7. VALIDATION

This section summarizes the validation of the NFC process model and the P&CE abstraction models. Section 7.1 documents the post-development validation of the NFC process level model. Section 7.2 describes validation exercises for the interpolation and extrapolation of chemical values from the lookup tables provided by the dilution/evaporation abstraction model. Section 7.3 is a summary of confidence building activities during model development. Section 7.4 is a summary of the validation process and results for the P&CE models.

The validation of the P&CE models is performed consistent with Level II, for a model of higher relative importance to repository system performance, as directed by SCI-PRO-002, *Planning for Science Activities*, Attachment 3. In addition to validation activities during model development, at least two post-development validation methods are required for Level II validation. One method, required by the technical work plan (TWP) governing the development of this report (SNL 2007 [DIRS 179287], Section 2.2.3), is a critical review, in accordance with SCI-PRO-006, Section 6.3.2, 5th bullet. In variance to the TWP, the critical review will evaluate only the P&CE abstraction models for drift seepage and invert pore water, and not the NFC model.

Near Field Chemistry Model Validation Methods and Criteria—The NFC model provides potential seepage water chemistries and ranges for in-drift CO_2 partial pressures through time. In accordance with the TWP (SNL 2007 [DIRS 179287], Section 2.2.3), the following two validation methods will be used to validate the NFC model:

- *Corroboration of model results with data acquired from the laboratory, field experiments, analog studies, or other relevant observations, not previously used to develop or calibrate the model* (SCI-PRO-006, Section 6.3.2, 1st bullet).

- *Corroboration of model results with other model results obtained from the implementation of other independent mathematical models developed for similar or comparable intended use/purpose* (SCI-PRO-006, Section 6.3.2, 2nd bullet).

Model validation is accomplished by comparison to pore-water compositions representing ambient conditions, to experimental data from the DST, and to predictions of the thermal-hydrologic-chemical (THC) seepage model, an independently derived model for seepage compositions. Validation criteria for the two NFC model outputs are as follows (SNL 2007 [DIRS 179287], Section 2.2.3):

Seepage water composition: The following validation criteria apply:

- The TWP (SNL 2007 [DIRS 179287], Section 2.2.3) states that the validity of the predicted alkali feldspar dissolution rate will be established if the rate calculated using the NFC model lies within an order of magnitude of the published range of feldspar dissolution rates. However, this comparison requires knowledge of the surface area of feldspar in the tuff, which is not available. In addition, published feldspar dissolution rates are poorly constrained with respect to the effective mineral surface area in the systems studied. In variance to the TWP, the NFC feldspar dissolution rate is validated using a different comparison. The NFC rate will be compared to feldspar dissolution

rates calculated from rock and pore-water strontium isotopic data from Yucca Mountain. As before, the validity of the predicted alkali feldspar dissolution rate will be established if the rate calculated using the NFC model lies within an order of magnitude of the range of rates developed from the strontium isotope data.

- The TWP (SNL 2007 [DIRS 179287], Section 2.2.3) states that the validity of the model predictions of seepage composition will be tested by showing that the NFC model approach for ambient conditions produces trends in water chemistry and mineralogy that are qualitatively consistent with observed trends in the field; (2) comparing predicted changes in water chemistry and mineralogy with those observed in the DST; and (3) comparing predicted water compositions to seepage waters selected from THC seepage model output by post-processing (Section 7.1.3). These comparisons of water compositions should agree to within an order of magnitude for each component, or if disagreements exist, they will be explained mechanistically in terms of the processes involved and the significance with respect to the intended use of the model.

  However, in variance to the TWP (SNL 2007 [DIRS 179287], Section 2.2.3), comparisons of the NFC model and measured water compositions are not carried out, as the NFC model does not model the processes of dilution and evaporation, which are the dominant processes affecting DST pore-water compositions. The duration of the DST experiment was too short for significant feldspar dissolution to occur.

CO_2 fugacity: The NFC model will generate maximum and minimum possible CO_2 fugacities through time, which will be sampled by TSPA at successive time steps. The following validation criteria apply:

- Validation of this approach will be achieved by showing that the range provided sufficiently bounds CO_2 fugacity values in the drift, and does so as the system evolves with time. This criterion will be evaluated by: (1) comparing the range with CO_2 concentration data from the DST; and (2) comparing the range for postclosure simulation with pCO_2 from the THC seepage model for comparable inputs. For comparison with DST data, the NFC model should bracket the observed range, with exceptions possible because the DST results may be affected by the transient response to dryout. For comparison with the THC seepage model the NFC model should also bracket the range, and the range should narrow with simulation time as the system cools. Exceptions are possible because the THC seepage model is a 2-D model that neglects axial gas-phase transport in the drift. Inconsistencies identified in these comparisons will be explained mechanistically in terms of the processes involved and the significance with respect to the intended use of the model.

The validation of the NFC model is described in Section 7.1. Section 7.1.1 uses strontium isotopic data for the tuff matrix and pore waters in the Topopah Spring Tuff (TSw) to evaluate the feldspar dissolution rate implemented in the NFC model. Section 7.1.2 compares observed trends in major ion compositional data for pore waters in the Paintbrush Tuff nonwelded unit (PTn) and in the TSw to NFC model predictions under ambient conditions. Section 7.1.3 compares THC seepage model predictions (SNL 2007 [DIRS 177404]) to NFC model results

developed with the same input data. Finally, Section 7.1.4 compares NFC model predictions to measured data from the DST experiment.

Seepage Dilution/Evaporation Abstraction Validation Methods and Criteria—The seepage dilution/evaporation abstraction predicts the composition of aqueous solutions in the drift, both on the waste package and drip shield surfaces, and in the invert. The integrated invert chemistry abstraction utilizes the same set of lookup tables, according to the implementation instructions found in Section 6.15.2. Because these two models are abstractions of the same model results, applied at different locations in the drift, the validation of the seepage dilution/evaporation abstraction also validates the integrated invert chemistry abstraction model.

In accordance with the TWP (SNL 2007 [DIRS 179287], Section 2.2.3), the following validation method (SCI-PRO-006, Attachment 3), in addition to the critical review, will be used to validate the NFC model:

- *Corroboration of abstraction model results to the results of the validated mathematical model(s) from which the abstraction model was derived* (SCI-PRO-006, Section 6.3.2, 7th bullet).

This consists of a comparison between output from the in-drift precipitates/salts (IDPS) process model (SNL 2007 [DIRS 177411]) and the seepage dilution/evaporation abstraction by implementing the interpolation and extrapolation discussed in Sections 6.9, 6.13.2, and 6.15.1. The post-development validation criteria state that the interpolation results are to be within the bounds of the uncertainty range of the IDPS model output. Section 7.2 documents the post-development validation of the seepage dilution/evaporation abstraction.

No further validation activities are required in accordance with the TWP (SNL 2007 [DIRS 179287], Section 2.2.3). The during- and post-development validation activities described below provide sufficient confidence that the models are valid for their intended uses, and that the associated uncertainties are propagated into the total system performance assessment (TSPA).

7.1 VALIDATION OF THE NEAR FIELD CHEMISTRY MODEL

The near-field chemistry (NFC) model is validated by comparison to field data under ambient conditions, to results of the THC seepage model, and to experimental data from the DST. Two different sets of ambient field data were examined. The first data set consists of strontium isotopic data for the tuff matrix and pore waters in the TSw (Section 7.1.1). The second data set consists of major ion compositional data for pore waters in the Paintbrush Tuff nonwelded unit (PTn) and in the TSw (Section 7.1.2). Model outputs from the NFC are also compared with model outputs from the THC seepage model (SNL 2007 [DIRS 177404]) (Section 7.1.3). Finally, experimental data from the DST are evaluated within the framework of the NFC model (Section 7.1.4). Each data set provides validation for different aspects of the NFC model, as discussed in the following sections.

Two specific aspects of the NFC model are not validated here, but are corroborated by results of calculations during model development, or have been validated in other model reports.

- The plug-flow implementation for pore-water transport is supported by the results of the FEHM calculations documented in Section 6.3.3.2.4. The FEHM results were used to optimize, or calibrate, the plug flow implementation, and hence cannot be used directly to validate the hydrologic model implemented, or transport times predicted, in the NFC. However, the FEHM results vary little (less than 15%) relative to the *uncalibrated* plug flow calculations, at all percolation fluxes from 1 mm yr^{-1} to 100 mm yr^{-1}. This provides corroboration for the main assumption required for the plug flow implementation, that matrix–fracture interactions are rapid relative to downward transport.

- The implementation of a conductive-heat-transfer-only model is consistent with use in other project models. *Multiscale Thermohydrologic Model* (SNL 2007 [DIRS 181383], Section 6.2.5) implements a conduction-only model and provides justification that heat flow is conduction-dominated. The method is also implemented, and validated, in *In-Drift Natural Convection and Condensation* (SNL 2007 [DIRS 181648]). Because this approach is validated in other project documents, this aspect of the NFC model requires no further validation.

7.1.1 Strontium Isotopic Data

Strontium isotopic data were collected during site characterization activities for several materials. These include whole rock analyses of core samples from rock units throughout the geologic section; analyses of soluble salts leached from crushed core, taken to represent pore-water compositions; and microanalysis of the Sr isotopic stratigraphy in calcite deposited in fractures through the TSw. The whole-rock and pore-water isotopic data are used here to evaluate the validity of the feldspar dissolution rate used by the NFC model. The feldspar dissolution rate derived from the Sr isotopic data will be considered corroborative of the mean NFC rate if they agree to within an order of magnitude.

The devitrified rhyolite core of the TSw consists almost entirely of silica polymorphs and feldspar (Section 4.1.6). Because silica polymorphs contain no significant strontium, the feldspar components of the TSw contain virtually all of the total Sr present. Changes in the strontium isotopic composition of pore water as it percolates downward through the devitrified rhyolitic core of the TSw can be used to estimate the rate of feldspar dissolution. If the rate determined by this method is consistent to within an order of magnitude with that used by the NFC model (which was determined from the abundance of secondary minerals in the tuff), then it will provide validation for that aspect of the NFC model. Consistency to within an order of magnitude is deemed sufficient because feldspar dissolution rates calculated from field measurements vary by over four orders of magnitude (White 1995 [DIRS 179312], Table 7), and uncertainties in the parameter values used in the derivation of the rate by either method are significant and difficult to fully quantify.

7.1.1.1 Data

Strontium isotopic data has been collected by the USGS as a function of depth for both core samples and leachate from core samples from three dry-cored boreholes through the TSw: SD-7, SD-9, and SD-12. The leachate data represent water-soluble salts leached from the coarsely crushed core by deionized water, with contact times of 1 hour (SD-9 and SD-12) or overnight (SD-7). The leachate data are taken to be representative of pore-water isotopic compositions from those locations in the geologic section; hereafter, they will be referred to as "pore-water" data. The sources for these data are listed in Table 7.1-1.

Table 7.1-1. Sources of Sr Abundance and Isotopic Data Used in This Validation Study

Borehole	Data Set	Source
SD-9, SD-12	Sr abundance and isotopic data for rocks, leachate	GS990308315215.004 [DIRS 145711]
SD-7	Sr abundance and isotopic data for rocks	GS970908315215.011 [DIRS 145702]
SD-7	Sr isotopic data for leachate	MO0708ISOTOPES.000 [DIRS 182333]
SD-7, SD-9, SD-12	Unit contact depths	MO0004QGFMPICK.000 [DIRS 152554]

* Sr isotopic data for leachates from SD-7 core fragments are not currently available in DTN form, but are available in a pair of RISweb documents.

Prior to use, the measured isotopic ratios, $(^{87}Sr/^{86}Sr)_m$, are converted to normalized isotopic values of the $\delta^{87}Sr$ notation. The value of $\delta^{87}Sr$ is defined as (Marshall and Futa 2001 [DIRS 156503], Equation 1):

$$\delta^{87}Sr = 1000 \times \left(\frac{\left({}^{87}Sr / {}^{86}Sr \right)_m}{0.7092} - 1 \right) \qquad \text{(Eq. 7.1-1)}$$

where the value of 0.7092 is the approximate $^{87}Sr/^{86}Sr$ value of modern seawater. This conversion is documented in Validation DTN: SN0705PAEBSPCE.014 (spreadsheet: *Sr calculations for NFC validation.xls*).

The Sr isotopic data for the pore waters from the entire sampled depth interval of these three boreholes is shown in Figure 7.1-1, and the rock isotopic data is shown in Figure 7.1-2. The upper and lower boundaries for the section representing the four repository host units, the Tptpul, Tptpmn, Tptpll, and Tptpln, are indicated. In each borehole, the $\delta^{87}Sr$ values for the pore water generally increase with depth. In boreholes SD-7 and SD-12 (but not in SD-9), this is especially notable through the devitrified rhyolitic core of the TSw. The rock $\delta^{87}Sr$ values are elevated in the Tiva Canyon tuff (TCw), drop to values below the pore-water values in the PTn and in the latitic top of the TSw, and then increase sharply at the top of the devitrified rhyolitic core of the TSw. Rock $\delta^{87}Sr$ values decrease gradually with depth through the rhyolitic core of the TSw, but are always higher than the pore-water values. In general, the pore-water values tend to evolve towards the rock values in any part of the section. The situation is complex at the top of the PTn,

possibly because of extensive zeolitization and scavenging of soil-derived strontium from the percolating waters. The pore-water $\delta^{87}Sr$ values at depths below the PTn exhibit a much narrower range than soil Sr values, indicating that the pore-water Sr is "derived almost entirely from the volcanic rocks, rather than the soils" (Marshall and Futa 2001 [DIRS 156503], Section II).

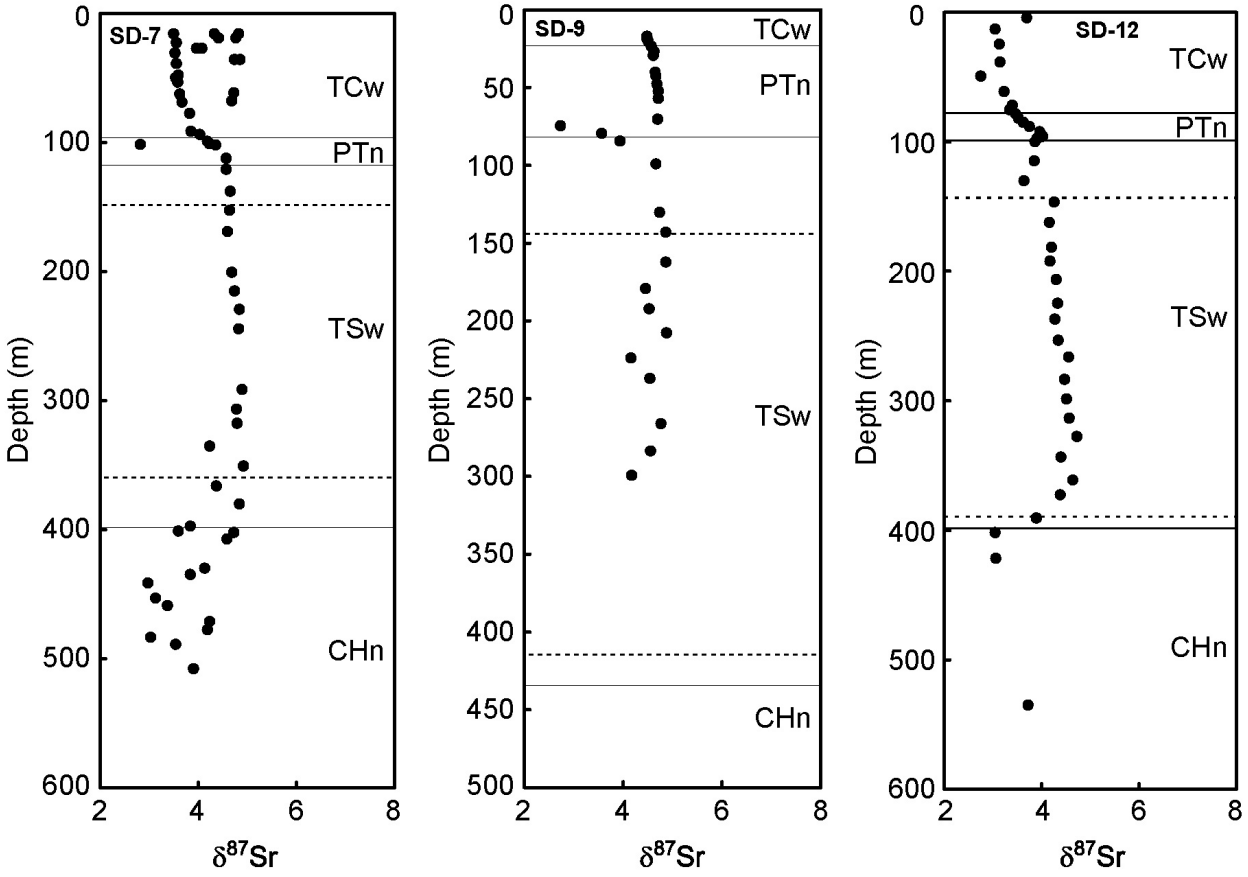

Source: Validation DTN: SN0705PAEBSPCE.014, spreadsheet: *Sr calculations for NFC validation.xls*.

NOTE: Geologic unit boundaries are shown by solid lines; dashed lines delineate the devitrified rhyolite core of the Topopah Spring Tuff. Units are defined as Tiva Canyon welded tuff (TCw), Paintbrush tuff non-welded (PTn), Topopah Spring welded tuff (TSw), and Calico Hills non-welded tuff (CHn).

Figure 7.1-1. Sr Isotopic Composition of Core Leachate Samples from Boreholes SD-7, SD-9, and SD-12

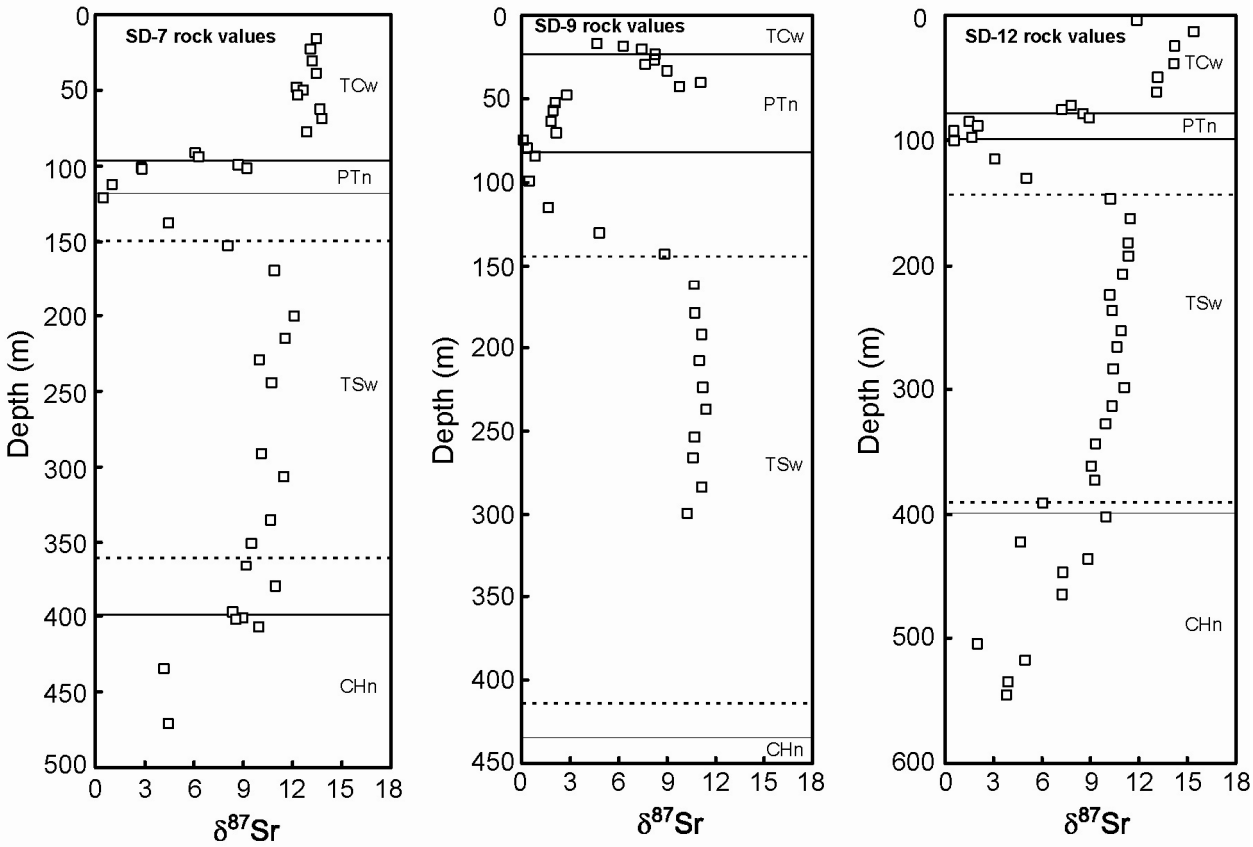

Source: Validation DTN: SN0705PAEBSPCE.014, spreadsheet: *Sr calculations for NFC validation.xls*.

NOTE: Geologic unit boundaries are shown by solid lines; dashed lines delineate the devitrified rhyolite core of the TSw. Units are defined as Tiva Canyon welded tuff (TCw), Paintbrush tuff non-welded (PTn), Topopah Spring welded tuff (TSw), and Calico Hills non-welded tuff (CHn).

Figure 7.1-2. Sr Isotopic Composition of Rock Samples from Boreholes SD-7, SD-9, and SD-12

The trend of increasing pore-water $\delta^{87}Sr$ with depth (Figure 7.1-1) has been interpreted to be due to water–rock interactions as the pore water percolates downward through the rock (Marshall and Futa 2001 [DIRS 156503]; Johnson and DePaolo 1994 [DIRS 162560]), and has been used to estimate pore-water flow velocities, or, alternatively, rates of Sr release by the rock. Feldspars (depicted in the NFC model as a single alkali feldspar) comprise the majority of the rock mass and contain nearly all of the Sr in the rock, as most of the remaining tuff consists of silica polymorphs which contain very little Sr. Note that while calcite is present in the rock and typically contains a few hundred mg kg^{-1} Sr (Paces et al. 2001 [DIRS 156507], Appendix 3), it contributes little to the total Sr concentration in the rock, because it is present in only small amounts (Section 4.1.6). Calcite does not contribute at all to the rate of Sr release by the rock because it precipitates rather than dissolves as the percolating water moves downwards through the rock.

Hence, the rate of Sr release by the rock represents the rate of feldspar dissolution, and the Sr isotopic data can be used to evaluate feldspar dissolution rates. Marshall and Futa 2001 ([DIRS 156503], Section II, last paragraph) evaluated the Sr isotopic data and estimated that pore-water transport times had to be "on the order of thousands of years." They also estimated a

whole-rock dissolution rate, as a volume fraction dissolved per unit time, for the entire sampled borehole depth (hence, an averaged value for both vitric and devitrified units). Their approach is modified here to evaluate the feldspar dissolution rate, as a mass fraction, only over the devitrified rhyolitic core of the TSw, the geologic interval considered in the NFC model.

The SD-9 data represent an incomplete sampling of the TSw section, and show more scatter than the other two data sets. In addition, the data represent two sampling intervals, with a gap of four to five months between them. Within the stratigraphic interval of interest, the three samples with the highest δ^{87}Sr values represent the first sampling period, while the remaining samples, scattered to lower values, represent the second. Given the scatter, the incomplete sampling of the stratigraphic section of interest, and the correlation with sampling time, the SD-9 data are not used in this analysis.

7.1.1.2 General Conceptual Model: Use of Sr Isotopes to Evaluate Water–Rock Interactions

The approach used by Marshall and Futa (2001 [DIRS 156503], Equation 2) is based on the formalism presented by Johnson and DePaolo (1994 [DIRS 162560]). Because of the necessary changes in the equation to describe dissolution of a single phase in the tuff, and to describe it in terms of mass fraction dissolved instead of volume fraction, it is easier to re-derive the equation from the general form presented by Johnson and DePaolo than to use the version presented by Marshall and Futa. The change in the isotopic composition of the pore water, as a function of time, at any given depth, is given by the following general equation (Johnson and DePaolo 1994 [DIRS 162560], Equation 11):

$$\frac{\partial \delta_f}{\partial t} = \nabla \cdot \left(D \nabla_{\delta_f}\right) + \frac{2D}{c_f} \nabla_{c_f} \cdot \nabla_{\delta_f} - v \cdot \nabla_{\delta_f} + M \sum_{i=1}^{n} \frac{R_i W_i c_i}{c_f} [\delta_i - \delta_f] + M \sum_{j=1}^{n} \frac{R_j W_j c_j}{c_f} [\Delta_j(T)] \quad \text{(Eq. 7.1-2)}$$

where:

- δ_f = δ^{87}Sr of the pore water
- c_f = Concentration of strontium in the pore water
- δ_i, δ_j = The δ^{87}Sr of a dissolving mineral phase i or a precipitating mineral phase j
- c_i, c_j = The concentration of strontium in a dissolving mineral phase i or a precipitating mineral phase j
- R_i R_j = The dissolution rate for mineral phase i or the precipitation rate of mineral phase j, expressed as a fractional change in the mass of the reactant per unit time
- W_i, W_j = The mass fraction of the dissolving mineral i or the precipitating mineral j
- ∇ = The change in a value per unit depth (z) (e.g., $\nabla\delta_f = \partial\delta_f/\partial z$)
- v = The average fluid velocity
- t = Time

D = The dispersion matrix

$\Delta_j(T)$ = The equilibrium difference between the δ values of the fluid and a precipitating phase j, as a function of temperature

M = The solid-to-fluid mass ratio, where:

$$M = \frac{(1-\phi)\rho_s}{\phi \rho_f S_w} \quad \text{(Eq. 7.1-3)}$$

where ϕ is the porosity, ρ_s is the solid density, ρ_f is the fluid density, and S_w is the saturation ratio (fraction of void space occupied by fluid).

The first two terms in Equation 7.1-2 are transport fluxes, while the third is the flux into the fluid from mineral dissolution, and the fourth, the flux out, due to mineral precipitation. Strontium isotopes do not fractionate under natural processes; thus, $\Delta_j(T)$ is equal to zero, and so is the final term in Equation 7.1-2. This means that mineral precipitation has no effect on the isotopic ratio, which is important, because calcite, which typically contains a few hundred mg kg^{-1} Sr (Paces et al. 2001 [DIRS 156507], Appendix 3), precipitates from the pore water as it percolates downward through the rock.

In addition, if dispersion is negligible relative to advective transport, the first two terms can be ignored, leaving:

$$\frac{\partial \delta_f}{\partial t} = -v\nabla_{\delta_f} + M\sum_{i=1}^{n}\frac{R_i W_i c_i}{c_f}\left(\delta_i - \delta_f\right) \quad \text{(Eq. 7.1-4)}$$

Finally, if the isotopic profile in the pore waters is assumed to represent steady-state conditions—that is, the isotopic ratio at any given depth does not change with time—then:

$$\frac{\partial \delta_f}{\partial t} = 0 \quad \text{(Eq. 7.1-5)}$$

Also, the tuff consists almost entirely of alkali feldspar plus silica phases (which contain negligible Sr), so there is only one phase in the rock that contributes significantly to the Sr content and isotopic composition, and that is alkali feldspar. Solving for $\nabla_{\delta f}$ (and renaming the variables for clarity):

$$\nabla_{\delta_f} = \frac{\partial \delta_{porewater}}{\partial z} = M\left(\delta_{feldspar} - \delta_{porewater}\right)\left(\frac{R_{feldspar} W_{feldspar}}{v}\right)\left(\frac{c_{feldspar}}{c_{porewater}}\right) \quad \text{(Eq. 7.1-6)}$$

This equation is similar to that used by Marshall and Futa (2001 [DIRS 156503], Equation 2), except for the conversion from volume fraction ($1 - \phi$) to rock-water mass ratio (M), and the

inclusion of the W term to make it specific to a single phase in the rock—feldspar. Finally, solving for the feldspar dissolution rate ($R_{feldspar}$) yields:

$$R_{feldspar} = \frac{\left(\frac{\partial \delta_{porewater}}{\partial z}\right) v}{W_{feldspar} M \left(\delta_{feldspar} - \delta_{porewater}\right) \left(\frac{c_{feldspar}}{c_{porewater}}\right)} \qquad \text{(Eq. 7.1-7)}$$

7.1.1.3 Model Parameterization

The parameter values for Equation 7.1-7 are estimated from the available data, as discussed below. Consistency is maintained with the NFC Model for all parameters. Calculations used to develop these parameters, unless otherwise stated are documented in Validation DTN: SN0705PAEBSPCE.014 (spreadsheet: *Sr calculations for NFC validation.xls*, tabs: "Calculation for SD-7" and "Calculation for SD-12").

$W_{feldspar}$ — obtained from the weighted mean of the mass fraction feldspar in the four repository units, which has already been calculated for use in the Near Field Chemistry model, as described in Section 6.3 and documented in Output DTN: SN0703PAEBSPCE.006 (spreadsheet: *Feldspar dissolution rate calculations.xls*, tab: "diss. Rate from mineralogy"). The weighted mean feldspar content, by mass, is 0.606.

M — The value of 19.6 is calculated from Equation 7.1-3 using the following values:

ϕ — The value of 0.139 represents the weighted mean of the porosity values for the four repository host units. The porosities are from DTN: LB0208UZDSCPMI.002 [DIRS 161243] (spreadsheet: *drift-scale calibrated properties for mean infiltration2.xls*). The weighted mean is calculated in Output DTN: SN0703PAEBSPCE.006 (file: *Feldspar dissolution rate calculations.xls*, tab: "Water-rock ratio").

ρs — The value of 2.526 g cm−3 represents the weighted mean of the grain density values for the four repository host units. The grain densities are taken from *Heat Capacity Analysis Report* (BSC 2004 [DIRS 170003], Table 6-8). This is a rock property that is held constant in both the development and validation cases to facilitate comparison. The weighted mean is calculated in Output DTN: SN0703PAEBSPCE.006 (file: *Feldspar dissolution rate calculations.xls*, tab: "Water-rock ratio").

Sw — The value of 0.798 represents the weighted mean of the saturation values for the four repository host units. Saturations are taken from *Heat Capacity Analysis Report* (BSC 2004 [DIRS 170003], Table 6-8). This is a rock property that is held constant in both the development and validation cases to facilitate comparison. The weighted mean is calculated in Output DTN: SN0703PAEBSPCE.006 (file: *Feldspar dissolution rate calculations.xls*, tab: "Water-rock ratio").

ρ_f — The value of 1.00 g cm^{-3} is used. The value of pure water at 21°C (an approximate median value for the TSw) would be ~0.9980 (Lide 2000 [DIRS 162229], p. 6-5), but the pore water is not pure water and will be a little denser. A value of 1.00 is chosen as being sufficiently accurate for this calculation.

$\delta_{feldspar}$ — The measured rock values for $\delta^{87}Sr$ are taken to represent the feldspar values, because the vast majority of the Sr in the rock is in the feldspar. As noted earlier, while calcite contains Sr, it is present in only trace quantities along fractures in the TSw and contributes negligibly to the bulk tuff Sr content or isotopic composition. The rock values vary with depth through the TSw; the chosen value is the average of the measured rock values for borehole depth interval corresponding to the devitrified rhyolitic core of the TSw (units Tptpul, Tptpmn, Tptpll, and Tptpln).

Borehole SD-7: Based on data from DTN: GS970908315215.011 [DIRS 145702], the average $\delta_{feldspar} = 10.51$.

Borehole SD-12: Based on data from DTN: GS990308315215.004 [DIRS 145711], the average $\delta_{feldspar} = 10.43$.

$\delta_{porewater}$ — This is the $\delta^{87}Sr$ value for the *starting* pore water (e.g., the value of the water at the top of the TSw devitrified rhyolite section). The leachate values from the rock cores are taken to be representative of pore-water values. Because there is scatter in the data, the actual value used here is not the value of the highest sample, but rather was derived by fitting the measured pore-water $\delta^{87}Sr$ values for the devitrified rhyolitic section to a straight line versus depth and using the predicted value corresponding to the depth of the highest measured value. The best fit lines for boreholes SD-7 and SD-12 are shown in Figure 7.1-3. Note that one data point within the interval of interest for SD-7 was not included in the analysis. The starting value for SD-7 $\delta^{87}Sr = 4.643$ while that for SD-12 $\delta^{87}Sr = 4.183$.

$c_{feldspar}$ — Since virtually all the Sr in the rock is in feldspar, the concentration of Sr in the feldspar is equal to the concentration in the rock, normalized to the mass fraction of feldspar in the rock ($W_{feldspar}$). Unfortunately, the concentration of Sr in the core samples from SD-7 and SD-12 was not measured. However, Sr concentrations were measured in a suite of rock samples collected along the ECRB, from all four of the TSw devitrified rhyolite units, the Tptpul, Tptpmn, Tptpll, and Tptpln. These data are archived in DTN: GS000308313211.001 [DIRS 162015]. The data show little variation through the units of interest, and have a mean and standard deviation of 25.1 ± 3.3 mg kg^{-1} (Validation DTN: SN0705PAEBSPCE.014, spreadsheet: *Sr calculations for NFC validation.xls*, tab: "Sr content of TSw rhyolite"). Given the average feldspar mass fraction of 0.606, this corresponds to a Sr concentration in the feldspar of 41.4 mg kg^{-1}.

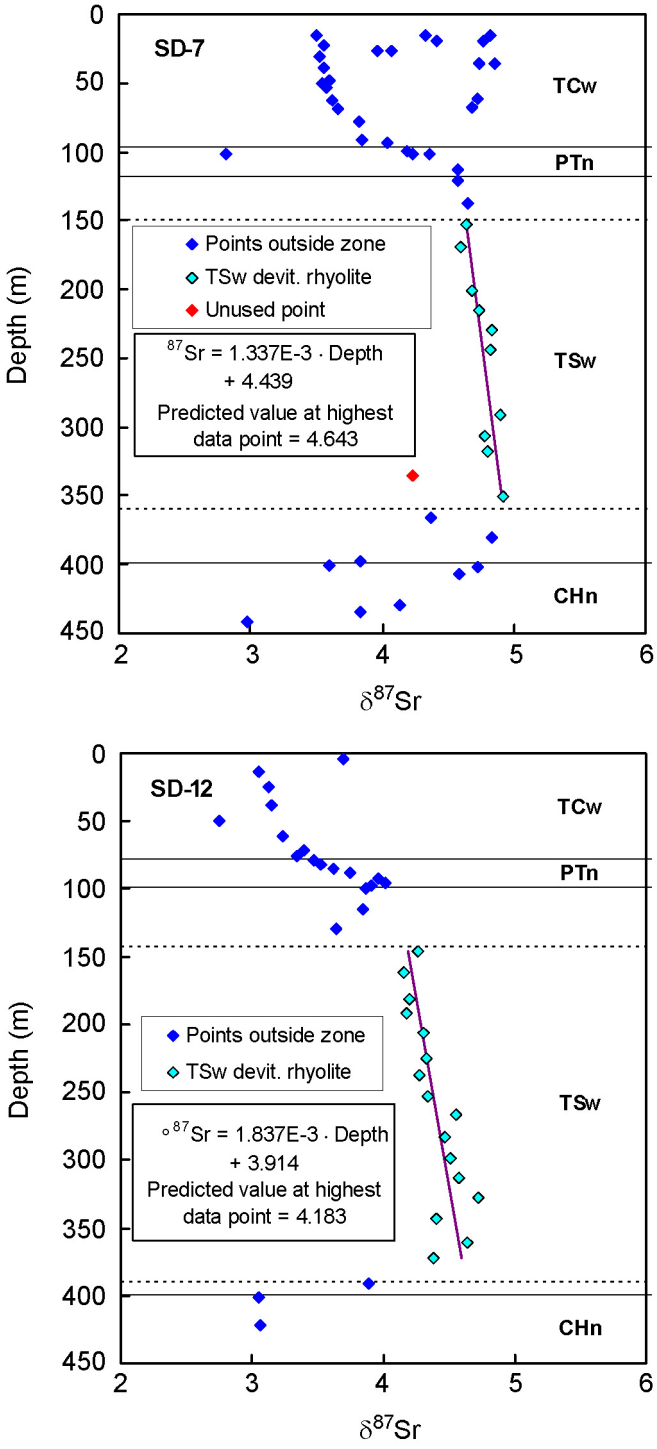

Source: Validation DTN: SN0705PAEBSPCE.014, spreadsheet: *Sr calculations for NFC validation.xls*.

NOTE: One point in the interval for SD-7 was not included in the fit. Geologic unit boundaries are shown by solid lines; dashed lines delineate the devitrified rhyolite core of the TSw. Units are defined as Tiva Canyon welded tuff (TCw), Paintbrush tuff non-welded (PTn), Topopah Spring welded tuff (TSw), and Calico Hills non-welded tuff (CHn).

Figure 7.1-3. Best Fit Line for $\delta^{87}Sr$ Core Leachate Data from the Devitrified Rhyolitic Center of the TSw, for Boreholes SD-7 and SD-12

$c_{porewater}$ — This value represents the Sr concentration in the pore water. It is the value with the greatest uncertainty, and an accurate estimate of this number is hard to determine. The measured leachate concentrations from the core samples from SD-12 are not direct measures of the Sr in pore water. They represent material leached from dried core, in units of milligrams leached per kilogram of tuff.

Multiplying these values by the rock-to-water mass ratio (M) of 19.6 yields a concentration for the pore water:

$$c_{porewater} = c_{leachate} \times M \quad \text{(Eq. 7.1-8)}$$

There are still large uncertainties in the pore-water concentration, however, associated with the degree to which the leachate represents the labile Sr originally present in pore water. The leaching process was done quickly to minimize dissolution of minerals in the tuff, and the efficiency of the process is unknown; not all soluble salts may have been extracted. Also, if calcite precipitated when the core dried, then the calculated concentration would be too low, but if more calcite was dissolved during the leaching step than was precipitated during dryout, then the observed concentration would be too high. Finally, if the initial core sample was not completely dry when it was leached, then the remaining pore water would contribute to the mass of the tuff sample leached, and the calculated pore-water concentration would be too high.

Even if multiplying the leachate concentration by the rock-to-water ratio yields an accurate measure of the pore-water concentration, there is considerable scatter in the Sr concentration in the leachates, and any single sample is unlikely to yield an accurate estimate of the initial value. Given the unknowns, a range of values is used in this calculation representing the mean value calculated from the leachate concentrations and M, plus or minus two standard deviations. The mean and standard deviation of the calculated pore-water concentrations is: $c_{porewater} = 0.284 \pm 0.112$ mg kg^{-1} (Validation DTN: SN0705PAEBSPCE.014, spreadsheet: *Sr calculations for NFC validation.xls*, tab: "Sr isotope data SD-9, SD-12"). Given the uncertainties, it is reassuring that the mean value is actually quite close to the mean Sr concentration for pore waters unaffected by microbial activity of 0.345 mg kg^{-1} (Output DTN: SN0705PAEBSPCE.015, spreadsheet: *Sr_Mn_data.xls*). It is important to note that the "pore water" Sr concentrations and isotopic compositions calculated here are from leachates extracted from dry core samples; hence, they here unlikely to have been affected by microbial activity during core storage.

Leachate Sr concentrations are not available for the SD-7 borehole, so the SD-12 range of values is also used for the SD-7 calculation.

$\partial\delta_{porewater}/\partial z$ — This value is the change in the isotopic composition of the pore water with depth, and is equal to the slope of the best fit line through the isotopic data, shown in Figure 7.1-3.

- SD-7: $\partial\delta_{porewater}/\partial z = 1.337 \times 10^{-3}$ m^{-1}
- SD-12: $\partial\delta_{porewater}/\partial z = 1.837 \times 10^{-3}$ m^{-1}

ν — The velocity of the pore water, in m yr^{-1}. This value is calculated using the assumption of plug flow, consistent with the NFC Model. Using this assumption, the volume of rock wetted by 1 liter of water is equal to $1/(\phi \times S_w)$. Using the values described above, this is equal to 9.00 liters of rock per liter of water. Hence, a percolation flux of 1 mm yr^{-1} corresponds to a flow velocity of 9 mm yr^{-1}. The flow velocity is treated parametrically in this analysis, with feldspar dissolution rates generated for percolation flux values ranging from 1 mm yr^{-1} to 15 mm yr^{-1}. This range was chosen because it represents the most probable range of values for fluxes at the PTn/TSw boundary, for the present-day climate state (DTN: LB0612PDPTNTSW.001 [DIRS 179150]).

These calculations yield a feldspar dissolution rate in terms mass fraction feldspar dissolved per year, which is converted to moles feldspar dissolved per kg tuff using the mass fraction of feldspar in the tuff and the formula weight of the feldspar. The calculations are documented in Validation DTN: SN0705PAEBSPCE.014 (spreadsheet: *Sr calculations for NFC validation.xls*).

7.1.1.4 Results and Summary

Feldspar dissolution rates estimated from the Sr isotopic data are compared to the NFC range in Figure 7.1-4. The feldspar dissolution rate used in the NFC model is implemented as a Beta distribution, with a mean value of 5.63×10^{-17} ($10^{-16.2}$) mol sec^{-1} kg tuff^{-1}, and maximum and minimum values of 9.96×10^{-17} ($10^{-16.0}$) mol yr^{-1} kg tuff^{-1} and 1.29×10^{-17} ($10^{-16.9}$) mol yr^{-1} kg tuff^{-1}, respectively (Output DTN: SN0703PAEBSPCE.007, spreadsheet: *Uncertainty in WR interaction parameter.xls*, tab: "1c) timing of alteration"). In Figure 7.1-4, for the NFC model, the heavy line is the mean value and the shaded area represents the range from the maximum to the minimum value of the Beta distribution. For the rates calculated from the borehole SD-7 and SD-12 Sr isotopic data, the darker shaded region represents the dissolution rates calculated using the mean $c_{porewater}$ value at percolation flux values ranging from 1 mm yr^{-1} (slowest feldspar dissolution rate) to 15 mm yr^{-1} (highest rate). The lighter region represents the range if two standard deviations in the $c_{porewater}$ value are considered.

For SD-7, the dissolution rates, using the mean $c_{porewater}$ value, vary from 8.40×10^{-17} ($10^{-16.1}$) mol sec^{-1} kg tuff^{-1} at a percolation flux of 1 mm yr^{-1}, to 1.26×10^{-15} ($10^{-14.9}$) mol yr^{-1} kg tuff^{-1} at a percolation flux of 15 mm yr^{-1}. For SD-12, the rates, using the mean $c_{porewater}$ value, vary from 1.08×10^{-16} ($10^{-16.0}$) mol sec^{-1} kg tuff^{-1} at a percolation flux of 1 mm yr^{-1}, to 1.63×10^{-15} ($10^{-14.8}$) mol yr^{-1} kg tuff^{-1} at a percolation flux of 15 mm yr^{-1}. These rates are very similar, and are slightly higher than those used in the NFC model. The difference is generally less than an order of magnitude, especially at percolation fluxes of a few millimeters per year, which are most consistent with the known age of the waters; the NFC and Sr ranges overlap at the lowest fluxes. At 1 mm yr^{-1} percolation flux, the SD-7 and SD-12 feldspar dissolution rates vary by

less than a factor of two from the mean rate used in the NFC model. If the uncertainty in the Sr data is included, then there is even more overlap between the rates derived from the two methods. In both cases, however, the feldspar dissolution rate used by the NFC model is most consistent with the rates derived from the Sr data using percolation fluxes at the lower end of the predicted present-day range.

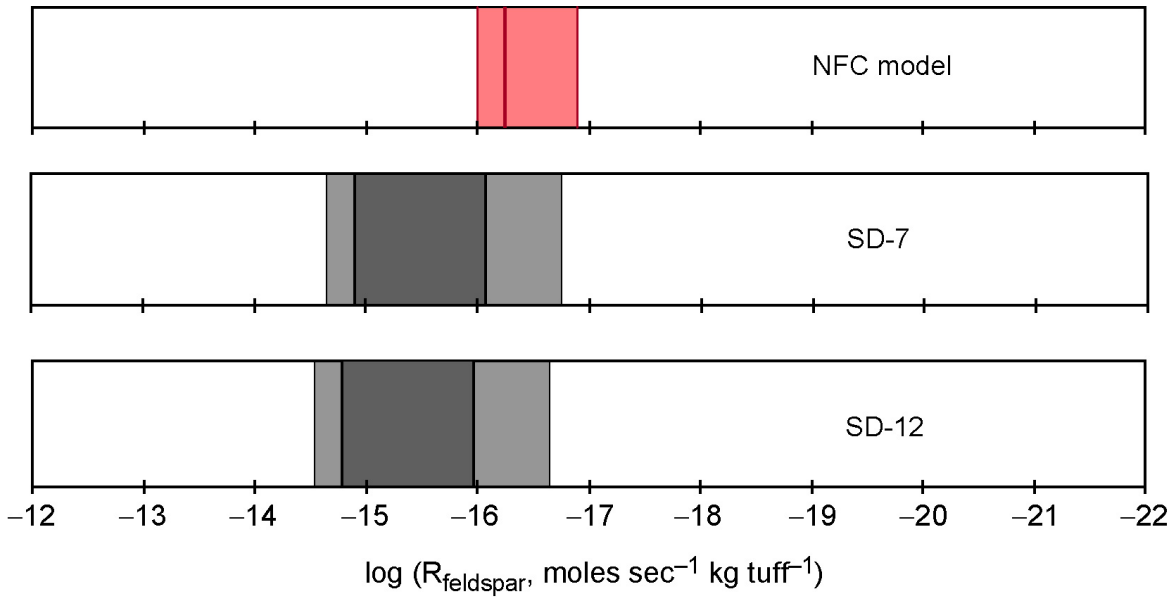

Source: Validation DTN: SN0705PAEBSPCE.014, spreadsheet: *Sr calculations for NFC validation.xls*.

NOTE: See text for discussion of the ranges shown.

Figure 7.1-4. Comparison of the NFC Model Feldspar Dissolution Rates with the Results of the Sr Isotopic Analysis for Boreholes SD-7 and SD-12

Although the feldspar dissolution rates determined from the Sr data are generally slightly higher than the range used by the NFC model, the ranges overlap. The dissolution rates vary by less than an order of magnitude, and the validation criteria for this aspect of the NFC model are met. The NFC feldspar dissolution rate can be considered validated.

7.1.2 Prediction of Ambient Pore-Water Compositional Trends and Mineral Assemblages

As pore waters percolate downwards through the geologic section, their compositions change. Viewed on a unit-to-unit basis, these changes are subtle, and are masked by the low sampling density, the variable thickness of the overlying rock units that percolating water has contacted, and the effect of combining water analyses from different depths within the unit itself. Despite these complications, general trends in pore-water composition are observed. In this section, the observed trends are documented, and EQ3/6 simulations using the NFC parameterization of water–rock interactions are used to evaluate whether the observed trends are consistent with the predicted trends. Validation criteria for this comparison require that the general compositional trends predicted by the NFC model match those observed in the ambient pore waters, and that predicted and measured compositions vary by less than an order of magnitude.

7.1.2.1 Pore-Water Data Considered

The pore-water data used in this validation test consist of two sets. The first set comprises the 34 TSw pore-water analyses that were evaluated and found to be minimally affected by microbial activity during core storage in Section 6.6. Although these waters are used in the NFC model simulations that feed TSPA, they are appropriate for use in model validation comparisons because the NFC model evaluates the WRIP value independently of water chemistry, and this calculation is in no way calibrated using water chemistry. Model outputs generated using the TSw pore waters are not being used in this section; instead, a simplified form of the model is applied to PTn pore waters using EQ3/6, and the unmodified TSw pore waters are used for comparison.

The second set consists of pore waters from the PTn hydrologic unit that overlies the TSw. These waters, too, have to be screened for potential microbial activity during storage. This was done using the same criteria as were used for the TSw waters. This analysis is documented in Validation DTN: SN0705PAEBSPCE.014 (spreadsheet: *PTn_Porewater_Data.xls*). First, all available PTn pore-water analyses were assembled (80 analyses). Of these, only 27 were "complete" analyses, including all major cations and anions (except for bicarbonate, which can be estimated by assuming equilibrium with a given pCO_2); the rest are missing values for potassium. Two samples are not considered because they are duplicates, and are nearly identical to the matching samples. Of the remaining 25 analyses, two have charge balance errors of greater than 10%, and are excluded on the basis of that. In a similar fashion to the TSw screening analysis, the remaining analyses were equilibrated using EQ3 at a pCO_2 of 10^{-3} bars, and the pH_{calc} determined. These files are in Validation DTN: SN0705PAEBSPCE.014. Only two of the 23 remaining samples failed the pH_{calc} criteria ($pH_{calc} > 8.35$) (see Section 6.6); however, two other samples were within 0.02 pH units of failing this criteria, and were also eliminated, because their pH values were significantly higher than the range of the other samples examined. The remaining 19 PTn pore-water analyses are complete and minimally affected by microbial activity, and are used in this analysis. These pore-water analyses are listed in Table 7.1-2, and the compositional data, in Table 7.1-3.

7.1.2.2 Modeling Changes in Pore-Water and Gas-Phase Composition with Depth

The NFC model predicts compositional changes in the pore water as it percolates downward through the thermally perturbed TSw devitrified rhyolite section above the drift. It predicts changes in potential seepage water composition (Section 6.3) by (1) implementing a thermal gradient calculated using a conduction-only line source heat flow solution, modified for the natural geothermal gradient; (2) assuming that the water is in equilibrium with calcite and amorphous silica; (3) summing the amount of alkali feldspar that dissolves into water as it percolates downwards, using a temperature-dependent feldspar dissolution rate, (4) assuming that the aqueous phase controls the local pCO_2; and (5), treating percolation flux rates parametrically.

Table 7.1-2. PTn Pore-Water Analyses Used in This Study

Sample Name	EQ3/6 Filename	Source
ESF-NR-MS#6/6.0-6.15/UC	ESFN-60	GS031008312272.008 [DIRS 166570]
ESF-NR-MS#6/6.15-6.3/UC	ESFN-61	
ESF-SR-MS#22/5.8-6.0/UC	ESFS-58	
ESF-SR-MS#22/6.0-6.3/UC	ESFS-60	
ESF-SR-MS#23/14.5-14.6/UC	ESFS-145	
ESF-SR-MS#23/14.6-14.9/UC	ESFS-146	
SD-6/501.3-501.6/UC	SD6-5013	
SD-9/93.3-93.4/UC	SD9-933	
SD-6/430.3 – 430.6/UP2	SD6-4303	GS011008312272.004 [DIRS 165859]
SD-6/430.6 – 431.0/UP1	SD6-4306	
SD-6/443.2 – 443.5/UP2	SD6-4432	
SD-6/443.5 – 443.8/UP1	SD6-4435	
SD-6/471.3 – 471.7/UP1	SD6-4713	
SD-6/491.2 – 491.5/UP2	SD6-4912	
SD-6/507.5 – 507.8/UP2	SD6-5075	
SD-6/522.5 – 522.6/UC1	SD6-5225	
SD-9/92.9-93.2/UC	SD9-929	GS041108312272.005 [DIRS 178057]
SD-9/93.4-93.5/UC	SD9-934	
UZ16-180.9-181.27/UP-4	UZ16	GS010708312272.002 [DIRS 156375]

To evaluate how the model predicts compositional changes as the water percolates downward through the stratigraphic section, the same general approach is used. EQ3/6 simulations implementing the major components of the NFC model—equilibrium with calcite and amorphous silica, kinetically limited feldspar dissolution with a temperature-dependent dissolution rate, local gas-phase equilibrium, and slow, plug flow percolation—are compared to the observed changes in ambient water composition as waters percolate from the PTn through the TSw.

In the ambient case, there is no thermal overprint—the geothermal gradient is used explicitly. The geothermal gradient is based on analysis of borehole temperature data from borehole SD-12 (Section 6.3). As with the NFC model, a repository depth of 300 m is assumed. The predicted geothermal gradient ranges from 17°C at the land surface, to 19.1°C at the top of the devitrified core of the TSw (~100 m), to 23.4°C at 300 m, the repository level (Validation DTN: SN0705PAEBSPCE.014, spreadsheet: *Calculations supporting PTn water validation test.xls*).

Table 7.1-3. PTn Pore-Water Compositional Data Used in This Analysis

EQ3/6 filename	pH	Na (mg/L)	K (mg/L)	Mg (mg/L)	Ca (mg/L)	Cl (mg/L)	SO_4 (mg/L)	HCO_3 (mg/L)	NO_3 (mg/L)	F (mg/L)	SiO_2 (mg/L)
ESFN-60	—	51	3.6	3.6	15	34	28	94	12	1.9	68.0
ESFN-61	—	47	3.7	3.6	15	41	26	91	8.3	1.3	61.0
ESFS-58	—	55	10.8	22.9	105	134	160	156	13	0.61	62.0
ESFS-60	7.5	55	9.6	23.1	108	113	140	154	15	0.85	69.0
ESFS-145	—	52	9.2	19.7	89	119	111	141	29	0.86	66.0
ESFS-146	7.7	47	9.3	19.6	90	109	116	133	37	0.83	62.0
SD6-4303	7.5	51	3.4	7.7	36.3	39.1	45	—	82.3	4	85.1
SD6-4306	7.4	54	3.8	8.7	46.3	45.8	50	99	76.6	4.9	66.9
SD6-4432	7.5	60.7	4.3	9.4	43	33.8	85	—	80.9	6.3	81.2
SD6-4435	7.4	65.5	4	11.7	48.2	47.3	98	101	86	6.3	84.4
SD6-4713	7.3	44.9	2.6	12.3	61.4	66.8	68	74	67.3	8.6	58.5
SD6-4912	7.3	53.4	1.7	16.1	62.7	60.6	57	135	65.5	26.9	91.7
SD6-5013	7.7	51	1.5	9.9	50	27	63	167	34	3.7	65.0
SD6-5075	7.4	48.3	2.4	24.6	125	20.3	299	92	25.7	3.1	64.0
SD6-5225	8.1	59	6	9.9	43.7	26.3	56	167	34.5	7.7	63.7
SD9-929	7.1	74	15.1	43.3	231	337	350	45	23	0.30	100.0
SD9-933	7.3	56	12.7	40.5	199	234	393	56	17	1.1	76.0
SD9-934	7.2	61	14.6	33.4	179	234	327	47	17	0.39	77.0
UZ16	7.3	20	3	11	55	38	38	146	33	—	—

NOTES: DTN sources listed in Table 7.2-1.

Some of the values presented above are rounded from the DTN values. The values reported in the source DTNs are as follows (mg/L): SD6-4306 – SO_4 49.8, HCO_3 98.9; SD6-4435 – SO_4 97.7; SD6-4713 – HCO_3 74.1; SD6-4912 – SO_4 56.6; SD6-5075 – Ca 125.1, HCO_3 92.4; SD6-5225 – SO_4 56.1; UZ-16: HCO_3 146.4. These slight differences are too small to have any effect on the calculation results. In any case, bicarbonate is recalculated on the basis of equilibrium with a fixed pCO_2 in the simulations, and sulfate is completely conserved in the NFC model and plays no role in the chemical reactions being evaluated.

It is also necessary to estimate water transport time as it passes downward through the TSw. This has been evaluated by Yang (2002 [DIRS 160839], Table 2), using ^{14}C residence times determined from borehole gas analysis (borehole UZ-1), and assumed to represent equilibrium with pore waters. Yang's estimates of pore water ages at the top of the TSw are 2,000 to 3,000 years, while those at the base of the unit are about 10,000 to 13,000 years, indicating transport times of on the order of 10,000 years for the entire section. This is also in agreement with the conclusion, based on pore-water hydrogen isotope data, that waters at the base of the TSw are more than 10,000 years old and isotopically reflect the cooler climate of the last ice age. Thus, in this analysis, it is assumed that the maximum transport time for the waters through the TSw is about 10,000 years, and that this is likely to be applicable to waters in the lower part of the unit.

Also, while the TSPA implementation of the NFC model sums up the feldspar dissolved and only calculates a composition at the end of the percolation pathway (at the drift wall), here it is necessary to calculate the change in composition with depth along the flow path. This is done in EQ6 simulations by use of the Transition State Theory (TST) model for mineral dissolution kinetics. The TST model calculates the feldspar dissolution rate from a reference rate as a function of temperature, by use of the Arrhenius relationship and the activation energy for feldspar dissolution. It also adjusts the alkali feldspar dissolution rate by the saturation index for the mineral, but this has no significant effect in the model implemented here, because alkali feldspar never approaches saturation in the pore waters. For use in the TST modeling, the alkali feldspar dissolution rates from the NFC model were converted to units of moles cm^{-2} sec^{-1} using a fixed value for the tuff specific surface area. This rate was used with a reactive surface area calculated from the same specific surface area and the water:rock ratio in the tuff. These calculations are documented in Validation DTN: SN0705PAEBSPCE.014 (spreadsheet: *Calculations supporting PTn water validation test.xls*).

Each EQ6 simulation was run for a fixed time, representing the transport time through the 200-m section of the TSw used in the NFC Model; usually, a value of 10,000 years was used. The geothermal gradient was implemented by setting the temperature to increase at a fixed rate, from the calculated temperature at the top of the unit (19.1°C) to the temperature at the repository (23.4°C), over the length of the time interval.

It is also necessary to assume a pCO_2 at the top of the modeled section. The pCO_2 is not held fixed, but rather is assumed to remain in equilibrium with the water chemistry as the water percolates downwards. The pCO_2 at the top of the simulated section (that is, at the top of the Tptpul) is assumed to be 10^{-3} bar (0.1%), based on the measured CO_2 concentrations in borehole UZ-1 over the time interval from 1988 to 1994. These data are plotted in Figure 7.1-5.

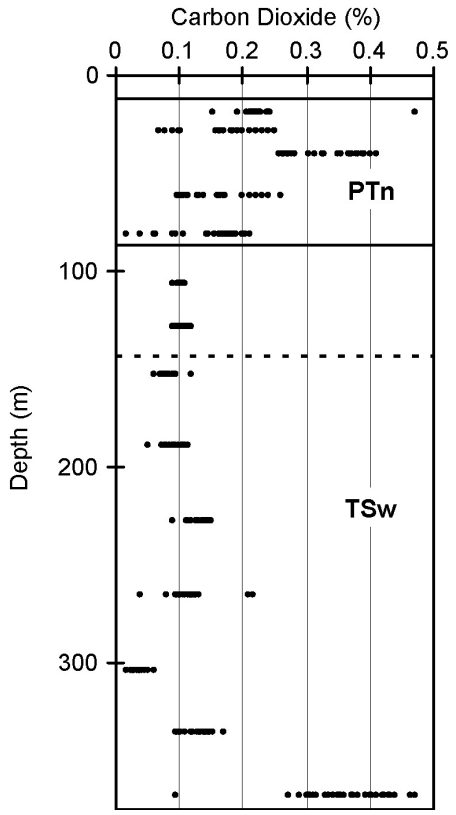

Source: DTNs: GS930408312271.014 [DIRS 145 533], GS911208312271.011 [DIRS 182482], GS930108312271.004 [DIRS 166448], GS940408312271.006 [DIRS 166451], GS940408312271.001 [DIRS 166450].

NOTE: Solid horizontal lines represent unit contacts, while the dotted line represents the top of the devitrified rhyolitic core of the TSw.

Figure 7.1-5. Measured CO_2 Concentrations in Borehole UZ-1, from 1988 to 1994

Before showing the results of specific simulations, it is useful to review the general chemical reactions that occur as increasing amounts of feldspar dissolve, as described in Section 6.3.2.6. First, at low amounts of feldspar dissolved, the following reaction occurs:

$$\underset{\text{(alkali feldspar)}}{2Na_{0.5}K_{0.5}AlSi_3O_8} + Ca^{2+} + SiO_2(aq) + 7H_2O \rightarrow \underset{\text{(stellerite)}}{\tfrac{1}{2}Ca_2Al_4Si_{14}O_{36}{:}14H_2O} + K^+ + Na^+$$

(Eq. 7.1-9)

This reaction consumes Ca^{2+}, while releasing K^+ and Na^+. As the solution becomes undersaturated with respect to calcite, it begins to dissolve. The reaction becomes:

$$\underset{\text{(alkali feldspar)}}{2Na_{0.5}K_{0.5}AlSi_3O_8} + \underset{\text{(calcite)}}{CaCO_3} + H^+ + SiO_2(aq) + 7H_2O \rightarrow \underset{\text{(stellerite)}}{\tfrac{1}{2}Ca_2Al_4Si_{14}O_{36}{:}14H_2O} + K^+ + Na^+ + HCO_3^-$$

(Eq. 7.1-10)

This reaction results in an increase in pH and solution alkalinity with increasing feldspar dissolution. In a system with limited gas-phase exchange, this has the effect of lowering the CO_2 concentrations in the gas phase, as it partitions into the aqueous phase.

Eventually, as greater amounts of feldspar dissolve, K^+ builds up in solution and a potassium-bearing clay phase saturates. In the NFC model, the K-phase is the mineral celadonite, and the reaction becomes:

$$6Na_{0.5}K_{0.5}AlSi_3O_8 + 2CaCO_3 + 2Mg^{2+} + 4SiO_2(aq) + 16H_2O \rightarrow$$
Alkali feldspar Calcite

$$Ca_2Al_4Si_{14}O_{36}{:}14H_2O + 2KMgAlSi_4O_{10}(OH)_2 + K^+ + 3Na^+ + 2CO_2$$
(stellerite) (celadonite)

(Eq. 7.1-11)

Once celadonite begins to precipitate, further dissolution of feldspar results in a drop in the pH. However, the amount of magnesium in solution is limited. With continued feldspar dissolution, this reaction rapidly becomes inhibited by lack of Mg^{2+}, and Equation 7.1-10 once again becomes dominant.

The above reactions are observed in the EQ6 simulations performed for this ambient condition validation case (Validation DTN: SN0705PAEBSPCE.014); in the NFC model simulations that support TSPA, greater amounts of feldspar can dissolve because of the elevated temperature conditions due to the thermal pulse. Under those conditions, other Na- and K-bearing silicates such as phillipsite can saturate and begin to precipitate.

In addition to the reaction of feldspar to form secondary minerals, other processes occur due to the temperature change as the water percolates downwards. Even in the ambient case, these reactions are significant with respect to the water composition. The increase in temperature causes CO_2 to degas from solution, and the rise in pCO_2 results in a slight decrease in pH. A very small amount of calcite precipitates, due to the reverse solubility of this mineral. Both calcium and carbonate concentrations decrease, while there is a slight increase in the silica concentration, because silica polymorphs are more soluble with increasing temperature.

Note that the effect of the increase in temperature is to cause calcite to precipitate, while feldspar dissolution consumes calcite. The relative rate of these two reactions determines whether calcite is predicted to precipitate or dissolve.

These trends are depicted graphically in Figures 7.1-6 through 7.1-8. In each figure, chemical constituents of PTn waters are plotted against those of TSw waters. The TSw waters are divided into those from the upper two rhyolitic units (the Tptpul and Tptpmn) and the lower two units (Tptpll and Tptpln), to illustrate that the chemical differences between the PTn and TSw waters are not solely due to glass dissolution in the PTn; the same chemical trends are observed between the upper and lower TSw samples. The predicted evolutionary paths of the waters are also indicated, assuming feldspar dissolution rates equal to the mean and maximum rates used in the NFC model; the maximum rate is about twice the mean rate. Also shown in these figures are the evolutionary paths using a feldspar dissolution rate of 5 times the mean rate. The evolutionary

pathways are calculated using the EQ3/6 TST method, assuming a 200-m thickness of devitrified rhyolitic TSw, the ambient geothermal gradient (19.1°C to 23.4°C), and a contact time of 10,000 years, the maximum reasonable value for TSw pore waters. When considering these figures, it is important to remember that the lowermost TSw waters are believed to be Pleistocence in age. It is not known how much of the observed differences in chemistry between the upper and lower TSw waters might be due to differences in percolation fluxes and in the composition of infiltrating waters in Pleistocene and recent times, as opposed to being due to differences in degree of water–rock interaction. It should also be noted that the samples from the lower two TSw units are all from the same location (Borehole SD-9), and hence are unlikely to represent the entire variation in pore waters from this stratigraphic level.

Potassium is the most sensitive measure of feldspar dissolution in the pore waters. Although potassium and sodium are released at an equal rate by feldspar dissolution, the initial potassium concentrations are much lower than the sodium concentrations, and hence the relative change in concentration is greater. Calcium is also quite sensitive, as it is depleted from solution by precipitation of stellerite, and also affected by the change in calcite solubility due to the geothermal gradient. Potassium and calcium concentrations in PTn and TSw waters are plotted against each other in Figure 7.1-6. Both sets of waters are equilibrated with calcite and silica, as in the NFC model. TSw data are shown for equilibration temperatures of both 19.1°C and 23.4°C, covering the likely range of temperatures for samples from the TSw; any single sample would have a value somewhere between the paired values. Also shown are the evolutionary pathways for the PTn waters, assuming the mean, maximum, and 5× mean NFC feldspar dissolution rates. The PTn waters are chemically distinct from the TSw waters; they are systematically more Ca-rich and K-poor. The calculated evolutionary paths illustrate that the major components of the NFC model (feldspar dissolution, equilibrium with calcite, and the local gas phase being controlled by equilibrium with the water) accurately predict the direction of compositional change. In addition, simulations using the mean and the maximum NFC feldspar dissolution rate accurately predict the degree of compositional change in the pore waters. In this plot, the simulations using 5× the mean NFC feldspar dissolution rate over-predict the degree of compositional change.

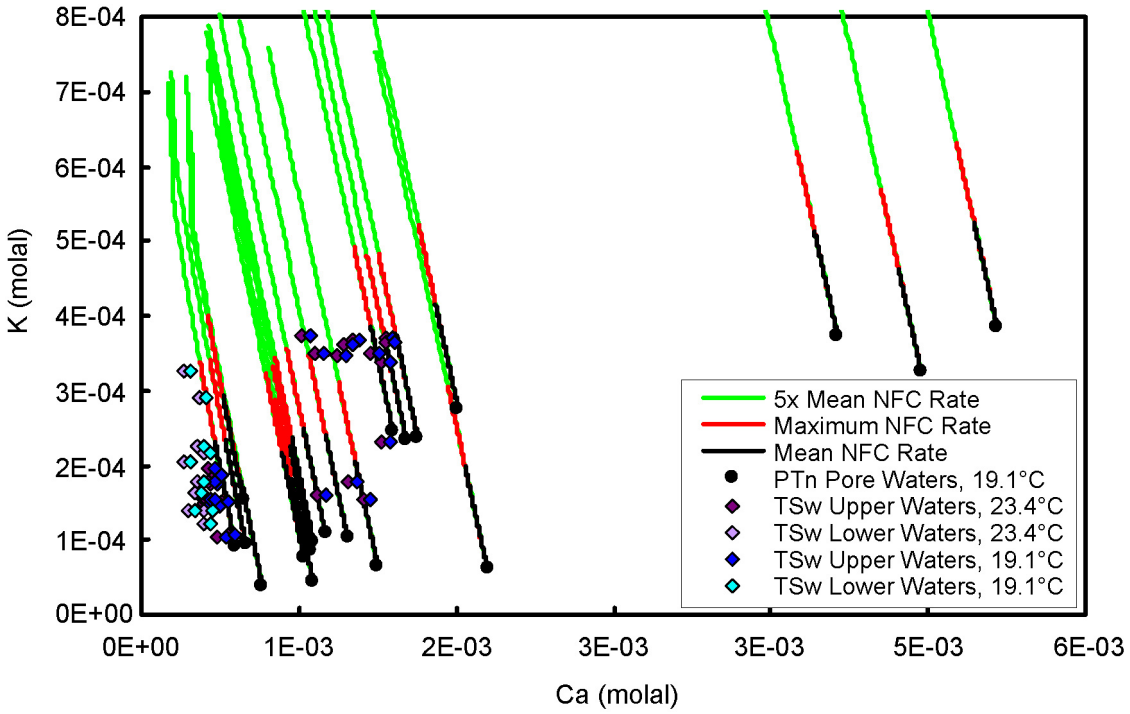

Source: Validation DTN: SN0705PAEBSPCE.014, spreadsheet: *PTn-TSw equilibrated waters and results.xls*.

NOTE: TSw waters are shown equilibrated at both 19.1°C and 23.4°C, covering the likely range of applicable temperatures.

Figure 7.1-6. K versus Ca Molalities for TSw and PTn Pore Waters, Showing Predicted Evolutionary Pathways for the PTn Waters, at Three Different Feldspar Dissolution Rates

In Figure 7.1-7, Na and Ca concentrations for PTn and TSw pore waters are plotted, along with the predicted evolutionary paths. In this and the following plot, only the 23.4°C data are shown for the lower TSw samples, because they represent depths too great to have equilibrated at the lower temperature. Na concentrations in the PTn are much higher than the K concentrations, so feldspar dissolution has little effect on the bulk Na concentration. The PTn and upper TSw pore waters largely overlap, although the lower TSw samples are slightly enriched in Na and depleted in Ca relative to the other samples. The NFC model again accurately predicts the direction of compositional change, although the composition of the lower TSw samples seems to be more consistent with a feldspar dissolution rate of two to five times the mean rate used by the NFC model (two times the mean rate is approximately equal to the maximum NFC rate). The inflection in some of the 5× simulations occurs when celadonite starts to precipitate, and the pH begins to drop (see Equation 7.1-11). The lower TSw samples are well predicted by this inflection, and this might indicate that the NFC feldspar dissolution rate is slightly low. However, given the paucity of the data from the lower TSw, and the fact that only a single location is represented, it is difficult to accurately evaluate this. In addition, the possibility that the difference between the PTn waters and the TSw waters might be in part due to glass dissolution in the PTn must be considered. The PTn waters were not collected at the base of the unit, but throughout it.

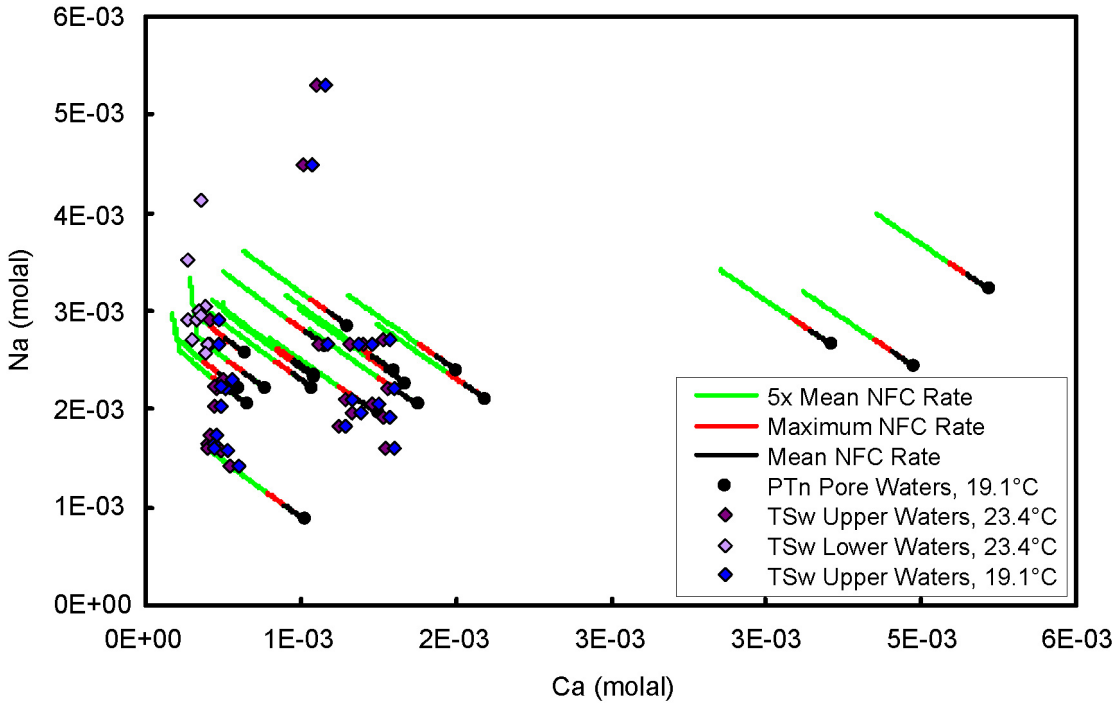

Source: Validation DTN: SN0705PAEBSPCE.014, spreadsheet *PTn-TSw equilibrated waters and results.xls*.

NOTE: TSw waters are shown equilibrated at both 19.1°C and 23.4°C, covering the likely range of applicable temperatures.

Figure 7.1-7. Plot of Na vs Ca Molalities for TSw and PTn Pore Waters, Showing Predicted Evolutionary Pathways for the PTn Waters, at Three Different Feldspar Dissolution Rates

The ratio of divalent to monovalent cations is plotted against the total carbon concentration in Figure 7.1-8. This plot is particularly sensitive to the assumed temperature, because of the effect of temperature on aqueous/gas phase CO_2 equilibria, and on the solubility of calcite; there is significantly more difference between the TSw data sets at 19.1°C and 23.4°C than there was on the two previous plots. Despite the scatter, the NFC model accurately depicts the evolution of the PTn waters, at feldspar dissolution rates consistent with, or slightly larger than, the NFC rates. The lower TSw waters again suggest a slightly higher dissolution rate, although this may be due to differences in the composition of Pleistocene relative to modern infiltration. The NFC model predictions capture the general compositional trends; the inflection in the predicted evolutionary pathways due to celadonite precipitation captures the upturn in the data at lower values of the divalent/monovalent ion ratio.

In Figure 7.1-9, model predictions for gas-phase CO_2 concentrations are compared with measured field data from packed-off intervals of borehole UZ-1. The measured data are a subset of the data shown in Figure 7.1-5, corresponding to the concentrations in the gas phase through the devitrified rhyolitic section of the TSw. In general, the measured data cluster tightly around 0.1% CO_2 (10^{-3} bar), and show almost no variation throughout the rhyolitic TSw section, the exception being the measured data at a depth of about 160 m, which indicate a slightly lower pCO_2 than the data sets from other levels. Model data are shown for four feldspar dissolution rates: the mean and maximum NFC feldspar dissolution rates, and values of 5× and 10× the mean NFC rate. The model predictions for the mean and maximum NFC rates do not vary

greatly from the assumed initial value of 10^{-3} bar, and are consistent with the measured values from borehole UZ-1. For simulations using higher feldspar dissolution rates, 5× and 10× the mean rate, the increase in alkalinity is sufficient to result in predicted pCO_2 values that fall below the measured values at 80, 120, and 190 m, although still above the anomalously low measured values at 160 m. The range of feldspar dissolution rates used in the NFC model is more consistent with the measured pCO_2 data than rates 5 to 10 times higher (Figure 7.1-8).

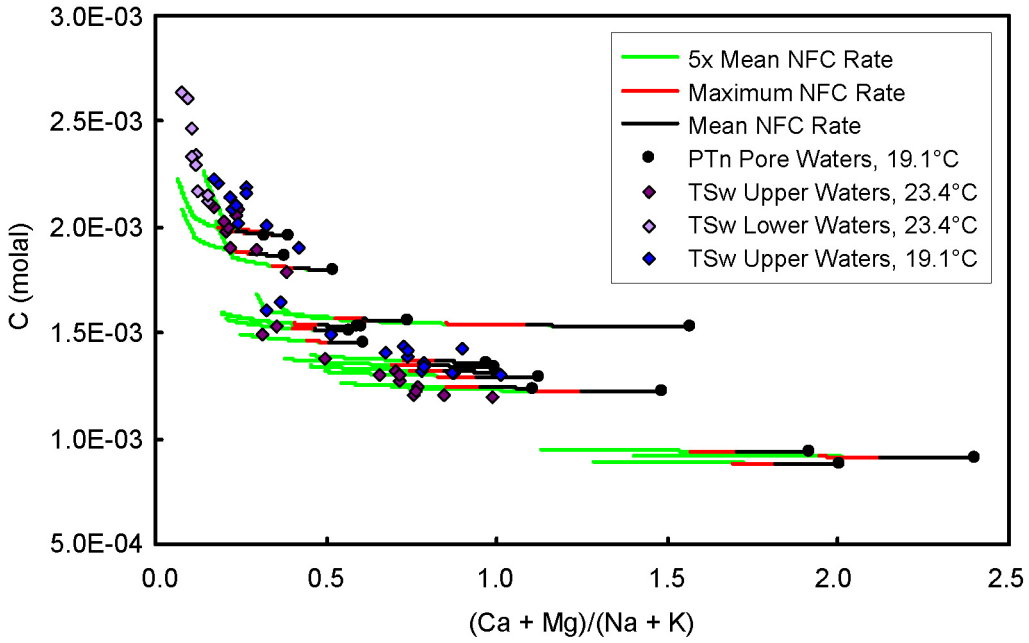

Source: Validation DTN: SN0705PAEBSPCE.014, spreadsheet: *PTn-TSw equilibrated waters and results.xls*.

NOTE: TSw waters are shown equilibrated at both 19.1°C and 23.4°C, covering the likely range of applicable temperatures.

Figure 7.1-8. Divalent/Monovalent Cation Ratio versus C Molality for TSw and PTn Pore Waters, Showing Predicted Evolutionary Pathways for the PTn Waters, at Three Different Feldspar Dissolution Rates

Predicted pH values versus depth are plotted in Figure 7.1-10. Initial calculated pH values cover a range of about 0.5 pH units, from 7.5 to 8.0. The effect of feldspar dissolution is a general rise in pH and alkalinity, with an inflection in the curves occurring when celadonite begins to precipitate. Using the mean and maximum NFC feldspar dissolution rates, the change in pH is relatively minor, perhaps 0.1 pH units. However, using the 5× and 10× mean feldspar dissolution rates, the predicted change in pH is larger. Predicted values evolve to between 8.0 and 8.5, and for a few waters in the 10× case exceed 9.0. All measured pH values for TSw pore waters, regardless of whether the samples were determined to be affected by microbial activity, are tabulated in Output DTN: SN0705PAEBSPCE.015 (spreadsheet: *TSw_Porewater_Data.xls*, tab: "All TSw"). Of the 68 measured values, 66 fall between pH 6.72 and 8.32; two samples, with reported measured pH values of 8.5, were collected prior to the development of data qualification procedures and are not considered reliable. Hence, the measured pH values are consistent with the results predicted using mean and maximum NFC feldspar dissolution rates, but not with the 5× and 10× dissolution rates.

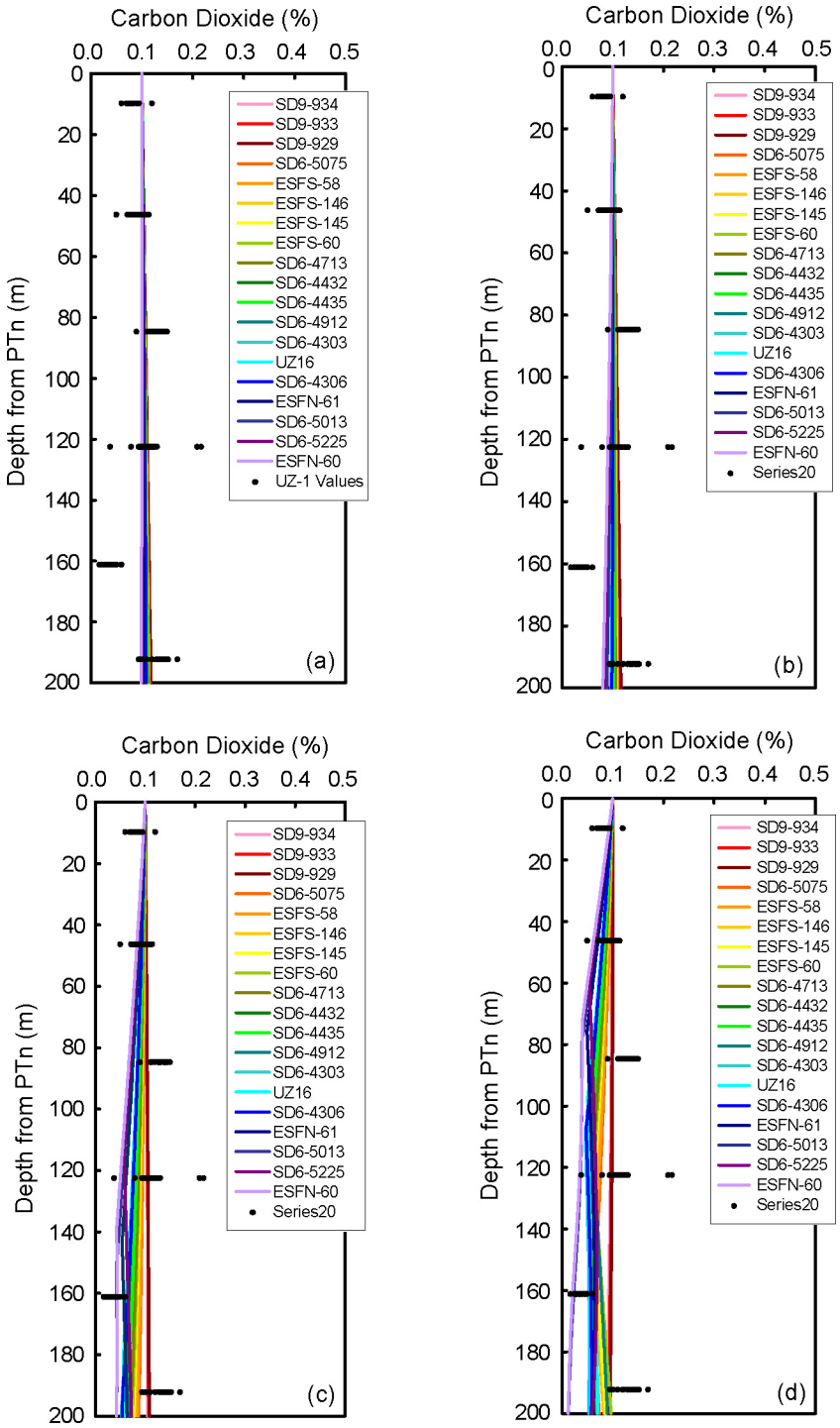

Source: Validation DTN: SN0705PAEBSPCE.014, spreadsheets: *PTn TST runs, avg rate.xls*, *PTn TST runs, max rate.xls*, *PTn TST runs, 5 X mean rate.xls*, and *PTn TST runs, 10 X mean rate.xls*.

Figure 7.1-9. Predicted CO_2 Gradients through a 200-m Section of the TSw, Compared to Measured Values in Borehole UZ-1: (a) NFC Mean Feldspar Dissolution Rate, (b) NFC Maximum Rate, (c) 5× NFC Mean Rate, (d) 10× NFC Mean Rate

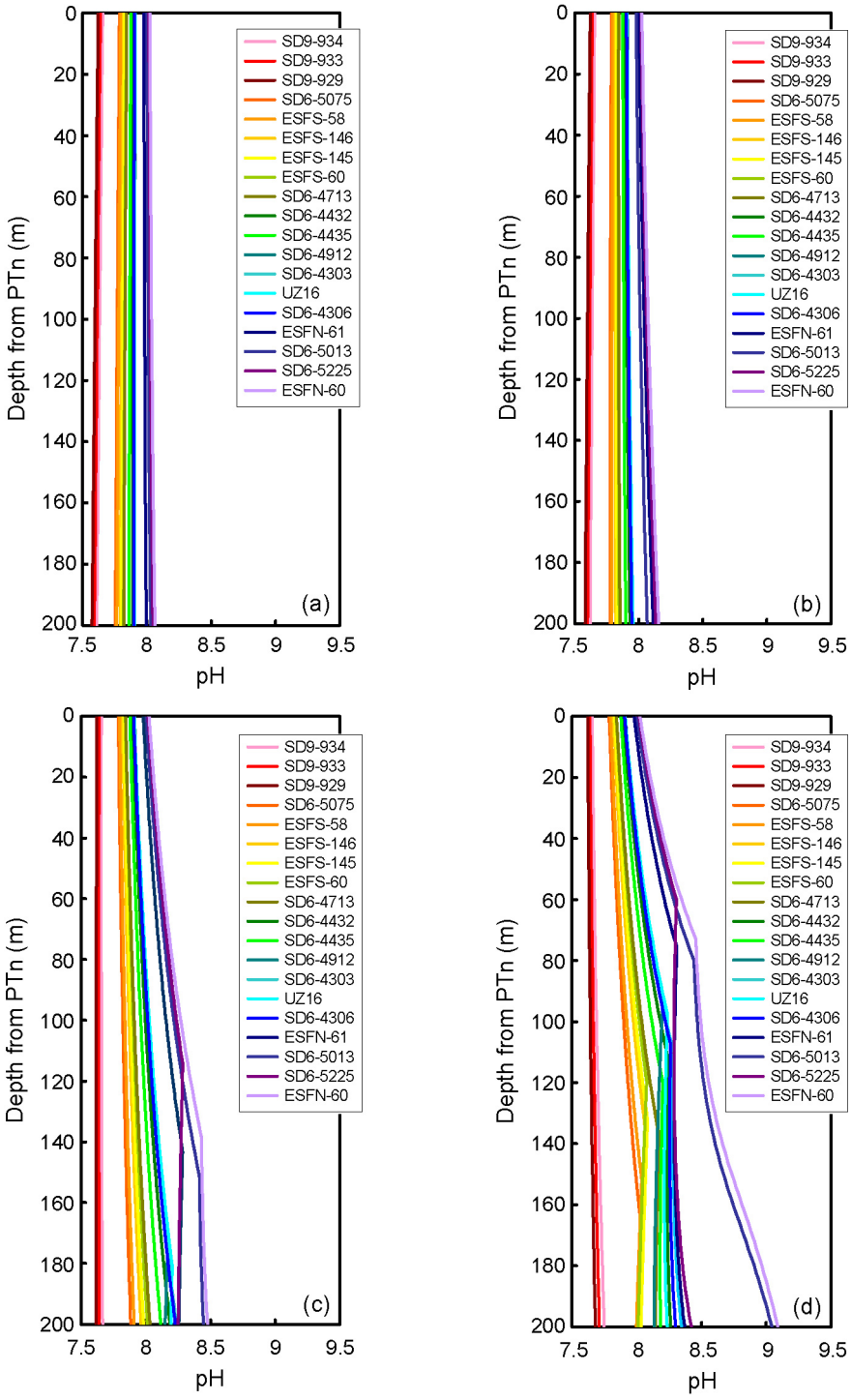

Source: Validation DTN: SN0705PAEBSPCE.014, spreadsheets: *PTn TST runs, avg rate.xls*, *PTn TST runs, max rate.xls*, *PTn TST runs, 5 X mean rate.xls*, and *PTn TST runs, 10 X mean rate.xls*.

Figure 7.1-10. Predicted Change in pH with Depth through a 200-m Section of the TSw: (a) NFC Mean Feldspar Dissolution Rate, (b) NFC Maximum Rate, (c) 5× NFC Mean Rate, (d) 10× NFC Mean Rate

7.1.2.3 Observed Mineral Assemblages

The NFC model assumes pore-water equilibrium with respect to calcite and amorphous silica. This approach is justified in Section 6.3.2.4.1, on the basis of generally observed trends in geothermal fields. The observation of calcite and opal on fracture surfaces throughout the TSw (Paces et al. 2001 [DIRS 156507], p. 7) validates the use of these phases.

Calcite precipitates as water percolates downwards through the TSw under ambient conditions, and has been doing so for millions of years (Paces et al. 2001 [DIRS 156507]). This is probably due to the temperature increase due to the geothermal gradient; the increase in temperature with depth lowers the solubility of calcite. The observation of calcite precipitation provides limits on possible rates of feldspar dissolution. EQ3/6 simulations with the PTn waters in Table 7.1-3, with no feldspar dissolution, predict minor amounts of calcite precipitation (approximately 10 μmoles liter^{-1}; Validation DTN: SN0705PAEBSPCE.014, spreadsheet: *PTn runs, no feldspar dissolved.xls*).

Using the NFC mean feldspar dissolution rate, minor calcite dissolution is predicted: on the average, <10 μmoles liter^{-1} at contact times of 10,000 years, and less at shorter times; calcite precipitation is predicted for a few waters at water–rock contact times of 2,000 years (Validation DTN: SN0705PAEBSPCE.014, spreadsheet *PTn TST runs, avg rate, calcite dissolved.xls*). However, using feldspar dissolution rates of 5× and 10× the mean NFC rate; calcite is predicted to dissolve at rates of approximately 0.1 and 0.5 millimoles liter^{-1}, respectively. Hence, the observation of calcite precipitation under ambient conditions suggests that the NFC mean feldspar dissolution rate might be a maximum value, and that rates of 5× and 10× the mean NFC rate are far too fast to be representative of the ambient case.

At feldspar dissolution rates characteristic of ambient conditions, the NFC model predicts only one secondary aluminosilicate, stellerite ($Ca_2Al_4Si1_4O_{36}$:$14H_2O$). A second phase, celadonite ($KMgAlSi_4O_{10}(OH)_2$) begins to precipitate at slightly higher degrees of feldspar dissolution than are predicted to occur under ambient conditions, and phillipsite ($K_{0.7}Na_{0.7}Ca_{1.1}Al_{3.6}Si1_{2.4}O_{32}$: $12.6H_2O$) is predicted in a few cases, at the highest degrees of feldspar dissolution (Validation DTN: SN0705PAEBSPCE.014, spreadsheets: *PTn TST runs,....xls*).

Zeolites are commonly observed associated with vitric horizons at Yucca Mountain, especially near the water table. These are mostly clinoptilolite and mordenite, although heulandite and chabazite are also found in the zeolitic zones. The NFC model does not predict the formation of clinoptilolite, mordenite, heulandite, or chabazite, but these appear to be dominantly associated with alteration of the vitric zones at Yucca Mountain, and the model domain considered by the NFC model is the devitrified rhyolitic core of the TSw, which contains no glass. Zeolites are much less common in the devitrified TSw rhyolite, but within this zone, stellerite is common in fractures (Bish et al. 2003 [DIRS 169638], p. 1893). It covered over 40% of the fracture surface in borehole core ESF-HD-TEMP-2 (SNL 2007 [DIRS 177414], Table 6.3-30), and has been observed as a significant component tuff in borehole UZ-16, where it comprises on the average 3% of the rock, for an interval of over 100 m (Chipera et al. 1995 [DIRS 111081], p. 16). Concomitant decreases in feldspar suggest that it may have formed at the expense of feldspar by scavenging of Ca out of groundwater. This is the exact reaction predicted by the NFC model.

These common occurrences of stellerite in the devitrified rhyolite offer validation of the dominant reaction predicted by the NFC model.

Celadonite has not been observed at Yucca Mountain. Commonly observed clay minerals at Yucca Mountain include illite and smectite. Illite is chemically and structurally very similar to celadonite. Both are K- and Mg-bearing micas, capable of having varying amounts of (Mg + Al) substituting for (K + Si) in the structure. The predicted occurrence of celadonite as opposed to illite may be a function of the particular fixed compositions present in the *data0.pce* database (Output DTN: SN0703PAEBSPCE.006). Celadonite is defined as ($KMgAlSi_4O_{10}(OH)_2$), and illite, as ($K_{0.6}Mg_{0.25}Al_{1.8}Al_{0.5}Si_{3.5}O_{10}(OH)_2$. Given the potential compositional variation within these minerals, and the fact that they are represented in the *data0.pce* thermodynamic database (Output DTN: SN0703PAEBSPCE.006) as single, compositionally-fixed phases, these two phases can be considered more or less equivalent, both representing, chemically, sinks for Al, K, and Mg in the NFC model.

Smectites are not predicted to form in the NFC model, although they are observed as a common alteration product in the rock. This may be a database limitation; several smectite clays are in the *data0.pce* database (Output DTN: SN0703PAEBSPCE.006), but they are fixed compositions—usually end-member compositions—which may not saturate under conditions when a mixed-phase would. Alternatively, smectites may not be predicted in the NFC model, but still be observed in the rock, because the initial conditions of secondary mineral formation may differ from the modeled conditions. Most of the alteration observed at Yucca Mountain occurred early in the history of the tuff, at elevated temperatures which persisted for at least a few million years (Section 6.12.2.2.1). Under these conditions, any calcite present may have been consumed as feldspar dissolved and Ca-bearing clays and zeolites formed. Saturation with respect to calcite may not have been maintained, and the pore waters may have become very Ca-poor. At the present time, however, ambient conditions have persisted for millions of years, and calcite has precipitated for much of that time, resulting in concentrations in the bulk rock of 0.1% to 0.5% by weight. The thermal period following repository closure will not persist long enough for all the calcite to be consumed, so rather than formation of Ca-poor smectites, K-Na-Ca-bearing zeolites (e.g., phillipsite) will form. Because initial conditions of secondary mineral formation do not match the expected future conditions, the absence of predicted smectite formation does not invalidate the NFC model.

As with the clays, the zeolites have very complex, variable compositions that are represented in the database as a few fixed-composition phases. Phillipsite is represented in the *data0.pce* database (Output DTN: SN0703PAEBSPCE.006) as $K_{0.7}Na_{0.7}Ca_{1.1}Al_{3.6}Si1_{2.4}O_{32}$:$12.6H_2O$. Although it has been observed as a rare mineral associated with altered vitric material at Yucca Mountain (Bish et al. 2003 [DIRS 169638], p. 1893), other zeolites such as clinoptilolite, heulandite, mordenite, and chabazite are more common. These are present in the *data0.pce* database (Output DTN: SN0703PAEBSPCE.006) as, respectively, three separate Ca, Na, and K species (clinoptilolite) plus five additional discrete compositions that include one solid solution phase, a Ca-Na species (mordenite), and an Na-K-Ca species (chabazite). Heulandite is included only as an Sr-Ba-Ca-K-Na species; hence, it could never precipitate in the NFC model, which does not include Sr and Ba. Given the simplicity of the representations in the database, it is most accurate to think of the zeolites in the NFC model as a group, representing mineral sinks for K and Na, once their concentrations build up sufficiently to saturate the solution with respect to the

zeolites. Phillipsite is the solubility-limiting phase that is predicted to form first; if it is suppressed, other Na, K (±Ca) zeolites will form. Hence, phillipsite represents the Na- and K-bearing zeolites as a group, and its predicted occurrence is validated by the general observation of Na-K-Ca-bearing zeolites as secondary minerals at Yucca Mountain. For additional discussion on the causes and effects of the observed mineral precipitates in the NFC model, see Sections 6.2.5 and 6.3.2.6.

7.1.2.4 Summary

In this section, the results of EQ3/6 simulations implementing the major components of the NFC model are compared to the observed changes in ambient water composition as waters percolate through the TSw. Although the comparisons are general because the data sets are limited (i.e., data from the lower part of the TSw is only available from one location) and some of the differences between the PTn waters and the TSw waters may be due to glass dissolution in the PTn, the general trends in pore-water compositions and in gas-phase composition are well captured by the NFC model. The simulations also indicate that the range of feldspar dissolution rates implemented by the NFC model reasonably accounts for the observed chemical trends in the pore water. The limited available data do not tightly constrain the feldspar dissolution rate, and some chemical parameters are consistent with slightly higher feldspar dissolution rates. However, the higher feldspar dissolution rates, 5× and 10× the NFC mean rate, are inconsistent with measured TSw gas phase compositions and pH values. The degree of water–rock reaction is limited under ambient conditions and predicted (and observed) changes in water composition with depth are minor—much less than an order of magnitude.

Because the NFC model captures the observed trends in ambient pore waters, and the modeled and measured results vary by less than an order of magnitude, the comparison with ambient pore-water data validates the general hydrologic and geochemical approach implemented by the NFC model.

Additional corroboration is offered by comparison with observed secondary mineral assemblages in the TSw devitrified rhyolite section. These are broadly consistent with the alteration products predicted by the NFC model and the feldspar dissolution rates used; the importance of reactions involving stellerite is well supported. In addition, the range of possible feldspar dissolution rates is limited by the observation that calcite precipitates in the ambient system. This is inconsistent with feldspar dissolution rates that significantly exceed the NFC mean feldspar rate.

In summary, the major processes in the NFC model qualitatively describe the observed ambient variation in water chemistry, and are consistent with the observed suite of secondary minerals.

7.1.3 NFC Model Comparisons to the THC Seepage Model

As described in Section 6.3.2 of SCI-PRO-006, one method of model validation is comparison of model results to another, independently derived model developed for a similar or comparable intended use. The NFC model calculates the interaction between percolating pore waters and the rock matrix of the TSw in order to bound the time-dependent chemistries of fluids entering the drift. Another model that has been used to model similar processes is the drift-scale thermal-hydrologic-chemical (THC) seepage model (SNL 2007 [DIRS 177404]), which uses the

TOUGHREACT code (TOUGHREACT V3.1.1 [DIRS 180937], STN: 10396-3.1.1-00) to calculate pore-water reaction and transport through the geologic section above and around the drift. In this section, model results from the THC seepage model are compared to results from a similarly parameterized NFC model simulation. The model validation criteria for the NFC/THC model comparison are as follows:

- *Potential seepage water compositions*: Comparisons of the water compositions predicted by each model should agree to within an order of magnitude for each component, or if disagreements exist, they will be explained mechanistically in terms of the processes involved and the significance with respect to the intended use of the model.

- *In-drift pCO_2*: The NFC model should bracket the range predicted by the THC model, and the range should narrow with simulation time as the system cools. Exceptions are possible because the THC seepage model is a 2-D model that neglects axial gas-phase transport in the drift. Inconsistencies identified in these comparisons will be explained mechanistically in terms of the processes involved and the significance with respect to the intended use of the model.

7.1.3.1 General Description of the THC and NFC Conceptual Models

Although both models predict the composition of potential seepage into the repository drifts, they differ significantly in terms of implementation. The THC model estimates multi-phase mass transport by simultaneously solving mass balance, mass action, and kinetic equations affecting all dissolved and gas-phase (in particular CO_2) species. The NFC model differs by predicting dissolved phase transport under bounding CO_2 scenarios. Whereas the THC model relies on a dual-continuum model prediction of fluid flow, the NFC uses an optimized plug-flow approximation. Unlike the NFC model, the THC model attempts to predict how reaction-induced rock porosity might change whole rock permeability. The NFC model uses a field-based feldspar alteration rate and assumes equilibrium with calcite and amorphous silica to predict pore-water evolution. The THC model implements kinetically limited mineral dissolution/precipitation rates, based on laboratory measurements combined with reactive surface areas based on geometric calculations, and reduced by an arbitrary amount to account for the generally slower rates observed in field studies. The NFC model generates time-dependent fluid chemistries at 16 locations in each of seven drifts distributed across the repository footprint, while the THC model uses a grid representing two-dimensional perpendicular slices across a drift at the repository center; a second grid with wider drift spacing simulates repository edge conditions. Neither of the two models actually predicts seepage compositions, but instead samples the composition of waters just behind the dryout front. The THC model samples pore-water compositions at the highest flux zone proximal to the drift crown, incorporating the effects of boiling, evaporation, and condensation. The NFC model focuses primarily on fluid–rock interactions as the pore water percolates through the TSw to the evaporation front around the drift, and does not incorporate boiling and condensation effects. Neither model explicitly considers ion exchange onto clays or zeolites, but both consider these implicitly, as the databases used for both models include many end-member clay and zeolite phases. Finally, neither model explicitly considers gas phase axial transport through the drift; the pCO_2 range predicted by the NFC model captures these effects (Section 6.3.2.8).

7.1.3.2 Source of THC Model Data

The NFC and THC models have been independently derived and are conceptually different, as discussed above. They are also implemented with different software. However, both models use many of the same inputs, to maintain consistency with other UZ thermal-hydrologic models. Both models implement the same thermal loading (Section 4.1.11), initial rock hydrologic properties based on the UZ calibrated properties set (Section 4.1.4.1), rock mineralogies based on the field data, as abstracted in the geologic framework model, and the same starting water compositions. The only major inputs to the NFC model that do not match those used in the THC seepage model are the feldspar dissolution rate and the activation energy (E_a) for feldspar dissolution. In order to do a relevant comparison, between the two models, the NFC model was run using the THC model feldspar dissolution rate and E_a values. These values were extracted from the input file *chemical.inp* for the THC seepage model using the Group 3 (W0) representative pore water, archived in DTN: LB0705DSTHC001.002 [DIRS 180854]. The THC seepage model utilizes two feldspar compositions, one representing the matrix "sanidine" in the TSw, equivalent to the alkali feldspar in the NFC model, and the other representing the trace plagioclase phenocrysts in the TSw. The "sanidine" rate was used in this comparison. The THC model rate is given at 25°C, in units of mol m^{-2} sec^{-1}, and was converted to the proper format for the NFC model (mol L^{-1} sec^{-1}) using the average mineral abundances and specific reactive mineral surface areas for the four repository host units (also from *chemical.inp*), and the water:rock ratio (19.6) used in the NFC model. The resulting rate was then corrected using the Arrhenius equation (Section 6.3.3.2.2) to yield a value at 23.4°C, the NFC model's ambient condition. The THC model feldspar dissolution rate at 23.4°C is 7.85×10^{-15} mol L^{-1} sec^{-1}, about seven times the NFC model's rate of 1.14×10^{-15} mol L^{-1} sec^{-1}. The E_a used by the THC model is 63 kJ mol^{-1}, somewhat higher than the NFC model rate of 49 kJ mol^{-1}. Because of the difference in activation energy, the THC model rate at 96°C (1.19×10^{-12} mol L^{-1} sec^{-1}) is approximately 21 times the 96°C NFC model rate (5.68×10^{-14} mol L^{-1} sec^{-1}). These calculations are documented in Validation DTN: SN0705PAEBSPCE.013 (spreadsheet: *Convert THC feldspar dissolution rate.xls*).

Other necessary inputs from the THC seepage model are the percolation fluxes used. These are listed in Table 7.1-4.

Table 7.1-4. Percolation Fluxes Used in the THC Seepage Model

Time (years)	Flux (mm/yr)
0 to 600	7.96
600 to 2,000	12.89
2,000 to 10,0000	20.45

Source: DTN: LB0704DSTHONLY.001 [DIRS 181164], spreadsheet: *th7_81.xls*.

Because the NFC model parametrically evaluates the evolving thermal field and percolation fluxes, any specific THC seepage model simulation can be used for the model comparison. The chosen data are from a repository-center THC seepage model simulation using the Group 3 representative water, ESF-HD-PERM-3/34.8-35.1/Alcove 5. In the terminology of the THC model, this is water "W0." The abstracted water compositions for this THC simulation are

archived in DTN: LB0705DSTHC001.001 [DIRS 181217] (spreadsheet: *frac_81_162_w0.xls*; in-drift CO_2 concentrations are in spreadsheet *frac_81_162_dr_w0.xls*).

7.1.3.3 Generating and Extracting NFC Model Results Using the THC Feldspar Dissolution Rate

In order to corroborate the PC&E model output with the THC model output, it is necessary that the data from each represent comparable thermal histories. To do this, the thermal measure (TM) (Section 6.15.1) for the THC simulation was calculated, by summing the drift wall boiling duration and the maximum drift wall temperature (data from DTN: LB0704DSTHONLY.001 [DIRS 181164], spreadsheet: *th7_81.xls*):

$$TM = (1268.9 \text{ years}) + (141.4 \text{ C}) = 1410.3 \qquad \text{(Eq. 7.1-12)}$$

Generating NFC data to compare to the THC results requires re-running only one part of the NFC model, the calculation of the WRIP value, which is summarized in Section 6.3.4. The nearest corresponding thermal measure in the WRIP lookup table (Output DTN: SN0703PAEBSPCE.006, spreadsheet: *WRIP lookup table.xls*) is 1412.1, a value generated using the 10th percentile thermal conductivity values. To generate WRIP values for the thermal history of interest using the THC feldspar data, the Mathcad file used to generate the 10th percentile NFC model results for TSPA was modified to use the THC model rate and E_a, and the file was rerun, to generate a new WRIP map for the TM = 1412.1 case. The same thermal field data files used in the 10th percentile thermal conductivity NFC model simulations for TSPA (*Drift 1.xls* to *Drift 7.xls*) were used. The original NFC model files are archived in Output DTN: SN0703PAEBSPCE.006; the simulations implementing the THC model feldspar are archived in Validation DTN: SN0705PAEBSPCE.013 (folder: \thermal-K, 10th percentile, THC rate). The WRIP map generated using the THC model feldspar data, and corresponding to the TM of 1412.1, is in spreadsheet *Water-rock interactions, 10th percentile, THC diss rate and Ea.xls*. It contains WRIP values for each of the 20 different percolation flux sets (Section 6.3.3.2.4), for 102 seepage times, from 50 years (repository closure) to 1 million years. This data was copied into spreadsheet *WRIP_Temp_values.xls* to facilitate cross referencing the THC model infiltration history (Table 7.1-4) with the PC&E WRIP values (Table 6.3-5). Using the "trend" function in Excel, WRIP values were calculated through time by interpolation between percolation flux sets as a function of the THC infiltration values.

The temperature at each time step was taken directly from the THC model output file *th7_81.xls*, (tab: "fractures-TH") The temperature used was the average of the drift crown and drift side temperatures. The time-WRIP value-temperature data are calculated in spreadsheet *WRIP_Temp_values.xls* and copied into *THC_GRP3_profiles_new_rate.xls* for the comparison; both are archived in Validation DTN: SN0705PAEBSPCE.013.

Using this information, predicted pore-water compositions were extracted from the EQ6 "seepage" output files for Group 3, archived in Output DTN: SN0701PAEBSPCE.002. This was done by extracting the water compositions at the temperature of interest from the output files with the bounding WRIP values (WRIP designations 0, B, C….I, J, L; see Table 6.3-5) and interpolating between the compositions using the WRIP value calculated using the THC feldspar

data. This procedure is documented in *THC_GRP3_profiles_new_rate.xls*. The end result of this calculation is a table of seepage compositions as a function of time.

The NFC model uncertainty in the WRIP values was also incorporated by modifying the WRIP values using the maximum and minimum multipliers as described in Section 6.12.2.2.5 and recalculating the pore-water compositions using the resulting maximum and minimum WRIP values as described above.

The in-drift pCO_2 range through time is calculated in the same manner as done by TSPA, as described in Section 6.15.1, except that the water vapor concentration in the drift at any given time step is taken directly from the THC model output (DTN: LB0704DSTHONLY.001 [DIRS 181164], spreadsheet: *th7_81.xls*).

7.1.3.4 Results of the NFC/THC Comparison

The results of the comparison are shown in Figure 7.1-11. Because the NFC model does not model dilution and evaporation, all parameter values in Figure 7.1-11 have been normalized to Cl. This is valid because dilution and evaporation of potential seepage waters has no effect on the predicted composition of evaporated seepage in the drift, the final concentration of which is a function of the in-drift RH. At any given point in time in the figure, a range of compositions is shown for the THC data, representing the six highest-flux nodes within 45 degrees of vertical in the model grid above the drift, locations likely to represent possible crown seepage into the drift. Figure 7.1-11 shows THC model-predicted potential seepage water chemistries—pH, Na/Cl, K/Cl, and Ca/Cl—for the repository-center location, using "W0," the Group 3 representative pore water. Also shown are the compositional profiles predicted by the NFC model, using WRIP values estimated with the same feldspar dissolution rate and activation energy used by the THC seepage model. The NFC model incorporates an uncertainty range on the WRIP value, which is sampled by TSPA. The results shown here are for the mean, maximum, and minimum WRIP values at each time step, defining the uncertainty range. NFC model results are not predicted if the WRIP value exceeds the maximum amount evaluated by the NFC model. This is not a conceptual limitation, but rather an implementation limitation—the WRIP value falls outside of the range of the eleven discrete WRIP values used to generate seepage water compositions for the TSPA baseline case, and extrapolating water chemistries based on the WRIP value is not valid. Because this only affects the curve representing the maximum limit of the NFC model WRIP range, the effect on the model validation comparison is negligible.

Mean predicted Na and K profiles of both the THC and NFC model outputs are similar, and generally within 50% of each other throughout each simulation. Na/Cl and K/Cl profiles (and to a lesser extent, pH) largely result from temperature-dependent feldspar alteration. The general agreement points to the importance of feldspar dissolution to the geochemical evolution predicted by both the THC and NFC models. Feldspar dissolution affects the pH by raising solution alkalinity, and the resulting increased bicarbonate concentrations depress Ca, and thus Ca/Cl, by limiting calcite solubility. Predicted pHs diverge during the boiling period, but are within 0.4 units of each other in the critical post-drift wall boiling period; recall that seepage does not occur until boiling ceases at the drift wall (~1,300 years for the repository-center location considered here). Ca levels are affected by calcite equilibria, pH, and equilibria with Ca-bearing silicate phases, which also control predicted CO_2 levels in the NFC model. Although

general trends in predicted Ca/Cl levels are the same between the two models over the whole time span, the otherwise close agreement does not exist between approximately 400 and 4,000 years. However, the uncertainty bands in the NFC model results do capture the THC model results, with the exception of the time interval over which the WRIP values exceed the maximum used in the TSPA baseline, and water compositions are not predicted.

NFC model-predicted Si/Cl values are a factor of three to eight times higher than those predicted by the THC model (Validation DTN: SN0705PAEBSPCE.013, spreadsheet *THC_GRP3_profiles_new_rate.xls*), possibly reflecting kinetic limitations on the dissolution rates of amorphous silica and other silica polymorphs in the THC seepage model; both models use the same thermodynamic data for SiO_2(am). Note that the pH, buffering capacity, and potential corrosivity of seepage are relatively insensitive to dissolved SiO_2(aq) levels.

To compare the pCO_2 data from the NFC model with that from the THC seepage model, equivalent data in terms of spatial location and thermal history must be extracted from their respective outputs. The P&CE model provides maximum and minimum values of in-drift pCO_2 though time, while the THC seepage model provides a single time history the in-drift pCO_2.

The minimum and maximum pCO_2 values through time were calculated in the spreadsheet *pCO2_drift_calc.xls* (Validation DTN: SN0705PAEBSPCE.013) by following the TSPA implementation outlined in Section 6.15.1. The air mass fraction and pressure data at the crown provided in the THC model output file *th7_81.xls* (DTN: LB0704DSTHONLY.001 [DIRS 181164]) were used to calculate T_{EF}. This value was used to query the *PCE_pCO2_max_Gp3.xls* lookup table (Output DTN: SN0701PAEBSPCE.002) for the maximum pCO_2 as a function of temperature, using the previously calculated WRIP value to interpolate between columns. In a similar manner, the total C was interpolated from the values in the lookup table in spreadsheet *Gp3_C_total.xls* (Output DTN: SN0701PAEBSPCE.002), and the minimum pCO_2 was calculated from Equation 6.15-5.

The resulting NFC model time histories are compared to the THC model predictions for pCO_2 from spreadsheet *frac_81_162_dr_w0.xls* (DTN: LB0705DSTHC001.001 [DIRS 181217]) in Figure 7.1-12. Examination of Figure 7.1-12 reveals that the NFC model's pCO_2 range captures the THC model results for most for the first 1,200 years. The results for the period from 50 to 100 years do not match, but this is in part because only 50- and 100-year data points were calculated for the NFC model. Over the 50 to 100-year time interval, the THC model predicts pCO_2 values that are lower than the amount of CO_2 which would be released by the boiling pore water. Once the drift wall drops below boiling, after 1,200 years, the THC model predicts a rapid rise in pCO_2 exceeding the maximum range of the NFC model for several thousands of years. At longer times, both models eventually converge back to their starting values, although this is somewhat above 10^{-3} bars for the THC seepage model. The discrepancies between the two models may be due to the two-dimensional nature of the THC model. In the THC model, water vapor displaces most of the non-condensable gases in the drift during the initial boiling period, resulting in very low partial pressures of CO_2; in a three-dimensional model, axial transport and condensation of water vapor in the cooler parts of the drift result in lower RH values in the drift, and less displacement of non-condensable gases (SNL 2007 [DIRS 181383], Section 7.8[a]). After the boiling period in the THC model, CO_2 cycles back into the rock in the gas phase, where it is absorbed by pore water, lowering the pH (Figure 7.1-11) and causing

calcite dissolution and release of more CO_2. In a three-dimensional drift, condensation of cooler water at the drift ends will provide a sink for the CO_2, limiting buildup.

It is notable that the THC model CO_2 predictions show similar behavior to the NFC model minimum pCO_2 values during the boiling period, and transition to showing similar behavior to the NFC model maximum pCO_2 values at longer times. This is interpreted to indicate that, for the THC seepage model, the composition of the gas phase is controlled dominantly by the boiling process during the boiling period, and by equilibrium with the fluid phase in the rock after the boiling period. Because of the effect of axial transport on the gas phase composition is poorly constrained, the NFC model uses these cases as end-members, and does not attempt to refine predicted in-drift CO_2 concentrations further.

7.1.3.5 Summary

The general similarity in THC and NFC model predictions for the validation case shown here provides confidence that both models capture the primary processes critical to the chemistry of seepage. It is clear that feldspar dissolution is the dominant control on water chemistry. The suite of secondary aluminosilicates predicted to form in each model differs, in part because of use of different thermodynamic data. However, both suites apparently capture the general behavior of the alteration minerals as sinks for Al, Ca, and, at higher amounts of feldspar dissolution, K and Na (Section 7.1.2.2). Because the NFC model ultimately relies on a field-calibrated feldspar dissolution rate that is lower than that used by the THC model, it will always predict less reaction with the host rock. Uncertainty in this important parameter is explicitly implemented in the NFC model. However, when both models are run using comparable inputs, predicted trends in seepage water chemistry are similar. The NFC model pCO_2 range does not capture the pCO_2 trend predicted by the THC model, possibly because the THC is a 2-D model that lacks axial gas transport.

THC model predictions of individual component concentrations are within an order of magnitude of the NFC model's range of values; in most cases, the NFC model's uncertainty bands bracket the THC model results. The NFC model's predicted pCO_2 range does not bracket the THC model's predictions; however, the THC seepage model results may be an artifact of the two-dimensional nature of that model. Because the NFC model meets the validation criteria with respect to this model–model comparison, except for the pCO_2 results, which can be mechanistically explained, the results provide corroboration of the NFC seepage model approach and predictive capability.

Reaction-transport modeling remains the focus of abundant scientific enquiry and debate, re-emphasizing the bounding nature of both the NFC and THC models. Two obvious technical obstacles to more accurate predictions of fluid–rock interaction are the field-relevant parameterization of reactive surface areas and the linking of porosity changes to permeability evolution. There presently exists no scientific consensus on either. Despite these and other technical challenges, the general similarity in THC and NFC model predictions provides confidence that the primary processes critical to the chemistry of seepage at Yucca Mountain are being captured.

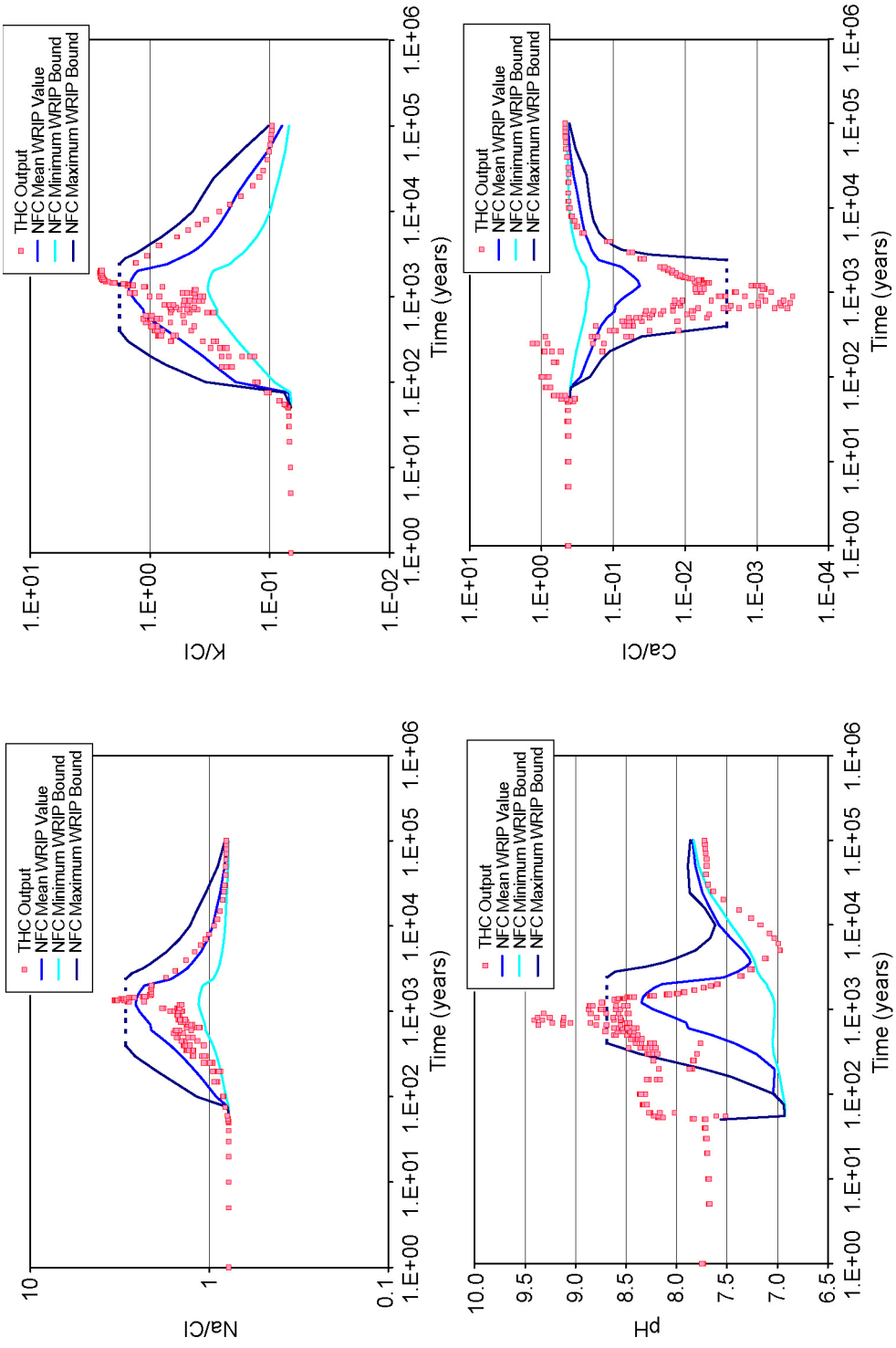

Source: Validation DTN: SN0705PAEBSPCE.013, spreadsheet: *THC_GRP3_profiles_new_rate.xls*.

NOTE: THC data are from the six highest-flux nodes above the drift. The NFC model incorporates an uncertainty range on the WRIP value; the NFC results shown here are for the mean, maximum, and minimum WRIP values at each time step. The NFC results are not predicted if the WRIP value exceeds the maximum amount evaluated by the NFC model, indicated by the dashed horizontal lines

Figure 7.1-11. Comparison of Potential Seepage Water Compositions Predicted by the THC and NFC Models for the Group 3 Represent ative Water

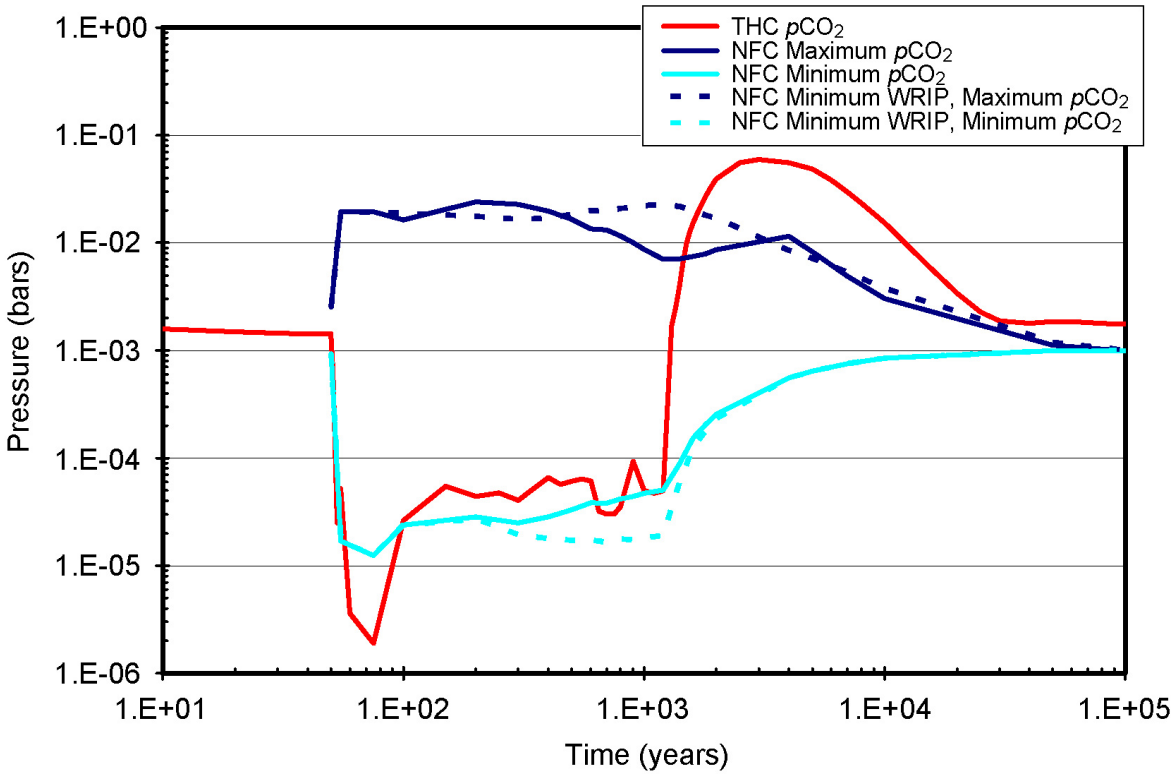

Source: Validation DTN: SN0705PAEBSPCE.013, spreadsheet: *pCO2_drift_calc.xls*.

NOTE: The NFC model range does not entirely bound the THC seepage model range.

Figure 7.1-12. Comparison of In-Drift CO_2 Partial Pressures Predicted by the NFC and THC Seepage Models

7.1.4 Comparison to Drift Scale Test Pore-Water and Gas-Phase Data

The DST was carried out in the Exploratory Studies Facility (ESF) at Yucca Mountain, Nevada. It was a large-scale test to evaluate the coupled thermal, hydrologic, chemical, and mechanical processes that take place in unsaturated fractured tuff over a range of temperatures (approximately 25°C to 200°C). The DST consisted of a 50-m-long drift, 5 m in diameter, with nine heaters placed axially in the drift to simulate water packages. Secondary heaters were placed in boreholes extending outward from the drift, to simulate the effects of adjacent drifts. The DST heaters were activated on December 3, 1997, and switched off on January 14, 2002, and since that time the test area has been slowly cooling. Water and gas samples were collected from packed borehole intervals surrounding the drift. Water samples were collected from June 1998 to January 2002; gas samples from February 1998 to November 2005. Details regarding the DST layout, borehole orientations, operation of the test, and measurements performed (as well as their uncertainties) are discussed in Section 6.3 of *Thermal Testing Measurements Report* (SNL 2007 [DIRS 177414]). Information on these aspects of the DST is not repeated in this report unless directly related to the geochemical data collected and used for model validation.

In this section, measured data from the DST are compared to results predicted by the NFC model. The model validation criteria for the NFC/DST data comparison are as follows:

- *In-drift pCO_2*: The NFC model should bracket the range observed in the DST data, and the predicted range should narrow as the system cools. Inconsistencies identified in these comparisons will be explained mechanistically in terms of the processes involved and the significance with respect to the intended use of the model.

- *Potential seepage water compositions*: An evaluation of the DST borehole waters is presented below. However, in variance to the TWP (SNL 2007 [DIRS 179287], Section 2.2.3), comparisons of the NFC model and measured water compositions are not carried out, as the NFC model does not model the processes of dilution and evaporation, which are the dominant processes affecting DST borehole water compositions.

7.1.4.1 Drift Scale Test Data

Four types of data from the DST were used in this analysis. These are (1) gas phase CO_2 concentrations, (2) borehole water samples, (3) borehole and drift wall temperature data, and (4) mineralogical data. These data were from packed-off borehole intervals around the heated drift, and, for the CO_2 data, from the drift itself. The sources of these data are shown in Table 7.1-5.

Borehole intervals sampled for water and gas samples are shown in Figure 7.1-13. Additional gas samples were taken from the observation drift, which did not significantly heat, and from the heated drift itself, after the boiling period. The water and gas sampling and analysis procedures are described in *Thermal Testing Measurements Report* (SNL 2007 ([DIRS 177414], Section 6.3.4). A summary is provided for each below.

CO_2 Concentrations—CO_2 samples were collected from February 8, 1998, to November 29, 2005. Samples collected at temperatures below 50°C were collected using a diaphragm pump with a moisture trap. For samples collected at temperatures above 50°C, a 4°C chiller was place in front of the pump. Following collection, samples were analyzed by two different instruments over different time intervals. Measured CO_2 concentrations in samples collected prior to January 2001 are approximately 16% low, if they exceed 0.2 volume% (v%) CO_2 (SNL 2007 [DIRS 177414], Section 6.3.4.2.2). Initial gas phase CO_2 data used in this study is summarized in Validation DTN: SN0705PAEBSPCE.014 (spreadsheet: *DST pCO2 comparison.xls*, tab: "Raw data"). Temperatures associated with each sample represent the temperature at the physically higher end of the borehole interval sampled.

Borehole Water Compositions—Borehole water compositions were collected from June 4, 1998, to January 9, 2002. Each sample was collected from the physically lower end of each interval sampled. As described in *Thermal Testing Measurements Report* (SNL 2007 [DIRS 177414], Sections 6.3.4.1 and 6.3.4.5), some samples were affected by interactions with introduced materials—specifically, degradation of the fluoroelastomer and chloroelastomer packers. The determination if a water sample was "affected," "not affected," or "possibly

affected" by interactions with introduced materials is listed in *Thermal Testing Measurements Report* (SNL 2007 [DIRS 177414], Table 6.3-32). All waters were considered here.

Table 7.1-5. Sources of Data from the Drift Scale Test

Data Type	Source
Borehole water sample compositions	Summarized in SNL 2007 [DIRS 177414], Table 6.3-25 DTN: LL020709923142.023 [DIRS 161677]
Gas phase CO_2 pressures in the drift and in boreholes	Summarized in SNL 2007 [DIRS 177414], Table 6.3-28 DTNs: LB980420123142.005 [DIRS 111471], LB980715123142.003 [DIRS 111472], LB0404ISODSTHP.003 [DIRS 169254], LB990630123142.003 [DIRS 111476], LB000121123142.003 [DIRS 146451], LB000718123142.003 [DIRS 158342], LB0011CO2DST08.001 [DIRS 153460], LB0102CO2DST98.001 [DIRS 159306], LB0108CO2DST05.001 [DIRS 156888], LB0203CO2DSTEH.001 [DIRS 158349], LB0206C14DSTEH.001 [DIRS 159303], LB0303ISODSTCP.001 [DIRS 177538], LB0309ISODSTCP.001 [DIRS 177539], LB0403ISODSTCP.001 [DIRS 177540], LB0410ISODSTCP.001 [DIRS 177541], LB0509ISODSTCP.001 [DIRS 177542].
Borehole and in-drift temperature data	DTNs: MO9807DSTSET01.000 [DIRS 113644], MO9810DSTSET02.000 [DIRS 113662], MO9906DSTSET03.000 [DIRS 113673], MO0001SEPDSTPC.000 [DIRS 153836], MO0007SEPDSTPC.001 [DIRS 153707], MO0012SEPDSTPC.002 [DIRS 153708], MO0107SEPDSTPC.003 [DIRS 158321], MO0202SEPDSTTV.001 [DIRS 158320], MO0208SEPDSTTD.001 [DIRS 161767], MO0303SEPDSTTM.000 [DIRS 165698], MO0307SEPDST31.000 [DIRS 165699], MO0403SEPDST32.000 [DIRS 177813], MO0408SEPDSTTD.000 [DIRS 177814], MO0509SEPDSTTD.000 [DIRS 177815], MO0603SEPDSTTD.000 [DIRS 177816]
Mineralogical changes in rock around the DST	Summarized in SNL 2007 [DIRS 177414], Table 4-3 DTN: LA0201SL831225.001 [DIRS 158426]

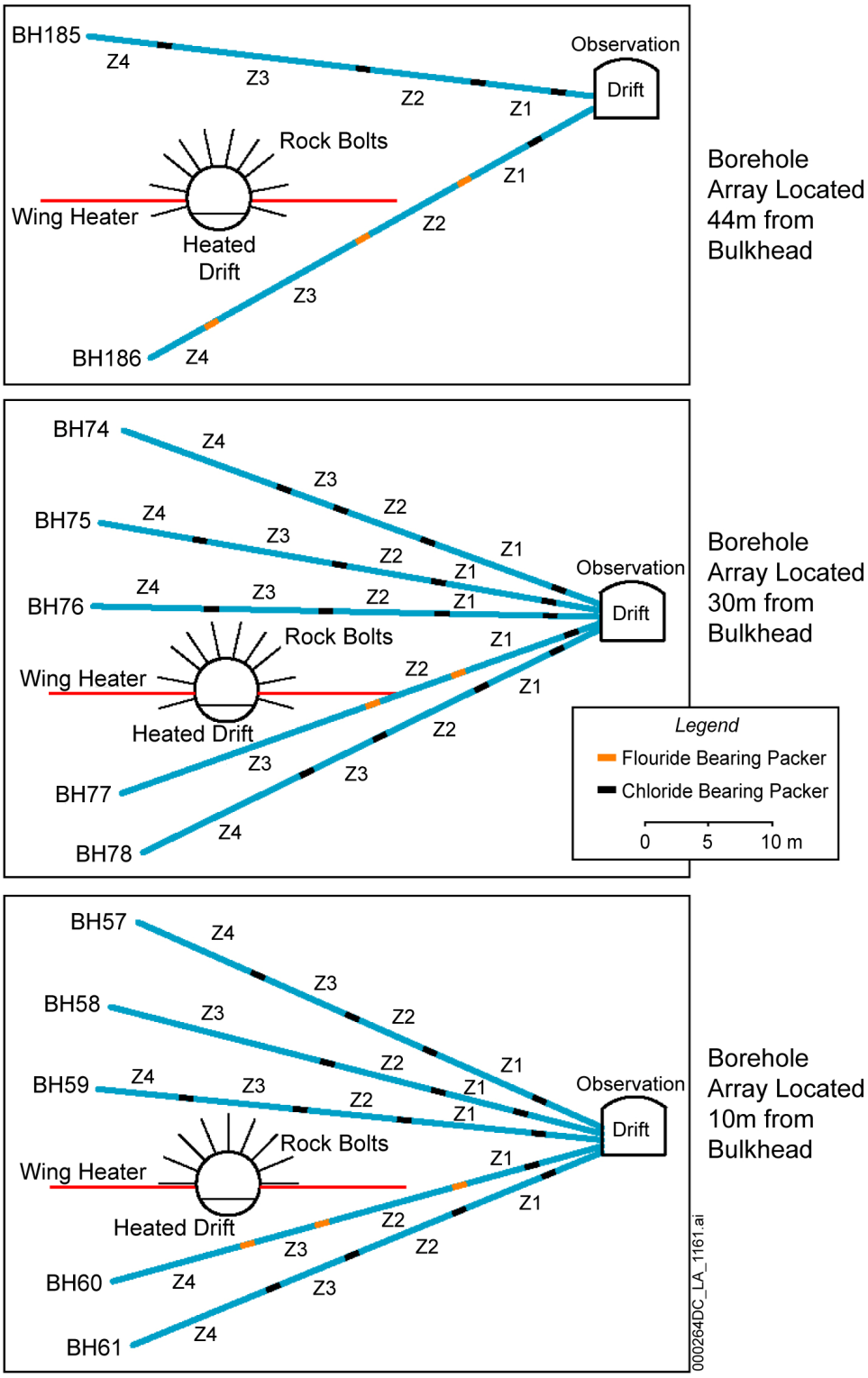

Source: SNL 2007 [DIRS 177414], Figure 6.3-44.

NOTE: Y-distance is the distance from the bulkhead.

Figure 7.1-13. Location of Boreholes and Gas and Water Sampling Zones around the Drift Scale Test

7.1.4.2 Drift Scale Test Gas-Phase CO_2 Comparison

Prior to evaluating the DST gas phase CO_2 data, the raw data have to be processed. Two different corrections were made to the data, as documented in Validation DTN: SN0705PAEBSPCE.014 (spreadsheet *DST pCO2 comparison.xls*). First, measured concentrations with values above 0.2 v% collected prior to January 2001 were corrected for the 16% measurement error. The second, most important adjustment required correcting for the water vapor that condensed out of the gas sample, either into the vapor trap on the diaphragm pump (assumed to be at 25°C), or into the 4°C chiller. At near-boiling conditions, this correction can be an order of magnitude or larger, because the gas phase consists largely of steam; removing the water vapor by condensation results in proportionally larger CO_2 concentrations in the remaining gas sample. This calculation was done by assuming that the gas sample was saturated at the temperature of collection, and using data from the NBS steam tables (Haar et al. 1984 [DIRS 105175]) to determine how much water vapor would condense out of the gas sample upon cooling. Also, the amount of CO_2 that partitioned into the condensed water was calculated and added back in. This was accomplished by performing EQ3 simulations with dilute water at pCO_2 values of 10^{-1}, 10^{-2}, 10^{-3}, 10^{-4}, and 10^{-5} bars, and 4°C and 25°C, to determine the CO_2 partitioning between the vapor and liquid phases, and interpolating between the results using the measured CO_2 concentrations. The result was then added back into the total before calculating the *in situ* CO_2 concentrations. This had only a minor effect on the final value. Only samples collected at below-boiling temperatures were considered, because correcting for these effects for samples collected at above-boiling temperatures is too sensitive to the exact temperature used in the correction.

An additional uncertainty that was evaluated was that due to the temperature differential along the interval from which the gas sample was collected. For a 5- to 10-m sampling interval, this could be tens of degrees, and in some cases, packers failed, so the borehole length actually being sampled was two or in some cases three times the length of a single interval. For any given sample, the temperature difference from one end of the sampled interval to the other had a significant effect on the correction for the amount of water vapor in the gas sample. However, the overall range of observed pCO_2 values was not significantly different (Validation DTN: SN0705PAEBSPCE.014, spreadsheet: *DST pCO2 comparison.xls*, tab: "Evaluate temp across zone"), and this effect can be ignored with respect to the analysis that follows.

Corrected gas-phase CO_2 concentrations are shown in Figure 7.1-14 (a). Three different pCO_2 data sets—borehole, in-drift, and observation drift—are shown. The borehole pCO_2 data were collected from the borehole intervals shown in Figure 7.1-13. One data set, from borehole BH-185 is plotted separately; this borehole has consistently higher pCO_2 values than the other boreholes. These values presumably represent pCO_2 levels in equilibrium with pore waters in the rock, although the degree of connection with the drift is not known. The in-drift pCO_2 data shown were collected only after the drift wall cooled back below boiling. The observation drift was open to the atmosphere, and did not significantly heat up during the test; measured pCO_2 values average $10^{-3.42}$, essentially identical to the current atmospheric levels. A time-temperature profile from an approximate drift-center location on the drift wall is shown in Figure 7.1-14(b). Heating was initiated in December 1997 and ceased in January 2002, after which the drift cooled rapidly. As the drift and the surrounding rock cooled, the range of observed pCO_2 data narrowed.

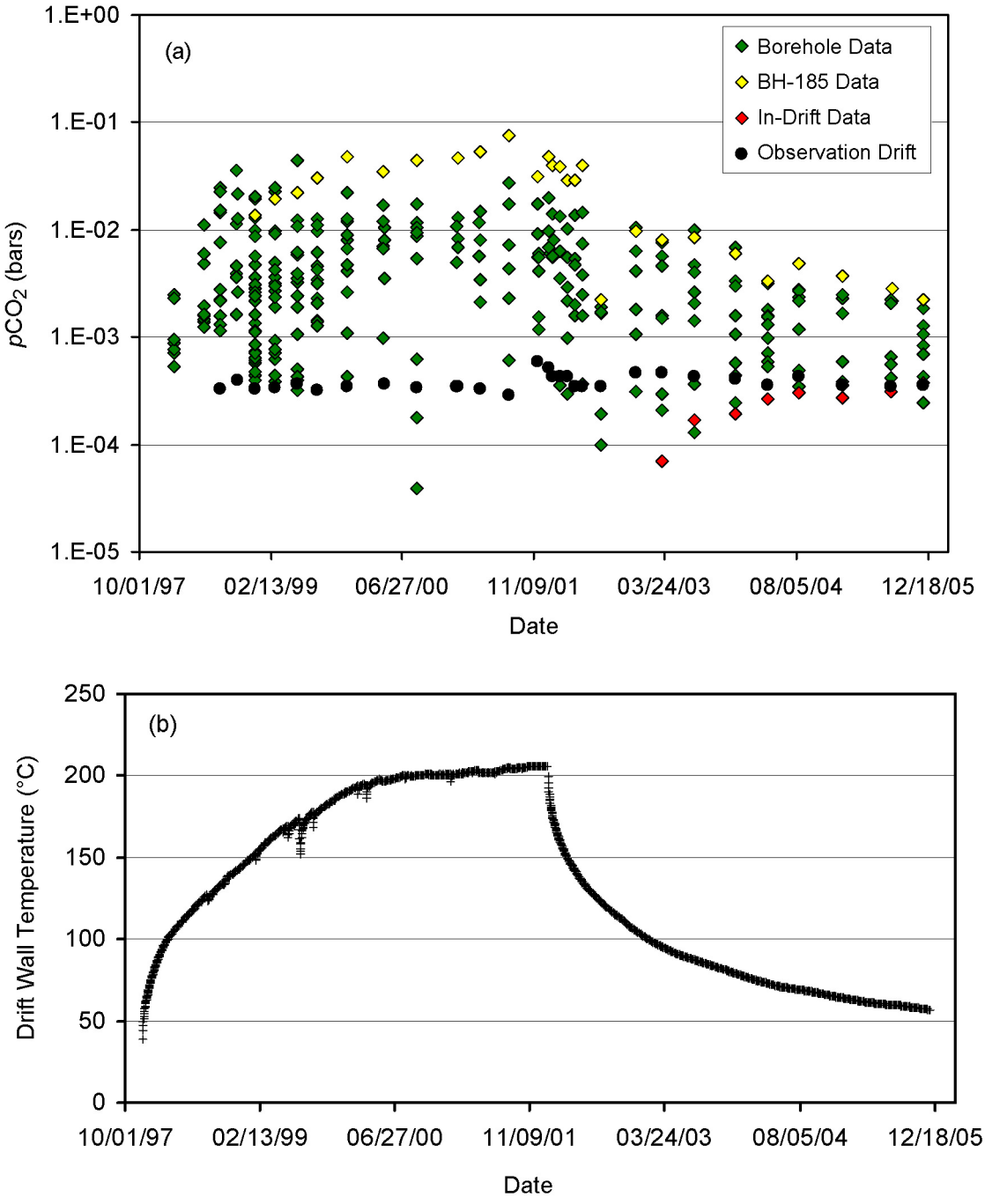

Source: Validation DTN: SN0705PAEBSPCE.014, spreadsheet: *DST pCO2 comparison.xls*, tabs: "Compare to NFC" and "Drift temperature data."

NOTE: As expected, the range of borehole and in-drift pCO_2 values narrows as drift wall temperature drop after the heaters were turned off in January, 2002.

Figure 7.1-14. (a) Measured Gas-Phase CO_2 Concentrations in and around the DST; (b) Drift Wall Temperatures, Approximate Drift Center Location

The NFC model predicts a range of pCO_2 values as a function of (1) the starting water, (2) the amount of feldspar dissolution, and (3) the temperature at the dryout front (either 96°C, or the drift wall temperature). The maximum value of that range is predicted on the basis of equilibrium with the predicted pore-water compositions at the temperature at the dryout front. The minimum value assumes that the in-drift atmosphere is a mixture of air with the ambient repository-level pCO_2 (10^{-3} bars), and steam generated by evaporation of the pore water at the dryout front, which releases CO_2 as it evaporates (Section 6.3.3.2.9). With respect to the DST, at any given time, the predicted NFC maximum value should bound the upper range of the observed data, which represents equilibrium with the local pore water; the predicted NFC minimum value should bound the lower range of the observed data.

Two possible choices for the starting water were considered, the Group 3 and Group 4 representative waters, both of which were collected from the HD-PERM boreholes in Alcove 5, near the site of the DST. Both yielded virtually identical results (Validation DTN: SN0705PAEBSPCE.014, spreadsheet: *DST pCO2 comparison.xls*, tab: "Compare to NFC"), so in the following discussion and figures, only the results using the Group 4 water are presented.

The TSPA process described in Section 6.15 for calculating the minimum and maximum pCO_2 values was used to calculate the NFC predictions for this comparison. This requires using the Group 4 P&CE lookup tables for pCO_2-max and $[C]_{total}$ (*Gp4_C_total.xls* and *PCE_pCO2_max_Gp4.xls*), which are archived in Output DTN: SN0701PAEBSPCE.002. Data in the lookup tables are provided as a function of temperature and WRIP value from "0" (no feldspar added) to "b," "c," "d,"…"j," "l," with "l" being the maximum amount of feldspar added. To determine the appropriate WRIP value, the potential amount of feldspar dissolution must be evaluated. Feldspar dissolution rates are quite slow; a maximum bound on the amount of feldspar dissolved was calculated by assuming 8 years of water–rock contact (the total gas sampling interval) at 96°C (the maximum temperature at the dryout front), and applying the feldspar dissolution rate derived in Section 6.3.3.2.2. This calculation is archived in Validation DTN: SN0705PAEBSPCE.014 (spreadsheet: *DST pCO2 comparison.xls*, tab: "Predicted max feld. dissolved"). Even using these maximum values, the calculated amount of feldspar dissolved is only about one-fifth of the amount used in the EQ3/6 simulations representing the WRIP value "b," and the "b" data differ only very slightly from the "0" data. Hence, for this comparison, the "0" WRIP value data in the pCO_2-max and $[C]_{total}$ lookup tables were used.

The final information used to calculate the pCO_2 range is the drift wall temperature. The data used are shown in Figure 7.1-14(b), and are from a single sensor, ESF-HD-SURF-TC-19, located approximately at the center of the 50-m heated drift. These data were extracted from the DTNs listed in Table 7.1-5, and are archived in Validation DTN: SN0705PAEBSPCE.014 (spreadsheet: *DST pCO2 comparison.xls*, tab: "Drift temperature data").

To calculate the NFC model-predicted pCO_2 values, the WRIP value "0" columns in the two P&CE lookup tables in spreadsheets *PCE_pCO2_max_Gp4.xls* and *Gp4_C_total.xls* (Output DTN: SN0701PAEBSPCE.002) are queried at each time step using the drift wall temperature, or 96°C if the drift wall temperature exceeds boiling. The pCO_2 maximum values are provided directly from *PCE_pCO2_max_Gp4.xls*. The minimum pCO_2 value is calculated using the

$[C]_{total}$ value from *Gp4_C_total.xls* and the ambient pCO_2 at the repository level, assumed to be 10^{-3} bars, as described in Section 6.15.1.

The results of this calculation are shown in Figure 7.1-15(a). The NFC maximum pCO_2 curve captures nearly all of the data, with two exceptions. Several points early in the heating history exceed the predicted values, and the data from one borehole towards the end of the heated drift, BH-185, are consistently higher than the other data, and are outside of the predicted range. It is not clear why this one location yields higher values than all others; however, three different ground support systems were tested in the DST, and over this end of the drift, a cast-in-place concrete liner, 20 cm thick, was used as ground support (CRWMS M&O 1998 [DIRS 111115], Section 3.4). The presence of the liner may have affected gas-phase transport or otherwise perturbed the system. The NFC model's minimum curve captures the variation during the boiling period; it appears to under-predict the data, but it must be remembered that samples collected at temperatures above boiling, which would have had the largest degree of dilution and the lowest pCO_2 values, are not included in this analysis. However, after the boiling period, the NFC minimum curve does not capture the spread of the data; the lower bound converges too rapidly back to the ambient value of 10^{-3} bars.

One likely explanation for this is that the air that moved back into the system as it cooled and water vapor condensed out of the gas phase was not representative of the gas phase in the host rock, but rather represented atmospheric air, that was drawn around the bulkhead. Current atmospheric pCO_2 values are about $10^{-3.42}$ bar, as opposed to the 10^{-3} bar observed in the gas phase in the host rock. In Figure 7.1-15(b), the NFC range is recalculated assuming that the non-condensable gas phase moving back into the drift has a pCO_2 of $10^{-3.42}$ bar, and the behavior of the data, especially the in-drift data after the drift wall boiling period, is very well captured. Note that the upper bound does not change, as it is not sensitive to the assumed pCO_2 in the non-condensable fraction of the gas phase. The model predictions in Figure 7.1-15(b) constrain the data very well, especially after the boiling period, and offer validation for the in-drift pCO_2 range implemented by the NFC model. Note that this does not suggest that a pCO_2 of $10^{-3.4}$ bar would be more appropriate than 10^{-3} bar for use in the NFC model; DST heating was terminated abruptly, resulting in rapid cooling and condensation of water vapor, and requiring relatively rapid air flow into the system to maintain atmospheric pressure. Thus, atmosphere from the ventilated drift was drawn through the rock around the bulkhead. These conditions do not apply to the repository itself, which will cool slowly and, after closure, will be isolated from the atmosphere.

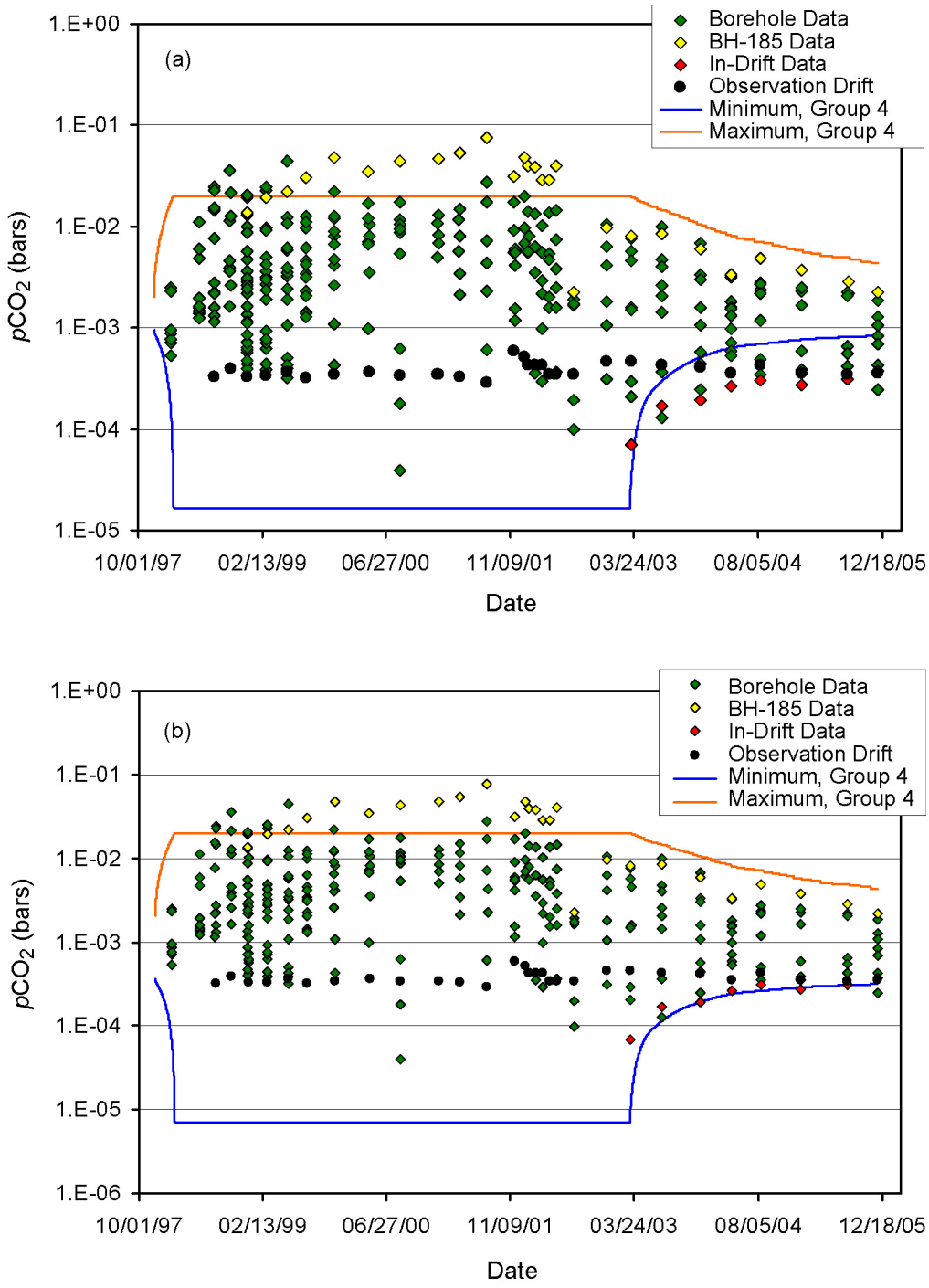

Source: Validation DTN: SN0705PAEBSPCE.014, spreadsheet: *DST pCO2 comparison.xls,* tab: "Compare to NFC."

Figure 7.1-15. Comparison of Predicted NFC pCO_2 Range and Measured Gas-Phase CO_2 Concentrations in and around the DST: (a) NFC Model Range Calculated Assuming Ambient $pCO_2 = 10^{-3}$ bar, the Repository-Level Value in the Rock; (b) NFC Model Range Calculated Assuming Ambient $pCO_2 = 10^{-3.42}$ bar, the Current Atmospheric Value

7.1.4.3 Drift Scale Test Borehole Waters

Borehole water samples were collected over the heating phase of the DST, from the borehole intervals shown in Figure 7.1-13. The pore-water samples were collected from the physically lower end of each interval, and may represent water that drained from higher parts of the interval. Many of the samples are highly dilute, and probably represent condensation within the borehole; virtually all are more dilute than the HDPERM pore waters collected from the nearby Alcove 5 prior to heating. The DST pore waters used in this analysis are not listed here, but are summarized in DTN: LL020709923142.023 [DIRS 161677], and tabulated in Validation DTN: SN0705PAEBSPCE.014 (spreadsheet: *DST borehole water evaluation.xls*, tab: "Raw data").

For several reasons, the DST borehole water compositions do not provide a useful comparison for the NFC model. The NFC model does not model the processes of condensation and evaporation, which are the dominant processes affecting the borehole waters. Element–element plots in Figure 7.1-16 show that the borehole water compositions plot linearly, intersecting the origin, consistent with dilution of the initial pore waters by condensation. Also shown on this plot are the compositions of pore-water samples from the nearby Alcove 5 (HD-PERM samples), which may represent starting pore-water compositions in the area of the DST. Also, as noted in the previous section, the DST test did not last sufficiently long to result in significant feldspar dissolution. Borehole water compositions were collected for about four years during the heating period. Even assuming the maximum temperature, 96°C, applying the NFC feldspar dissolution rate only results in an increase in K concentration in solution of about 0.1 mg/L (Validation DTN: SN0705PAEBSPCE.014, spreadsheet: *DST borehole water evaluation.xls*, tab: "Max predicted feldspar diss."), and K is the most sensitive indicator of feldspar dissolution. Thus, the DST borehole waters offer little validation of the ability of the NFC to predict pore-water compositions, and are not considered further here.

7.1.4.4 Mineralogical Data

Mineralogical data available from the DST are relatively limited, and are summarized in *Thermal Testing Measurements Report* (SNL 2007 [DIRS 177414], Section 6.3.4.3). The data are based on two sets of sidehole cores that were collected during the heating phase of the DST. These data are archived in DTN: LA0201SL831225.001 [DIRS 158426]. Both sets were collected from boreholes in the boiling zone. Examination of the cores allowed identification of newly precipitated minerals, because the boreholes surfaces were initially clear. The only three minerals observed to have precipitated were calcite, amorphous silica, and gypsum. The presence amorphous silica corroborates the NFC model's use of this phase as the solubility-limiting phase for silica in solution, rather than another silica polymorph.

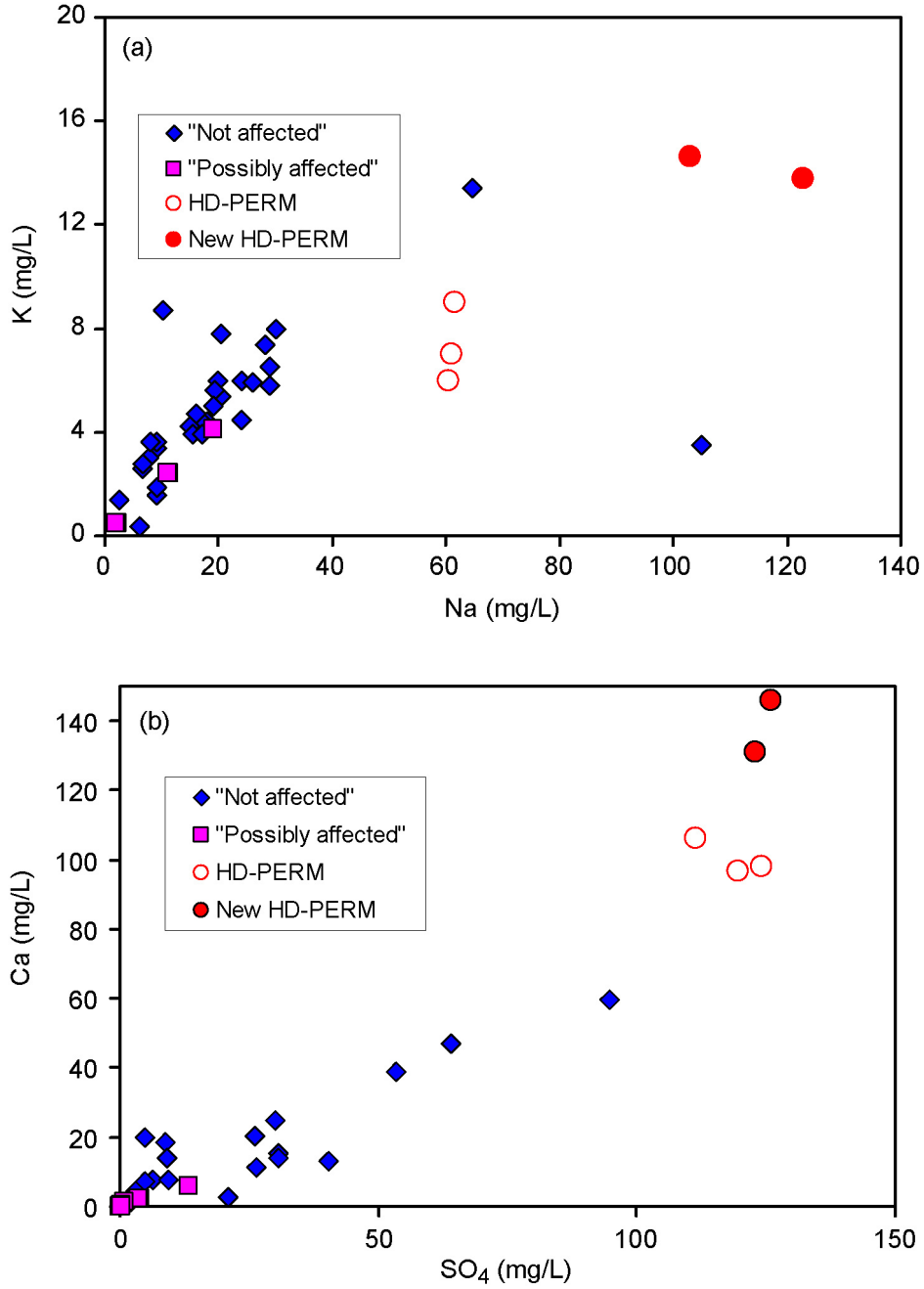

Source: Validation DTN: SN0705PAEBSPCE.014, spreadsheet: *DST borehole water evaluation.xls*, tab: "Data, formatted."

NOTE: The data form a straight line, intersecting the origin, suggesting that the dominant variation is due to dilution. Note that two more concentrated samples were not plotted, to allow for an expanded view of the more dilute samples. "Not affected" refers to waters that were not affected by interactions with engineered materials, while the "possibly affected" waters may have been (SNL 2007 [DIRS 177414], Table 6.3-32). "Affected" waters (one per plot) are not shown, again, to allow for the scale expansion.

Figure 7.1-16. DST Borehole Water Concentrations of (a) Na versus K, and (b) SO_4 versus Ca

7.1.4.5 Summary

In this section, measured DST pCO_2 concentrations were compared to NFC model predictions. The predicted NFC pCO_2 range bounded the data well, especially during the cool-down period, after the cessation of drift wall boiling. However, it was necessary to modify the model slightly, using a pCO_2 concentration of $10^{-3.42}$ bar (atmospheric pCO_2 level) for the non-condensable air in the drift, consistent with air movement from the ventilated drift, around the bulkhead and into the heated drift during cooling. Samples from BH-185, towards the end of the heated drift, were above the NFC model-predicted upper bound. However, that portion of the heated drift was lined with a cast-in-place cement liner, 20 cm thick, which may have affected water compositions or gas-phase movement. Because the compositions predicted by the NFC model accurately bound the DST data collected from the majority of sampling localities, the DST data corroborate the NFC model for the in-drift pCO_2 range. There is little evidence for significant mineral precipitation or dissolution during the DST experiment, but the observation of amorphous silica as a precipitate supports the use of this model as the solubility-limiting phase for aqueous silica in the NFC model.

7.2 VALIDATION OF THE P&CE ABSTRACTION MODELS

The P&CE abstraction models for seepage dilution/evaporation and integrated invert water chemistries instruct TSPA-LA to both interpolate and extrapolate key chemical parameters over a limited set of conditions (Section 6.15). This section validates the interpolation and extrapolation of key chemical parameters by direct comparison to output from the IDPS model (SNL 2007 [DIRS 177411]). Because the integrated invert water chemistry abstraction model utilizes the same set of lookup tables in the same manner as the seepage dilution/evaporation abstraction model, a single set of validation test cases is provided in the sections below to validate both P&CE abstraction models. Not every combination of temperature and pCO_2 is necessary to validate the phase space of the P&CE abstraction models. The validation test cases described below include two temperatures and two pCO_2 values, the combination of which validates temperatures from 30 to 100, by assessing interpolation between 30°C and 70°C and then 70°C and 100°C. Likewise, the validation of the interpolation of pCO_2 also covers the range from log pCO_2 = −4 to −2, by selecting validation test cases between log pCO_2 values of −2 and −3 and then −3 and −4. There is a third dimension in the phase space of interest and that is the starting water chemistry. To evaluate this, the two most chemically distinct waters (Group 1 and Group 3) were selected for the validation test cases. Therefore, the phase space encompassed by the P&CE abstraction models is validated.

7.2.1 Comparison of P&CE Seepage Dilution/Evaporation Abstraction to EQ3/6 Model Outputs

In accordance with the validation criterion (SNL 2007 [DIRS 179287], Section 2.2.3.1), the P&CE seepage dilution/evaporation abstraction results (i.e., interpolated lookup table values) are compared with specific EQ6 simulations to ensure that the interpolation results adequately estimate the IDPS process model output, within the bounds of the model uncertainty (from Table 6.12-1).

The EQ6 evaporation input and output files (denoted in the list below by an "e" before the file type) selected for this validation exercise are from the Groups 1 and 3 evaporation simulations archived in Output DTN: SN0701PAEBSPCE.001. The seepage simulations (files: *1GT70.6i* and *3GT96.6i*) were taken from Output DTN: SN0701PAEBSPCE.002. These EQ6 evaporation simulations output files listed below were used to construct the lookup tables of the same name that are also archived in Output DTN: SN0701PAEBSPCE.001.

- *3gp3t70e.6i*
- *3GT96.6i*
- *3gp3t70e.6o*
- *3gp2t70e.6o*
- *3gp3t1e.6o*
- *3gp2t1e.6o*
- *1gp3t30e.6i*
- *1GT70.6i*
- *1gp3t70e.6o*
- *1gp4t70e.6o*
- *1gp3t30e.6o*
- *1gp4t30e.6o*.

The EQ6 input files *1gp3t30e.6i* and *3gp3t70e.6i* listed above were modified to replace the temperature and pCO_2 and renamed *Gp1_val.6i* and *Gp3_val_b.6i*. The selected temperature and pCO_2 in those two files for these abstraction validation calculation simulations were 56°C and $10^{-3.2}$ bar, and 95.6°C and $10^{-2.4}$ bar, respectively. In addition, two new seepage simulations were created, called *Gp1_seep.6i* and *Gp3_seep.6i*, by modifying the *1GT70.6i* and *3GT96.6i* files. The only modifications made to the initial seepage files were to change the end-point seepage temperatures to match the validation cases, thus producing the appropriate pickup files. These pickup files were appended to the validation simulations (*Gp1_val.6i* and *Gp3_val.6i*). Additionally, a single relative humidity point is selected for each of these temperature and pCO_2 cases; these are 98 and 66% RH, respectively. The basis for this choice is that during higher temperature conditions, the relative humidity is generally lower, and upon cooling the RH is known to increase. The modified files described here and used in this validation exercise are archived in Validation DTN: SN0705PAEBSPCE.008.

Software application EQ3/6 V8.0 was used along with the *data0.pce* database (Output DTN: SN0703PAEBSPCE.006) to create *gp1_val.6o* and *gp3_val.6o*. GETEQDATA was then used to extract the results from those output files along with the results of the lookup table output files listed above into *PCE_evap_validation.xls*. The relevant files can be found in Validation DTN: SN0705PAEBSPCE.008.

In the validation, values for pH, ionic strength, Cl^-, and Cl^-/NO_3^- (represented by total [Cl] and total [N]) are first interpolated with respect to pCO_2, and then the two nearest temperatures in the set of lookup table outputs. For example, interpolation for $10^{-3.2}$ bar pCO_2 is accomplished by linearly interpolating the logarithms of CO_2 partial pressure. In this case, the two nearest logarithms of pCO_2 in the lookup tables are −3 and −4. This procedure exactly follows that used for TSPA, as described in Section 6.15. The interpolated values are then plotted at 30°C and

70°C and connected by a straight line to determine the interpolated value at 56°C and $10^{-3.2}$ bar of CO_2.

Figure 7.2-1, for ionic strength, pH, Cl^-, and Cl^-/NO_3^-, shows that even with dependence on both pCO_2 and temperature, the exact values generated by the EQ6 simulations (green squares) are well represented by the interpolated values at 56°C (red lines). The P&CE model uncertainties for ionic strength and pH (from Table 6.12-1) encompass the ranges of interpolated values for pCO_2 and temperature.

The uncertainties for Cl^- and Cl^-/NO_3^- are defined as zero in the *RH* range that includes 98% (Table 6.12-1). Therefore, no uncertainty bar is applicable to Figures 7.2-1(c) and 7.2-1(d). A numerical evaluation of these quantities and their deviations from interpolated values is archived in Validation DTN: SN0705PAEBSPCE.008 (spreadsheet: *PCE_evap_validation.xls*, tab: "Results Gp1_val"). There is a slight difference between the measured and calculated value for the log of the Cl concentration in molal of approximately 0.002. This difference is insignificant when compared to other model uncertainties. Furthermore, there is no deviation from the measured to the interpolated value for the Cl:N value (to the tenth place past the decimal); the difference is zero.

Examination of the second validation case, at 95.6°C, $10^{-2.4}$ bar of pCO_2, and 66% RH, is presented in Figure 7.2-2. Ionic strength is not included in this low-RH example because it is below 85% RH; this is where the ionic strength is greater than 3 molal (about 10 molal here) and does not support any implementation in TSPA-LA (see Table 6.12-1). For pH, Cl^-, and Cl^-/NO_3^- the differences between the seepage evaporation abstraction and the EQ6 simulations that implement the IDPS process model are much smaller than the uncertainty bars.

These two validation cases indicate that the P&CE seepage dilution/evaporation abstraction is a valid representation of evaporated seepage water compositions as calculated using EQ6 simulations to implement the IDPS process model, especially when propagation of the model uncertainty is included. Where the IDPS model uncertainty is nonzero, the abstraction model falls within those bounds, and where the IDPS model uncertainty is zero, the differences are quantitatively insignificant and the validation criterion is met.

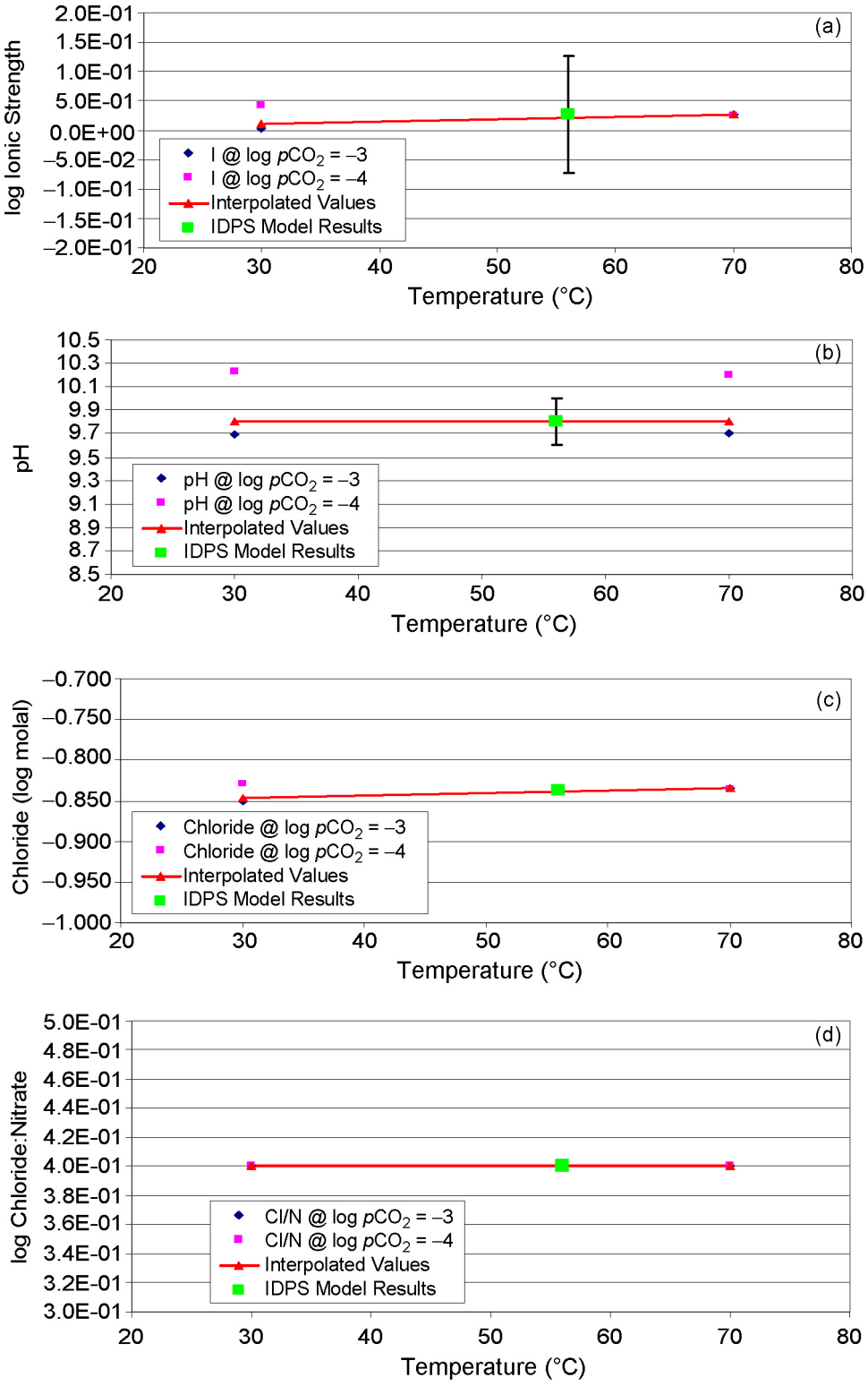

Source: Validation DTN: SN0705PAEBSPCE.008.

Figure 7.2-1. Seepage Evaporation Abstraction Validation at 56°C, $10^{-3.2}$ pCO_2, and 98% RH

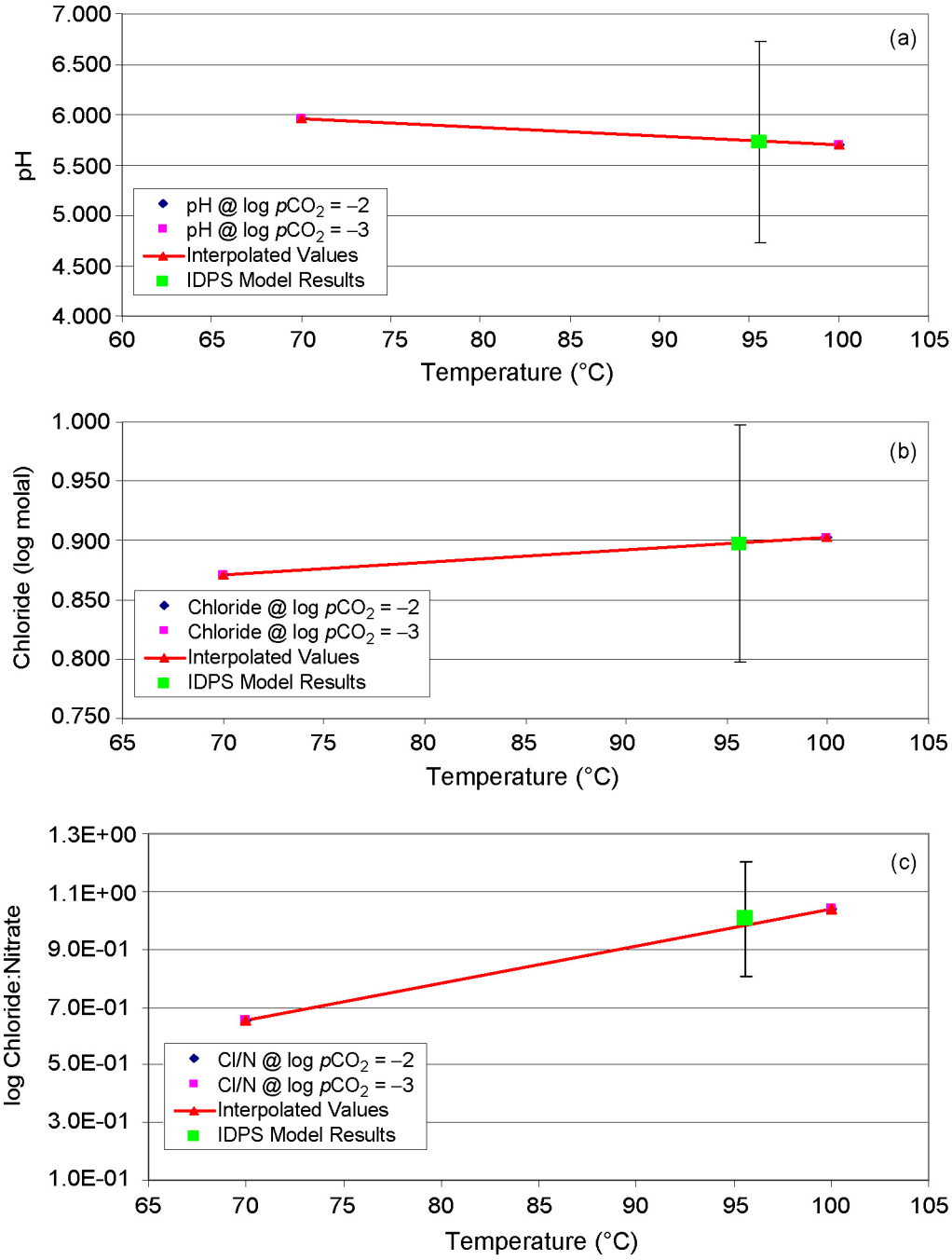

Source: Validation DTN: SN0705PAEBSPCE.008.

Figure 7.2-2. Seepage Evaporation Abstraction Validation at 95.6°C, $10^{-2.4}$ pCO_2, and 66% RH

7.2.2 Extrapolating pCO_2 Values beyond the Lookup Tables

As discussed in Section 6.15, extrapolation can be made when pCO_2 is outside the given range of the P&CE seepage dilution/evaporation lookup tables. This sensitivity study gives the predictive range over which the lookup tables can be extrapolated. Results indicate that valid log linear extrapolation as a function of pCO_2 can be performed for values of ionic strength, chloride and nitrogen concentrations, and pH.

7.2.2.1 Calculation Framework

Two cases were examined to assess the effects of the possible range of pCO_2 on seepage water chemistry. Based on the total possible range of in-drift pCO_2 of approximately 2×10^{-2} to 1×10^{-5} bar (discussed in Section 6.7.2), there is a possibility that the seepage water chemistry lookup tables from the dilution/evaporation abstraction model used in TSPA-LA could be utilized outside the 10^{-2} to 10^{-4} bar range specified for their creation (Section 6.9). Sensitivity calculations were conducted and are documented here using $pCO_2 = 10^{-5}$ and 2×10^{-2} bar to evaluate the effects of extrapolation on the key chemical parameters of interest to TSPA (pH, *I*, [Cl], [N]). For these simulations, Group 1 water was selected with a moderate WRIP value, G, at a temperature of 70°C and the pCO_2 values discussed above. The waters were evaporated and the chemistry was extracted as a function of the activity of water. These model values were then compared to the extrapolated values that were calculated using the data from the seepage dilution/evaporation lookup tables archived in Output DTN: SN0701PAEBSPCE.001 at RH values of 98% and 70%. These validation simulations and calculations are archived in Validation DTN: SN0705PAEBSPCE.008.

7.2.2.2 Result of pCO_2 Extrapolations

Figure 7.2-3 shows the variation in pH when pCO_2 gas values fall outside the range of the provided lookup tables. The trend is about half a pH unit increase for every order of magnitude decrease in pCO_2 below 10^{-4} bar.

For ionic strength and nitrate, there is only a small dependence upon pCO_2 and only at intermediate RH (Figures 7.2-4 and 7.2-6). Chloride, however, shows some linearly predictable trends. These trends are strongly associated with the activity at which calcite and halite precipitate (Figure 7.2-5).

A numerical evaluation of the differences between the extrapolated and the modeled values is presented in Table 7.2-1 and the calculations are archived in Validation DTN: SN0705PAEBSPCE.008. The uncertainties on these values are described in Section 6.12.3, Tables 6.12-1 and 6.12-2, and are given here for comparison. Note that the uncertainty for the pH at RH of 98% is estimated to be ±0.2 units from Output DTN: SN0703PAEBSPCE.007 (spreadsheet: *Re-evaluation of pH uncertainty.xls*, tab: "CDF of pH uncertainty," figure labeled "Error vs. Frequency").

At an RH of 98%, the IDPS uncertainties for chlorine and nitrogen concentration are listed as zero. The deviation from the modeled data for these two quantities as a function of the pCO_2 extrapolation is nonzero. However, the deviations are small, < 0.001 molal for the sensitivity

case at $pCO_2 = 2 \times 10^{-2}$ bar and < 0.01 molal for the sensitivity case at $pCO_2 = 10^{-5}$ bar (Table 7.2-1). The deviation between the extrapolated and modeled data for pH never exceeded 0.08 units, well within the model uncertainty of approximately 0.2 units. The ionic strength is predicted well by the log linear extrapolation of pCO_2, with differences between extrapolated and modeled data of 0.02 and 0.13 molal for $pCO_2 = 2 \times 10^{-2}$ and 10^{-5} respectively. The IDPS uncertainties were applied to these values and the calculated uncertainty ranges are presented in Table 7.2-1. Aside from the negligible differences for the chlorine and nitrogen concentrations, the extrapolated and modeled data agree within the stated uncertainties.

Table 7.2-1. Numerical Evaluation of the Uncertainty Introduced by Extrapolating Key Chemical Parameters as a Log Linear Function of pCO_2

RH = 98% and pCO_2 = 0.02				
	pH	**I (molal)**	**Cl (molal)**	**N (molal)**
Extrapolated data	8.97	0.8967	0.1333	0.0530
Uncertainty	±0.2 units	±0.1 log molal	±0.0 log molal	±0.0 log molal
Uncertainty range	8.77 to 9.17	0.7123 to 1.1289	N/A	N/A
Modeled data	8.94	0.8784	0.1319	0.0525
RH = 70% and pCO_2 = 0.02				
	pH	**I (molal)**	**Cl (molal)**	**N (molal)**
Extrapolated data	9.15	N/A	4.9325	1.9619
Uncertainty	±0.1 units	N/A	±0.1 log molal	±0.2 log molal
Uncertainty range	8.15 to 10.15	N/A	3.9180 to 6.2096	1.2379 to 3.1094
Modeled data	9.07	N/A	5.1721	2.0572
RH = 98% and pCO_2 = 0.00001				
	pH	**I (molal)**	**Cl (molal)**	**N (molal)**
Extrapolated data	10.70	1.0530	0.1460	0.0581
Uncertainty	±0.2 units	±0.1 log molal	±0.0 log molal	±0.0 log molal
Uncertainty range	10.50 to 10.90	0.8364 to 1.3257	N/A	N/A
Modeled data	10.62	0.9199	0.1359	0.0541
RH = 70% and pCO_2 = 0.00001				
	pH	**I (molal)**	**Cl (molal)**	**N (molal)**
Extrapolated data	10.92	N/A	4.3555	1.7324
Uncertainty	±0.1 units	N/A	±0.1 log molal	±0.2 log molal
Uncertainty range	9.92 to 11.92	N/A	3.4555 to 5.4833	1.0931 to 2.7457
Modeled data	10.93	N/A	4.1024	1.6318

Source: Validation DTN: SN0705PAEBSPCE.008, spreadsheet: *CO2_validation.xls*.

At an RH of 70%, the IDPS uncertainties for chlorine and nitrogen concentration are given as 0.1 and 0.2 log molal, respectively. The calculated differences between the extrapolated and modeled data fall within these uncertainty ranges (Table 7.2-1). The ionic strength is not utilized by TSPA below an RH of 85%, and so no comparison is required. There is a large pH uncertainty at this RH, ±1.0 units. The extrapolated pH values match the modeled values within 0.1 pH units, well within the uncertainty.

It is concluded from these analyses that the key chemical parameters of pH, I, [Cl], and [N] can be extrapolated as a log linear function of pCO_2 down to a value of 10^{-5} and up to a value of 2×10^{-2} bar without incurring significant uncertainties on the extrapolated values when compared to the reported model uncertainties (Table 6.12-1). The pCO_2 extrapolation range is, therefore, validated.

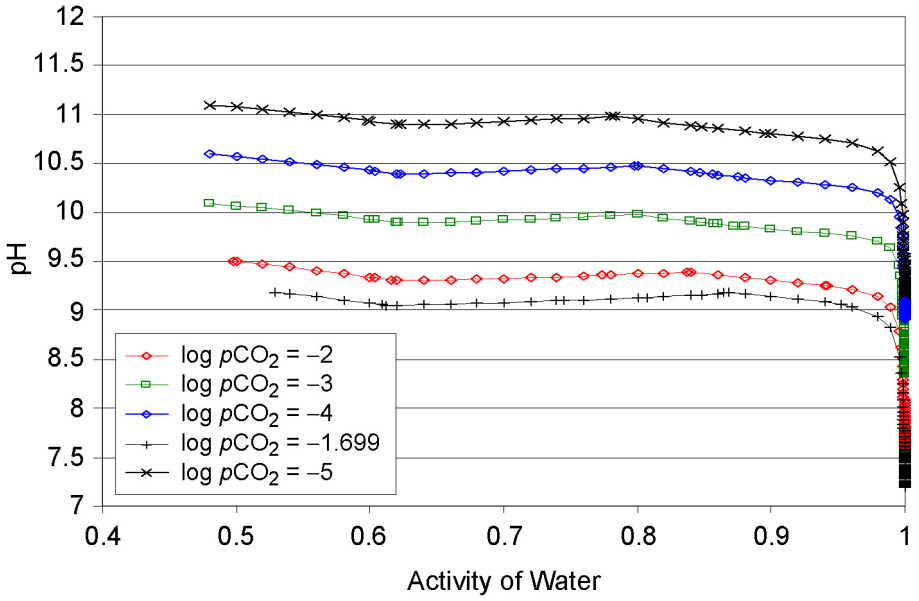

Source: Validation DTN: SN0705PAEBSPCE.008, spreadsheet: *CO2_validation.xls*.

Figure 7.2-3. Variation in pH as a Function of pCO_2 for Group 1 water, T = 70°C with a WRIP = G

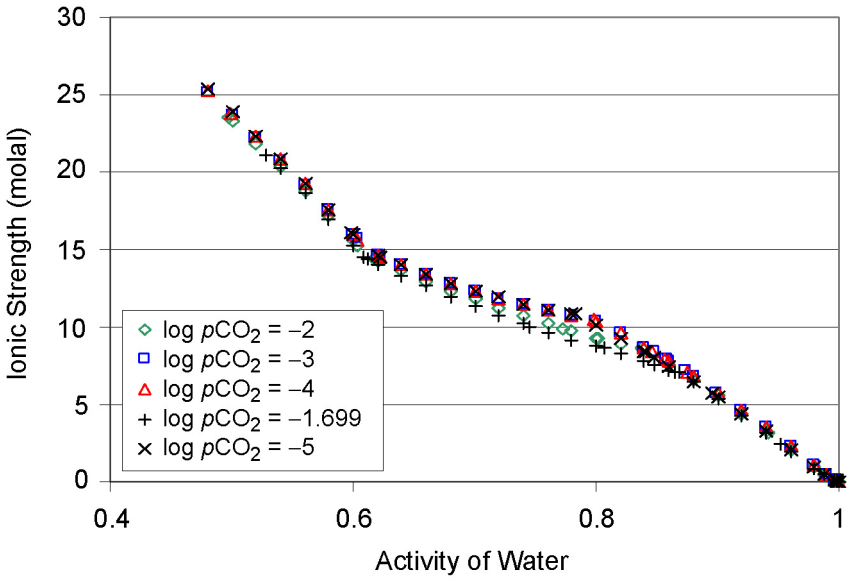

Source: Validation DTN: SN0705PAEBSPCE.008, spreadsheet: *CO2_validation.xls*.

Figure 7.2-4. Variation in Ionic Strength as a Function of pCO_2 for Group 1 water, T = 70°C with a WRIP = G

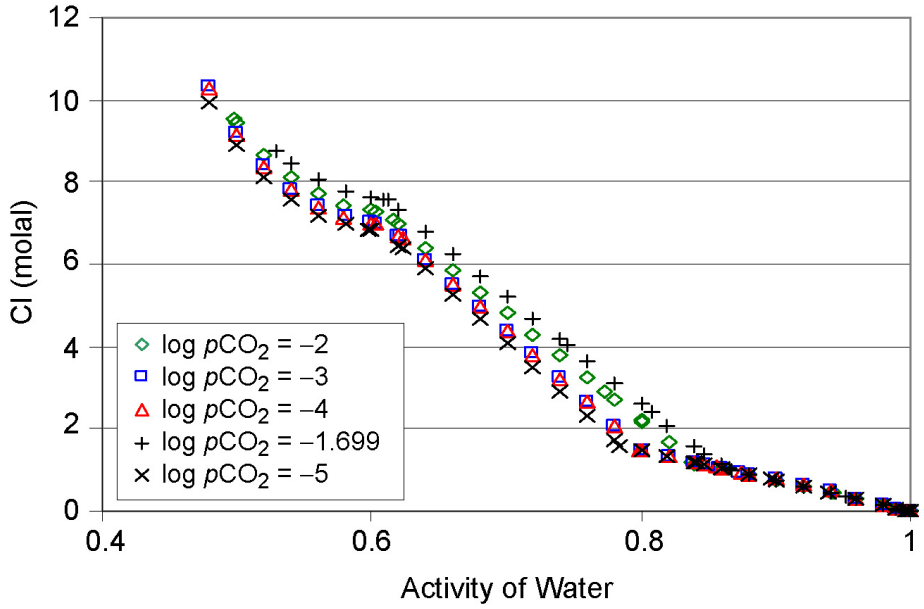

Source: Validation DTN: SN0705PAEBSPCE.008, spreadsheet: *CO2_validation.xls*.

Figure 7.2-5. Variation in Cl Concentration as a Function of pCO_2 for Group 1 Water, T = 70°C with a WRIP = G

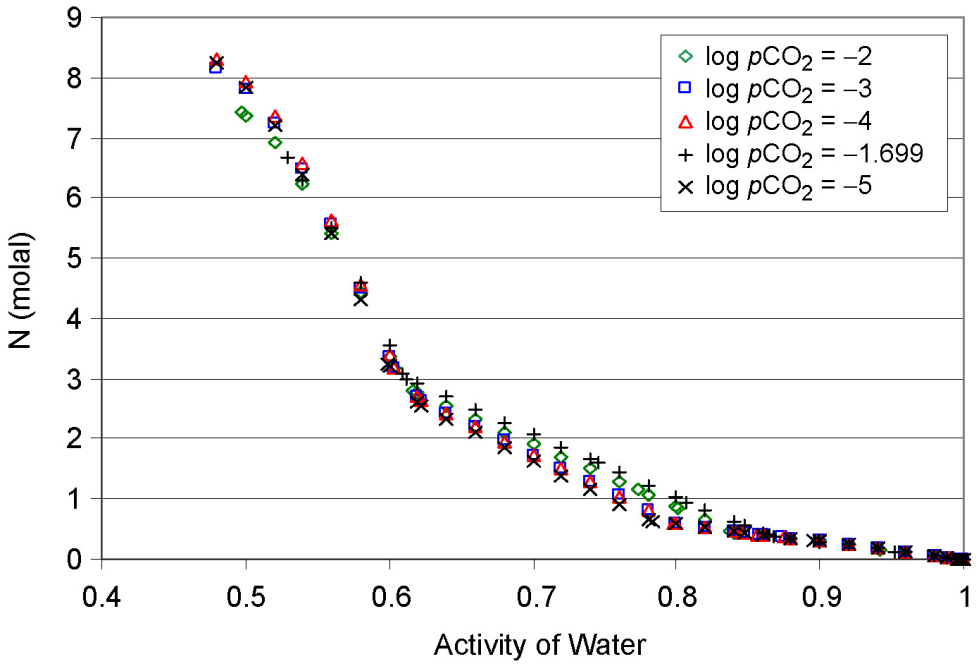

Source: Validation DTN: SN0705PAEBSPCE.008, spreadsheet: *CO2_validation.xls*.

Figure 7.2-6. Variation in N Concentration as a Function of pCO_2 for Group 1 Water, T = 70°C with a WRIP = G

7.3 CONFIDENCE BUILDING DURING DEVELOPMENT

Confidence building performed during the development of the models is documented in accordance with the requirements of SCI-PRO-002, Attachment 3. This confidence building includes the following:

Selection of input parameters and/or input data, and a discussion of how the selection process builds confidence in the model.

- Discussion of the input parameters for the NFC process model and the P&CE abstraction models and the bases for their selection is provided in Section 4.1. The NFC model is developed and justification provided for model inputs, and uncertainty selections are provided in Sections 4.1, 6.3, and 6.12. For the seepage dilution/evaporation abstraction and, hence for the integrated invert chemistry abstraction, the rationale for equilibrium modeling, and for including or excluding precipitating minerals and trace elements, is documented in a technically defensible manner (Sections 6.2 and 6.9).

- The rationale for equilibrium modeling is documented in Sections 6.2.3 and 6.2.4, which provide background discussion, and 6.2.4.1, which specifies explicit criteria used for selecting minerals for inclusion or exclusion, including criteria based on kinetics.

- The rationale for excluding the chemical effects from corrosion of introduced materials on water composition is documented in Section 6.8.

- The analysis of available pore-water data, for multiple samples acquired from the host rock units, is presented in Section 6.6. This analysis supports selection of the four different starting pore-water compositions for the initial and boundary conditions for the NFC seepage model and subsequently the P&CE abstraction models for use as output to TSPA, and thus supports the propagation of uncertainty from the NFC seepage model, through the P&CE abstraction models, to TSPA-LA.

Description of initial and boundary conditions runs, and/or run convergences, and a discussion of how the activity or activities build confidence in the model. If appropriate, include a discussion of impacts of any non-convergence runs.

- Initial and boundary conditions for the P&CE abstraction models are discussed in Sections 6.3 and 6.9. For the seepage dilution/evaporation abstraction, nonconvergence of EQ3/6 runs was encountered when calculating dryout (eutectic compositions) at very low water activity values (Section 6.15.1). If the nonconvergence resulted in an upturn in the activity of water at low RH, then the data were truncated at that point. The representation of nitrate and chloride concentrations for these conditions is based on the known solubility behaviors of nitrate and chloride salts, and the abstraction provides a reasonable lower bound on the chloride:nitrate ratio.

Discussion of the impacts of uncertainties to the model results.

- For the NFC process model and the P&CE abstraction models, the predictive model uncertainty associated with use of the IDPS model is propagated to TSPA using uncertainty lookup tables, as described in Section 6.12. Uncertainty on the NFC model parameters is discussed in detail, also in Section 6.12, and specific instructions for model propagation and justification of uncertainty distributions can also be found in Section 6.12. Uncertainties specific to the interpolation and extrapolation of lookup table parameters, as is stated in the implementation instructions for TSPA (Section 6.15), are evaluated in Section 7.2 and found to be small, and much less than the model uncertainty from the IDPS model and overall model uncertainty.

Documentation of the NFC process model and the P&CE abstraction models includes defensible assumptions (Section 5) and simplifications in model development (addressed in Sections 6.2, 6.3, 6.9, and 6.12). The suite of P&CE models maintain consistency with physical principles, such as conservation of mass and energy, using EQ3/6 V8.0 software (Section 6.2.1).

7.4 VALIDATION SUMMARY

The P&CE models have been validated by applying acceptance criteria (Level II) based on an evaluation of the overall model's relative importance to the potential performance of the repository system. All validation requirements for the NFC model have been fulfilled, including corroboration of model results with ambient field data, experimental data from the DST, and comparison to the predictions of the independently derived THC seepage model. Validation requirements for the P&CE abstraction models have also been fulfilled, by corroboration of interpolated/extrapolated results from the abstraction with directly determined values, and by critical review (Appendix A). Activities requirements for confidence building during model development have also been satisfied. The model development activities and post-development validation activities described establish the scientific bases for the P&CE models. Based on this, the P&CE models are considered to be sufficiently accurate and adequate for the intended purpose and to the level of confidence required by the relative importance of the models to the potential performance of the repository system. No future validation activities are required for the P&CE models.

INTENTIONALLLY LEFT BLANK

8. CONCLUSIONS

8.1 SUMMARY AND MODEL FINDINGS

The engineered barrier system (EBS) physical and chemical environment abstractions provide a quantitative description of the pH, ionic strength (I), and major ionic and elemental compositions of waters in contact with the waste package, drip shield, and the invert. Brines that form by evaporative concentration of the seepage water can potentially affect corrosion on the waste package and drip shield, and influence radionuclide mobility in the invert. Compositional parameters of the waters contacting the drip shield and waste package, such as pH or the ratio of chloride to nitrate, are important in assessing potential corrosion (SNL 2007 [DIRS 178519]). Acidic or alkaline pH values in the water of the invert may affect the solubility of radionuclides. Changes in ionic strength of the water in the invert may reduce the mobility of colloidal particles transporting adsorbed radionuclides.

Potential water compositions of seepage from the NFC process model were evaluated, and represented by four water compositions that form different brine types upon evaporation (Section 6.6). These waters are used to generate a set of 396 lookup tables to represent evaporated seepage and invert waters for TSPA-LA. The lookup tables represent an equilibrium chemical response surface for each starting water (Groups 1 through 4) with varying amounts of alkali feldspar (WRIP = 0,B,C…J,L) (Table 6.3-5), covering a range of temperatures (100°C to 30°C), pCO_2 (10^{-4} to 10^{-2} bar), and relative humidity. The generation of these tables is discussed in Section 6.9. The predicted range in chemistry of the seepage and invert waters as a function of RH (e.g., pH, I, Cl^-, NO_3^-/Cl^-), as predicted by the lookup tables, is discussed in Section 6.13.

The physical and chemical environment (P&CE) seepage dilution/evaporation abstraction shows that corrosive calcium and magnesium chloride brines only form for the Group 3 starting water at low WRIP values (WRIP ≤ "E", 4.64×10^{-4}) (Table 6.13-3 and Figures 6.13-3). The most likely brines to form are sodium and potassium chloride or carbonate-type brines (Tables 6.13-1 to 6.13-4). Chloride:nitrate ratios for a representative few of the predicted evaporated waters expected to contact drip shields and waste packages are shown in Figures 6.13-9 to 6.13-12. The mineral assemblages that precipitate during evaporation of the brines for a subset of the lookup tables are reported in Table 6.13-5.

Lookup tables that represent both evaporated seepage water and invert water have been provided with instructions (Section 6.15) on how to select the appropriate chemical values from the lookup tables. These lookup tables can be used as source chemistry for waters flowing into the drift including the invert.

Stainless steel ground support and low-alloy or carbon steel committed materials have their chemical composition and corrosion rates compiled in Section 6.5. The short-lived materials, such as low-alloy or carbon steel, corrode rapidly in the high humidity environment of the drift and do not affect seepage water that could impact the drip shield or waste packages because they are located in the invert. Oxygen gas pressure of the in-drift atmosphere is determined to be sufficient to maintain an oxidative environment during the corrosion of the low-alloy or carbon steels (Section 6.7).

Dust that settles onto the waste package and drip shield from natural sources and repository construction processes will not affect repository performance with respect to corrosion. During and for a while after the heat pulse, when temperatures are above 100°C, no liquid water is expected to flow in the drift (Section 6.3). Thus, the only waters likely to be present are those formed by deliquescence of the salt within dust, and the effect of those is discussed in Section 6.10.

8.2 SUMMARY OF MODEL ABSTRACTION FOR TSPA

8.2.1 Summary of the Total System Performance Assessment Lookup Tables

The recommended TSPA-LA implementation of the lookup tables for the determination of seepage water chemistries for both the dilution/evaporation and the integrated invert chemistry abstractions is documented in Section 6.15. The propagation of uncertainties on each of the key chemical parameters provided to TSPA-LA by the P&CE suite of models is discussed in Section 6.12. The development of the two P&CE abstraction models is documented in Section 6.9. Section 8.2.2 lists the lookup table data tracking numbers (DTNs).

8.2.2 Data Tracking Numbers for Data Generated in This Report

Tables 8.2-1 and 8.2-2 list the DTNs for data generated in this report. Table 8.2-1 is for data generated to feed TSPA-LA, and Table 8.2-2 is for supporting data used in development of the TSPA-LA data feeds.

Table 8.2-1. P&CE Model Output DTNs Derived for Use in the TSPA-LA Model

DTN	Location In Text	Description of TSPA Parameters
SN0701PAEBSPCE.001	Sections 6.3.1, 6.3.3.2.9, 6.8.1.4, 6.9, 6.12.3, 6.13.1.2, 6.13.3, 6.15, and 7.2	396 dilution/evaporation lookup tables containing pH, *I*, and ion concentrations as a function of in-drift relative humidity, associated with the four starting water compositions, for each of the eleven WRIP values (0, B, C, D, E, F, G, H, I, J, L) (defined in Table 6.3-5), at three maximum drift wall temperatures (100°C, 70°C, and 30°C) and three pCO_2 values (10^{-4}, 10^{-3}, and 10^{-2} bar). These 396 tables provide both dilution and evaporation simulation results.
SN0701PAEBSPCE.002	Sections 6.3, 6.7.2, 6.8.1.4, 6.8.2, 6.9.1, 6.12.3, 6.13.2, 6.15, and 7.1.3.2	This DTN contains lookup tables used by TSPA for calculating maximum and minimum values for the in-drift CO_2 concentrations.
SN0703PAEBSPCE.006	Sections 4.1, 6.3, 6.6.3, 6.7, 6.8, 6.12, 6.13.6, 6.15, 7.1, 7.2.1, and 8.4.1.3	This DTN contains a lookup table used by TSPA for determining the WRIP, which is a metric for the amount of feldspar that dissolves as groundwater percolates downward through the TSw to the drift. It also contains the data files used to develop the WRIP lookup table. Furthermore, this DTN contains a set of lookup tables that report the relative humidity at which halite or sylvite first precipitate, i.e., the relative humidity at which salt separation can occur.
SN0703PAEBSPCE.007	Sections 4.1, 6.1, 6.3.3.2.4, 6.12, and 6.13	This DTN contains a description of uncertainty parameters to be applied to the water-rock interaction parameter and to in-drift water compositional parameters (Cl and NO_3 concentrations, ionic strength, and pH).

Table 8.2-2. P&CE Model Supplemental Output DTNs

Output DTN	Location In Text	Title
SN0705PAEBSPCE.009	Sections 4.1.8 and 6.3	Miscellaneous supporting calculations; the normative calculation of mineral abundances in the repository host rock; the example calculation of a WRIP parameter
SN0705PAEBSPCE.010	Sections 6.3.1 and 6.8.2.1	The EQ3/6 simulations and supporting calculations for the validation of the modified thermodynamic database used by this report: *data0.pce*
SN0705PAEBSPCE.011	Section 6.8	The EQ3/6 simulations and supporting calculations for the assessment of the interaction of introduced steels with seepage waters
SN0705PAEBSPCE.012	Section 6.11	EQ3/6 simulations and supporting calculations that aided the development of the alternative conceptual model
SN0705PAEBSPCE.015	Section 6.6	EQ3/6 simulations and supporting calculations for the pore-water selection analysis
MO0705OXYBALAN.000	Sections 4.1 and 6.7.1	EQ3/6 simulations and supporting calculations for the analysis of oxygen consumption by corrosion of in-drift materials

Table 8.2-3. P&CE Model Validation DTNs

Output DTN	Location In Text	Title
SN0705PAEBSPCE.008	Section 7.2	P&CE abstraction model validation EQ3/6 simulation files and supporting calculations
SN0705PAEBSPCE.013	Section 7.1.3	EQ3/6 simulations and supporting calculations for the comparison between the THC and NFC model outputs
SN0705PAEBSPCE.014	Section 7.1	EQ3/6 simulations and supporting calculations for the validation of the NFC process model

8.3 ABSTRACTION MODEL UNCERTAINTY AND RESTRICTIONS

Uncertainties in the output from the EBS physical and chemical environment (P&CE) model are summarized in this section. Direct inputs to the model are tabulated and discussed in Section 4.1, but the uncertainties associated with those inputs are discussed in the subsections of Section 6 where they are used. The effects of input uncertainties are discussed in more detail in Sections 6.3 and 6.12. Limitations and constraints on the use of the model and its outputs are discussed in Sections 6.12 and 6.15 with the discussions of the various components and features of the overall P&CE model. Specific limitations involved in the model are listed in Section 1.3.

The P&CE model uses four primary inputs, and each has uncertainty associated with it. These inputs are:

- Composition of water entering the drift
- The IDPS model (SNL 2007 [DIRS 177411]) and its associated databases (thermodynamic data and other technical information not specific to the site used in the geochemical modeling that results in the model output)
- Composition and flux of in-drift gases
- Amounts and characteristics of engineered materials to be placed in the drift (ground support, emplacement rails, etc.).

For evaluating repository performance, four parameters have been identified as output from this model that will be used as direct input to TSPA calculations: (1) chloride ion concentration, (2) chloride/nitrate molar ratio, (3) ionic strength, and (4) pH.

As explained in Section 6.12, of the four inputs, only two were found to have uncertainties that would propagate into the output parameters that feed the TSPA: (1) the IDPS model, and (2) the boundary incoming seepage waters.

An evaluation of the IDPS model was conducted to determine its contribution to error in predicting the parameters of interest as explained in Section 6.12. A re-examination of the uncertainty on pH values at relatively high RH was conducted in this report and a new distribution was generated (Section 6.12).

Uncertainties from these sources are propagated in a realistic and representative way to TSPA. There the NFC process model and IDPS uncertainties are directly combined to generate total uncertainty bands for the parameters of interest to TSPA. Appropriate distributions for the error ranges were selected, and instructions for how to implement the errors are developed and described in Section 6.12 and 6.15.

No confirmatory actions are deemed necessary at this time.

8.4 YUCCA MOUNTAIN REVIEW PLAN CRITERIA ASSESSMENT

This report predicts results that directly pertain to the abstraction of the quantity and chemistry of water contacting engineered barriers and waste forms. This section summarizes the contents of this report as they apply to U.S. Nuclear Regulatory Commission criteria for a detailed review of that abstraction.

8.4.1 Acceptance Criteria for Quantity and Chemistry of Water Contacting Engineered Barriers and Waste Forms

These criteria are from *Yucca Mountain Review Plan, Final Report* (NRC 2003 [DIRS 163274], Section 2.2.1.3.3.3), which is based on requirements set forth in 10 CFR 63.114(a)–(c) and (e)–(g) [DIRS 173273]).

8.4.1.1 Acceptance Criterion 1—System Description and Model Integration Are Adequate

(1) TSPA adequately incorporates important design features, physical phenomena, and couplings, and uses consistent and appropriate assumptions throughout the quantity and chemistry of water contacting engineered barriers and waste forms abstraction process.

The effects of coupled processes (Section 6.4) have been considered in part in the development of this model. For example, THC effects on input water compositions are incorporated in the NFC model output (Sections 4.1.4 and 6.3.2.1) used as input to the P&CE model. Thermal-hydrologic-chemical processes are at the heart of the in-drift water chemistry evolution presented in this report. The analyses presented in this report use current design information (Sections 4.1 and 6.5), and are based on physical phenomena expected within repository drifts (Sections 6.3 and 6.9). Coupled processes that were considered and screened out from further consideration in this report, and their rationale for exclusion, are presented in DTN: MO0706SPAFEPLA.001 [DIRS 181613]. Assumptions (Section 5) contained in this report are appropriate and are consistent with similar assumptions in related documents. These factors are included in the analyses leading to the output parameters (Section 6.13), which may be used to assess engineered barrier and waste form degradation.

(2) The abstraction of the quantity and chemistry of water contacting engineered barriers and waste forms uses assumptions, technical bases, data, and models that are appropriate and consistent with other related DOE abstractions. For example, the assumptions used for the quantity and chemistry of water contacting engineered barriers and waste forms are consistent with the abstractions of "Degradation of Engineered Barriers" (Section 2.2.1.3.1); "Mechanical Disruption of Engineered Barriers" (Section 2.2.1.3.2); "Radionuclide Release Rates and Solubility Limits" (Section 2.2.1.3.4); "Climate and Infiltration" (Section 2.2.1.3.5); and "Flow Paths in the Unsaturated Zone" (Section 2.2.1.3.6). The descriptions and technical bases provide transparent and traceable support for the abstraction of quantity and chemistry of water contacting engineered barriers and waste forms.

This report uses the same technical bases and other information used in other LA-supporting documents concerned with engineered barrier and waste form performance. The conceptual model that forms the basis for this report (Section 6.3), and its assumptions (Section 5), are consistent with other engineered system models and repository design. Primary input (Section 4.1) is developed in this report as a new process model, the NFC model, and provides both the in-drift water and gas chemistries. The IDPS model is used in conjunction with the NFC model to generate in-drift water chemistry. Section 6.3 provides details of these model interfaces. The descriptions and technical bases are recorded to provide inherently transparent and traceable support for the abstraction of in-drift water chemistry.

(3) Important design features, such as waste package design and material selection, backfill, drip shield, ground support, thermal loading strategy, and degradation processes, are adequate to determine the initial and boundary

conditions for calculations of the quantity and chemistry of water contacting engineered barriers and waste forms.

Initial and boundary conditions for this model are based on descriptions of design features (Section 6.5) and predicted behavior of the EBS (Section 6.3) as documented in YMP design documents and in other barrier-specific models and abstractions. This model includes consideration of the chemical effects of corrosion on engineered materials (Sections 6.7 and 6.8).

(4) Spatial and temporal abstractions appropriately address physical couplings (thermal-hydrologic-mechanical-chemical). For example, the DOE evaluates the potential for focusing of water flow into drifts, caused by coupled thermal-hydrologic-mechanical-chemical processes.

The abstractions in the P&CE model incorporate the effects of a number of different coupled processes in its evaluation of in-drift water chemistry. For example, thermal-hydrologic-chemical physical couplings are included implicitly through the NFC model. Another example is the analysis addressing the impact of corrosion of introduced materials. This analysis takes into account various thermal-hydrological-mechanical-chemical effects, as do the corrosion rates used in the analysis. Coupled processes formally classified as features, events, or processes (FEPs) are discussed briefly in Section 6.14 and documented in more detail in DTN: MO0706SPAFEPLA.001 [DIRS 181613]. This DTN contains straightforward screening justifications if the FEP is excluded from further consideration and a description of the TSPA disposition if it is included.

(5) Sufficient technical bases and justification are provided for total system performance assessment assumptions and approximations for modeling coupled thermal-hydrological-mechanical-chemical effects on seepage and flow, the waste package chemical environment, and the chemical environment for radionuclide release. The effects of distribution of flow on the amount of water contacting the engineered barriers and waste forms are consistently addressed, in all relevant abstractions.

Assumptions (Section 5) and approximations pertaining to coupled processes in the P&CE model, as well as their technical bases and justification, are provided throughout the report. FEPs involving coupled processes are discussed with their technical bases in Section 6.14. The seepage dilution/evaporation abstraction is consistent with the NFC seepage model, and the TSPA-LA lookup tables are designed to couple the thermal hydrology of the drift with the chemical environment in drift. This model report is not concerned with distribution of flow within the drift.

(6) The expected ranges of environmental conditions within the waste package emplacement drifts, inside of breached waste packages, and contacting the waste forms and their evolution with time are identified. These ranges may be developed to include:

(i) Effects of the drip shield and backfill on the quantity and chemistry of water (e.g., the potential for condensate formation and dripping from the underside of the shield)

(ii) Conditions that promote corrosion of engineered barriers and degradation of waste forms;

(iii) Irregular wet and dry cycles;

(iv) Gamma-radiolysis; and

(v) Size and distribution of penetrations of engineered barriers.

This report develops and presents the expected ranges of environmental conditions within the drifts (Sections 6.7, 6.8, 6.9, and 6.13). Although this model does characterize conditions that affect corrosion of engineered barriers (Section 6.13), it does not consider the effect of the drip shield or backfill (current design does not include backfill) on the quantity and chemistry of water. Wet and dry cycles, gamma radiolysis, and size and distribution of engineered barriers are not the subject of this report, although information from it may be used to assess those factors.

(7) The model abstraction for quantity and chemistry of water contacting engineered barriers and waste forms is consistent with the detailed information on engineered barrier design and other engineered features. For example, consistency is demonstrated for:

(i) Dimensionality of the abstractions;

(ii) Various design features and site characteristics; and

(iii) Alternative conceptual approaches.

Analyses are adequate to demonstrate that no deleterious effects are caused by design or site features that the DOE does not take into account in this abstraction.

The chemistry of water contacting engineered barriers was developed using detailed information on various designed (engineered) features and site characteristics (Section 4.1), although this report does not address dimensionality of the abstractions as they relate to water contacting engineered barriers. This report includes consideration of potential impacts from engineered materials: for example, the effect of introduced steels on in-drift water composition (Section 6.8) and the effect of evaporative concentration coupled with transport on the chemical environment at the surface of the waste package (Section 6.13). In addition, treatment of alternative conceptual approaches (Section 6.11) is consistent with engineered barrier design and other

engineered features. For those design or site features not incorporated in the P&CE model, analyses were done to ensure that there were no adverse impacts caused by their exclusion (see Section 6.14, as well as the relevant FEPs, for further details).

(8) Adequate technical bases are provided, including activities such as independent modeling, laboratory or field data, or sensitivity studies, for inclusion of any thermal-hydrologic-mechanical-chemical couplings and features, events, and processes.

This report summarizes the inclusion of coupled processes by development and use of the NFC process model. In addition, this report includes a brief evaluation of Onsager coupled processes, which are dominated by direct processes that are appropriately represented in the abstractions (Section 6.4). This report also includes sensitivity analyses that address the effects from engineered materials on the in-drift chemical environment (Sections 6.7 and 6.8).

(9) Performance-affecting processes that have been observed in thermal-hydrologic tests and experiments are included into the performance assessment. For example, the U.S. Department of Energy either demonstrates that liquid water will not reflux into the underground facility or incorporates refluxing water into the performance assessment calculation, and bounds the potential adverse effects of alteration of the hydraulic pathway that result from refluxing water.

The effects observed in thermal-hydrologic tests and experiments (from the DST) and ambient field data are used for validation of the NFC model (see Section 7.1). Results from the thermal-hydrological validated NFC model are developed and used in this report (Section 6.6) to generate results used by TSPA-LA (Sections 6.12 and 6.15).

(10) Likely modes for container corrosion (Section 2.2.1.3.1 of the Yucca Mountain Review Plan) are identified and considered in determining the quantity and chemistry of water entering the engineered barriers and contacting waste forms. For example, the model abstractions consistently address the role of parameters, such as pH, carbonate concentration, and the effect of corrosion on the quantity and chemistry of water contacting engineered barriers and waste forms.

As indicated in Section 1.2, one of the intended uses of this model is to provide TSPA-LA with quantified inputs for ionic strength, chloride and nitrate concentrations, and pH as functions of *RH*, pCO_2, and temperature. This information is then used in conjunction with another model supplying the *RH* and temperature information to then implement a third model—that developed in *General Corrosion and Localized Corrosion of Waste Package Outer Barrier* (SNL 2007 [DIRS 178519], Sections 6.3.1 and 6.3.2)—to determine if localized corrosion is occurring on the waste packages.

(12) Guidance in NUREG–1297 (Altman et al. 1988 [DIRS 103597]) and NUREG-1298 (Altman et al. 1988 [DIRS 103750]), or other acceptable approaches, is followed.

Inputs were selected and documented according to applicable Lead Lab procedures, which comply with NUREG-1297 and -1298 (Section 4.1).

8.4.1.2 Acceptance Criterion 2—Data Are Sufficient for Model Justification

(1) Geological, hydrological, and geochemical values used in the license application are adequately justified. Adequate description of how the data were used, interpreted, and appropriately synthesized into the parameters is provided.

The selection and justification of geological, hydrological, and geochemical values for use, along with sources of input data, are contained in Section 4.1 and tabulated in the Document Input Reference System. Further details of model development as related to the use, interpretation, and synthesis of data into parameters are presented throughout Section 6, especially in Section 6.3. The model was developed using water chemistry data collected in the ESF and adjoining facilities. The geochemical analyses presented in this report are based on a chemical thermodynamic database developed for this use from internationally accepted thermodynamic data (Sections 6.2 and 6.3).

(2) Sufficient data were collected on the characteristics of the natural system and engineered materials to establish initial and boundary conditions for conceptual models of thermal-hydrological-mechanical-chemical coupled processes, that affect seepage and flow and the engineered barrier chemical environment.

Data and technical information collected from field and experimental sources, and from literature searches for this model, are discussed for engineered materials in Section 4.1 (engineered components) and Section 6.5 (design features), and for natural system characteristics and the NFC model in Sections 6.3 and 6.6 (pore-water selection). Natural system data are used to develop the NFC model, which is developed and documented in this report and provides major feeds to the P&CE abstraction models (Section 6.3). The natural system data are used to establish initial and boundary conditions that affect seepage and flow and are discussed in Section 6.3. The discussion of the initial and boundary conditions that affect seepage and flow for the engineered material data is provided in Section 6.8. The effects on the chemical environment in the waste package from collected data are discussed in *In-Package Chemistry Abstraction* (SNL 2007 [DIRS 180506]).

(4) Sufficient information to formulate the conceptual approach(es) for analyzing water contact with the drip shield, engineered barriers, and waste forms is provided.

The conceptual approaches of this report's modeling of diluted and evaporated seepage waters are supported. This support comes both from other reports (e.g., SNL 2007 [DIRS 177411] and SNL 2007 [DIRS 177404] for support in Section 6.2; SNL 2007 [DIRS 181267] for support in Section 6.10), and from the analyses presented within this report: e.g., mineral inclusion or suppression (Section 6.2.5), oxygen availability (Section 6.7), and seepage water interaction with the introduced steels (Section 6.8).

8.4.1.3 Acceptance Criterion 3—Data Uncertainty Is Characterized and Propagated Through the Model Abstraction

(1) Models use parameter values, assumed ranges, probability distributions, and bounding assumptions that are technically defensible, reasonably account for uncertainties and variabilities, and do not result in an under-representation of the risk estimate.

The model parameter values were selected based on the characteristics of the input and are considered representative of the natural and engineered systems (Sections 4.1, 6.3, 6.5, 6.6, and 6.9). Ranges, probability distributions, and bounding assumptions were considered in assessing boundary conditions and input uncertainties and variabilities, which were propagated through the model as described in Section 6.12. Further propagation through TSPA-LA implementation is described in Section 6.15. When modeling decisions were necessary, the choices were made to result in conservative outcomes that avoid dilution of overall risk (Sections 6.3, 6.9, and 6.12).

(2) Parameter values, assumed ranges, probability distributions, and bounding assumptions used in the total system performance assessment calculations of quantity and chemistry of water contacting engineered barriers and waste forms are technically defensible and reasonable, based on data from the Yucca Mountain region (e.g., results from large block and drift-scale heater and niche tests), and a combination of techniques that may include laboratory experiments, field measurements, natural analog research, and process-level modeling studies.

The parameter values, assumed ranges, probability distributions, and bounding assumptions developed by other models based on site-specific data are discussed in Sections 5.1.1, 6.3, and 6.12. Values, ranges, and distributions obtained from other techniques mentioned above include such information as the thermodynamic databases, discussed in Section 4.1.3 with additional discussion in *In-Drift Precipitates/Salts Model* (SNL 2007 [DIRS 177411]); and corrosion data, discussed in Sections 6.5 and 6.8. The pore-water data founding model development was collected in the ESF and adjoining facilities. Environmental conditions imposed on model development (temperatures, *RH*, and moisture contents) were consistent with data collected from the DST and other related tests. The validation for the seepage dilution/evaporation and integrated invert chemistry abstractions has been performed by comparison against results directly from the IDPS process model (Section 7.2). Other laboratory and natural analogue information were used for additional confidence-building for this model (Section 7.3).

(3) Input values used in the total system performance assessment calculations of quantity and chemistry of water contacting engineered barriers (e.g., drip shield and waste package) are consistent with the initial and boundary conditions and the assumptions of the conceptual models and design concepts for the Yucca Mountain site. Correlations between input values are appropriately established in the U.S. Department of Energy total system performance assessment. Parameters used to define initial conditions, boundary conditions, and computational domain in sensitivity analyses

involving coupled thermal-hydrological-mechanical-chemical effects on seepage and flow, the waste package chemical environment, and the chemical environment for radionuclide release, are consistent with available data. Reasonable or conservative ranges of parameters or functional relations are established.

The input values (Section 4.1) were developed using initial and boundary conditions and assumptions (Section 5) common to other conceptual models and compatible with design concepts. Sensitivity studies involving coupled effects on the chemical environment were conducted (e.g., Sections 6.7 and 6.8). The initial and boundary conditions and computational domain for these sensitivity analyses were determined using parameters that are consistent with available data. This report uses the same technical bases and other information used in other TSPA-LA-supporting documents concerned with engineered barrier and waste form performance. The conceptual model that forms the basis for this report is consistent with other engineered system models and repository design. Primary input is taken from the IDPS model and is developed within this report as the NFC process model (Section 6.3); this input is used to generate in-drift water chemistry. Sections 6.3 and 6.12.3 provide details of these model interfaces.

Correlations between input values were established and used at various points in the P&CE model (Sections 6.3, 6.7, and 6.13). For example, the NFC input water and gas chemistries are correlated to each other, to temperature, and to relative humidity. Additionally, the correlation of chloride and nitrate are accounted for in the way their uncertainties are determined (Section 6.12) and implemented (Section 6.15).

The ranges of parameters and functional relations developed in this report, primarily as lookup tables (Section 6.9), are considered reasonable or conservative. Section 6.15 discusses the appropriate use of these tables, which are equilibrium chemical response surfaces that relate water chemistry to relative humidity, temperature, and pCO_2.

(4) Adequate representation of uncertainties in the characteristics of the natural system and engineered materials is provided in parameter development for conceptual models, process-level models, and alternative conceptual models. The U.S. Department of Energy may constrain these uncertainties using sensitivity analyses or conservative limits. For example, the U.S. Department of Energy demonstrates how parameters used to describe flow through the EBS bound the effects of backfill and excavation-induced changes.

Uncertainties in natural system characteristics are included in the NFC model (Sections 6.3 and 6.12), which is used by the P&CE abstraction models. Uncertainties in the Pitzer database have been modified for one-time use by this report, renamed as file *data0.pce* (Output DTN: SN0703PAEBSPCE.006) This has been used as direct input to this model and is discussed in Section 6.3. Engineered materials uncertainties are specifically considered in Section 6.5, and discussions on the effects of dust in Section 6.10. Section 6.12 discusses all key uncertainties in the NFC process model and the P&CE abstraction models developed in this report.

8.4.1.4 Acceptance Criterion 4—Model Uncertainty Is Characterized and Propagated Through the Model Abstraction

(1) Alternative modeling approaches of features, events, and processes are considered and are consistent with available data and current scientific understanding, and the results and limitations are appropriately considered in the abstraction.

The evaluation of FEPs documented in Section 6.14 is based on the model results developed in this report, including the alternative model discussed in Section 6.11. This alternative modeling is consistent with available data and scientific understanding. The results and limitations of the alternative FEP modeling and their impact on the engineered barrier chemical environment are presented in Section 6.14.

(2) Alternative modeling approaches are considered and the selected modeling approach is consistent with available data and current scientific understanding. A description that includes a discussion of alternative modeling approaches not considered in the final analysis and the limitations and uncertainties of the chosen model is provided.

Section 6.11 describes an alternative modeling approach considered for the development of the NFC process model, the key feed for the P&CE abstraction models The alternative model was not selected for further use. For the alternative model, brief descriptions and the rationale for exclusion are included as well as references to other reports and sections within this report for further detail. These references also contain information about the models that were selected, including their technical bases, limitations, and uncertainties.

(3) Consideration of conceptual model uncertainty is consistent with available site characterization data, laboratory experiments, field measurements, natural analog information and process-level modeling studies; and the treatment of conceptual model uncertainty does not result in an under-representation of the risk estimate.

Uncertainties in inputs and in analytical methodology are considered in the development of the conceptual model (Section 6.3) and output parameters (Section 6.15). Discussion of uncertainty in the conceptual model appears in various places throughout the report. The uncertainty evaluation is consistent with available site-specific data, laboratory experiments, field studies, natural analogue data, and process-level modeling studies. In addition, model validation is based on available site characterization data, laboratory experiments, and comparisons of NFC model outputs to outputs from the THC seepage report (SNL 2007 [DIRS 177404]) that was independently developed for a similar intended use (Section 7.1). The treatment of conceptual model uncertainty described in this report does not under-represent risk.

(4) Adequate consideration is given to effects of thermal-hydrological-mechanical-chemical coupled processes in the assessment of alternative conceptual models. These effects may include:

(i) Thermal-hydrologic effects on gas, water, and mineral chemistry;

(ii) Effects of microbial processes on the engineered barrier chemical environment and the chemical environment for radionuclide release;

(iii) Changes in water chemistry that may result from the release of corrosion products from the waste package and interactions between engineered materials and ground water; and

(iv) Changes in boundary conditions (e.g., drift shape and size) and hydrologic properties, relating to the response of the geomechanical system to thermal loading.

The effects of coupled processes were considered during the assessment of alternative conceptual models (Section 6.11). Section 6.11 provides details on an investigation of an alternative method for deriving NFC seepage waters. This alternative method incorporates coupled thermal-hydrologic-chemical processes as does the NFC process model (Section 6.3).

8.4.1.5 Acceptance Criterion 5—Model Abstraction Output Is Supported by Objective Comparisons

(1) The models implemented in this total system performance assessment abstraction provide results consistent with output from detailed process-level models and/or empirical observations (laboratory and field testings and/or natural analogs).

Information provided to the TSPA-LA was developed using two detailed process-level models: the NFC model (Section 6.3) and the IDPS model (SNL 2007 [DIRS 177411]). The resulting abstracted model output provided for implementation in TSPA-LA is consistent with the related process-level model output (Section 7). For appropriate cases, validation against empirical observation is also provided (Section 7).

(2) Abstracted models for coupled thermal-hydrological-mechanical-chemical effects on seepage and flow and the engineered barrier chemical environment, as well as on the chemical environment for radionuclide release, are based on the same assumptions and approximations demonstrated to be appropriate for process-level models or closely analogous natural or experimental systems. For example, abstractions of processes, such as thermally induced changes in hydrological properties, or estimated diversion of percolation away from the drifts, are adequately justified by comparison to results of process-level modeling, that are consistent with direct observations and field studies.

The abstracted model is based on the same assumptions and approximations demonstrated to be appropriate for process-level models. Coupled thermal-hydrologic-chemical considerations are the dominant factor in the development of this model abstraction. The output of this model is a tabulation of chemical conditions as a function of physical environmental conditions that is consistent with process-level modeling as demonstrated by model validation results (Section 7), which are in turn consistent with direct observations from laboratory and field studies.

(3) Accepted and well-documented procedures are used to construct and test the numerical models that simulate coupled thermal-hydrological-mechanical-chemical effects on seepage and flow, engineered barrier chemical environment, and the chemical environment for radionuclide release. Analytical and numerical models are appropriately supported. Abstracted model results are compared with different mathematical models, to judge robustness of results.

Accepted and well-documented procedures contained in the Quality Assurance Program (Section 2) governed the development of this report and the work it documents. The P&CE suite of models were constructed, supported, and documented according to SCI-PRO-002. Test and validation methods (Section 7), including comparison of abstracted output with that of other relevant models, also comply with SCI-PRO-002, as well as with applicable written guidance. This report was generated according to the requirements of *Technical Work Plan for: Near-Field Environment and Transport In-Drift Geochemistry Model Report Integration* (SNL 2007 [DIRS 179287]), as directed by SCI-PRO-006.

9. REFERENCES

9.1 DOCUMENTS CITED

127579 AISC (American Institute of Steel Construction) 1991. *Manual of Steel Construction, Allowable Stress Design.* 9th Edition, 1st Revision. Chicago, Illinois: American Institute of Steel Construction. TIC: 4254.

103750 Altman, W.D.; Donnelly, J.P.; and Kennedy, J.E. 1988. *Qualification of Existing Data for High-Level Nuclear Waste Repositories: Generic Technical Position.* NUREG-1298. Washington, D.C.: U.S. Nuclear Regulatory Commission. TIC: 200652.

103597 Altman, W.D.; Donnelly, J.P.; and Kennedy, J.E. 1988. *Peer Review for High-Level Nuclear Waste Repositories: Generic Technical Position.* NUREG-1297. Washington, D.C.: U.S. Nuclear Regulatory Commission. TIC: 200651.

105701 Amonette, J.E. and Rai, D. 1990. "Identification of Noncrystalline (Fe,Cr)(OH)3 by Infrared Spectroscopy." *Clays and Clay Minerals, 38,* (2), 129-136. Boulder, Colorado: Clay Minerals Society. TIC: 243615.

172858 Apted, M.; King, F.; Langmuir, D.; Arthur, R.; and Kessler, J. 2005. "The Unlikelihood of Localized Corrosion of Nuclear Waste Packages Arising from Deliquescent Brine Formation." *Journal of Metals, 57,* (1), 43-48. Warrendale, Pennsylvania: The Minerals, Metals & Materials Society. TIC: 257253.

103753 ASM International. 1987. *Corrosion.* Volume 13 of *Metals Handbook.* 9th Edition. Metals Park, Ohio: ASM International. TIC: 209807.

163015 Ball, J.W. and Nordstrom, D.K. 1998. "Critical Evaluation and Selection of Standard State Thermodynamic Properties for Chromium Metal and its Aqueous Ions, Hydrolysis Species, Oxides, and Hydroxides." *Journal of Chemical & Engineering Data, 43,* (6), 895-918. Washington, D.C.: American Chemical Society. TIC: 254015.

105730 Baron, D. and Palmer, C.D. 1996. "Solubility of KFe3(CrO4)2(OH)6 at 4 to 35°C." *Geochimica et Cosmochimica Acta, 60,* (20), 3815-3824. New York, New York: Elsevier. TIC: 243731.

162270 Bethke, C.M. 1996. *Geochemical Reaction Modeling, Concepts and Applications.* New York, New York: Oxford University Press. TIC: 252884.

100006 Bish, D.L. and Aronson, J.L. 1993. "Paleogeothermal and Paleohydrologic Conditions in Silicic Tuff from Yucca Mountain, Nevada." *Clays and Clay Minerals, 41,* (2), 148-161. Long Island City, New York: Pergamon Press. TIC: 224613.

101196 Bish, D.L. and Vaniman, D.T. 1985. *Mineralogic Summary of Yucca Mountain, Nevada.* LA-10543-MS. Los Alamos, New Mexico: Los Alamos National Laboratory. ACC: MOL.19950412.0041.

169638 Bish, D.L.; Vaniman, D.T.; Chipera, S.J.; and Carey, J.W. 2003. "The Distribution of Zeolites and their Effects on the Performance of a Nuclear Waste Repository at Yucca Mountain, Nevada, U.S.A.." *American Mineralogist, 88,* (11-12, Part 2), 1889–1902. Washington, D.C.: Mineralogical Society of America. TIC: 255986.

126590 Blum, A.E. and Stillings, L.L. 1995. "Feldspar Dissolution Kinetics." Chapter 7 of *Chemical Weathering Rates of Silicate Minerals.* White, A.F. and Brantley, S.L., eds. Reviews in Mineralogy Volume 31. Washington, D.C.: Mineralogical Society of America. TIC: 222496.

163699 Bomberger, H.B.; Cambourelis, P.J.; and Hutchinson, G.E. 1954. "Corrosion Properties of Titanium in Marine Environments." *Journal of the Electrochemical Society, 101,* (9), 442-447. New York, New York: Electrochemical Society. TIC: 254366.

156639 Borchardt, G. 1995. "Smectites." Chapter 14 of *Minerals in Soil Environments.* 2nd Edition. Dixon J.B. and Weed, S.B., eds. SSSA Book Series, No. 1. Madison, Wisconsin: Soil Science Society of America. TIC: 237222.

182475 Brady, P.V. 1991. "The Effect of Silicate Weathering on Global Temperature and Atmospheric CO_2." *Journal of Geophysical Research, 96,* (B11), 18101-18106. Washington, D.C.: American Geophysical Union. TIC: 259671.

100883 Brasher, D.M. and Mercer, A.D. 1968. "Comparative Study of Factors Influencing the Action of Corrosion Inhibitors for Mild Steel in Neutral Solution, I. Sodium Benzoate." *British Corrosion Journal, 3,* 120-129. London, England: British Joint Corrosion Group. TIC: 236434.

105092 Brookins, D.G. 1988. *Eh-pH Diagrams for Geochemistry.* New York, New York: Springer-Verlag. TIC: 237943.

110969 Bruno, J.; Duro, L.; de Pablo, J.; Casas, I.; Ayora, C.; Delgado, J.; Gimeno, M.J.; Peña, J.; Linklater, C.; Pérez del Villar, L.; and Gómez, P. 1998. "Estimation of the Concentrations of Trace Metals in Natural Systems. The Application of Codissolution and Coprecipitation Approaches to El Berrocal (Spain) and Poços de Caldas (Brazil)." *Chemical Geology, 151,* 277-291. Amsterdam, The Netherlands: Elsevier. TIC: 246492.

169982 BSC (Bechtel SAIC Company) 2004. *Aqueous Corrosion Rates for Waste Package Materials.* ANL-DSD-MD-000001 REV 01. Las Vegas, Nevada: Bechtel SAIC Company. ACC: DOC.20041012.0003; DOC.20060403.0001.

169991 BSC 2004. *Evaluation of Potential Impacts of Microbial Activities on Drift Chemistry.* ANL-EBS-MD-000038 REV 01. Las Vegas, Nevada: Bechtel SAIC Company. ACC: DOC.20041118.0005; DOC.20050505.0001; DOC.20050609.0001.

170003 BSC 2004. *Heat Capacity Analysis Report.* ANL-NBS-GS-000013 REV 01. Las Vegas, Nevada: Bechtel SAIC Company. ACC: DOC.20041101.0003.

164327 BSC 2004. *In-Drift Natural Convection and Condensation.* MDL-EBS-MD-000001 REV 00. Las Vegas, Nevada: Bechtel SAIC Company. ACC: DOC.20041025.0006; DOC.20050330.0001; DOC.20051122.0005.

170031 BSC 2004. *Mineralogic Model (MM3.0) Report.* MDL-NBS-GS-000003 REV 01. Las Vegas, Nevada: Bechtel SAIC Company. ACC: DOC.20040908.0006.

169862 BSC 2004. *Ventilation Model and Analysis Report.* ANL-EBS-MD-000030 REV 04. Las Vegas, Nevada: Bechtel SAIC Company. ACC: DOC.20041025.0002.

169734 BSC 2004. *Yucca Mountain Site Description.* TDR-CRW-GS-000001 REV 02 ICN 01. Two volumes. Las Vegas, Nevada: Bechtel SAIC Company. ACC: DOC.20040504.0008.

175539 BSC 2005. *Q-List.* 000-30R-MGR0-00500-000-003. Las Vegas, Nevada: Bechtel SAIC Company. ACC: ENG.20050929.0008.

102177 Byers, F.M., Jr.; Carr, W.J.; and Orkild, P.P. 1989. "Volcanic Centers of Southwestern Nevada: Evolution of Understanding, 1960-1988." *Journal of Geophysical Research, 94,* (B5), 5908-5924. Washington, D.C.: American Geophysical Union. TIC: 224013.

105213 Carlos, B.A.; Chipera, S.J.; Bish, D.L.; and Raymond, R. 1995. "Distribution and Chemistry of Fracture-Lining Zeolites at Yucca Mountain, Nevada." *Natural Zeolites '93: Occurrence, Properties, Use, Proceedings of the 4th International Conference on the Occurrence, Properties, and Utilization of Natural Zeolites, June 20-28, 1993, Boise, Idaho.* Ming, D.W. and Mumpton, F.A., eds. Pages 547-563. Brockport, New York: International Committee on Natural Zeolites. TIC: 243086.

138706 Carnahan, C.L. 1987. *Effects of Coupled Thermal, Hydrological and Chemical Processes on Nuclide Transport.* LBL-23186. Berkeley, California: Lawrence Berkeley National Laboratory. TIC: 232514.

100968 Carslaw, H.S. and Jaeger, J.C. 1959. *Conduction of Heat in Solids.* 2nd Edition. Oxford, Great Britain: Oxford University Press. TIC: 206085.

111081 Chipera, S.J.; Vaniman, D.T.; Carlos, B.A.; and Bish, D.L. 1995. *Mineralogic Variation in Drill Core UE-25 UZ#16, Yucca Mountain, Nevada.* LA-12810-MS. Los Alamos, New Mexico: Los Alamos National Laboratory. ACC: NNA.19940427.0099.

105735 Claassen, H.C. and White, A.F. 1979. "Application of Geochemical Kinetic Data to Groundwater Systems: A Tuffaceous-Rock System in Southern Nevada." Chapter 34 of *Chemical Modeling in Aqueous Systems: Speciation, Sorption, Solubility, and Kinetics.* Jenne, E.A., ed. ACS Symposium Series 93. Washington, D.C.: American Chemical Society. TIC: 208922.

105732 Cotton, F.A. and Wilkinson, G. 1988. *Advanced Inorganic Chemistry.* 5th Edition. New York, New York: John Wiley & Sons. TIC: 236867.

100359 CRWMS (Civilian Radioactive Waste Management System) M&O (Management and Operating Contractor) 1998. "Waste Package Degradation Modeling and Abstraction." Chapter 5 of *Total System Performance Assessment-Viability Assessment (TSPA-VA) Analyses Technical Basis Document.* B00000000-01717-4301-00005 REV 01. Las Vegas, Nevada: CRWMS M&O. ACC: MOL.19981008.0005.

111115 CRWMS M&O 1998. *Drift Scale Test As-Built Report.* BAB000000-01717-5700-00003 REV 01. Las Vegas, Nevada: CRWMS M&O. ACC: MOL.19990107.0223.

162482 Davies, C.W. 1962. *Ion Association.* Washington, D.C.: Butterworths. TIC: 244840.

100439 de Marsily, G. 1986. *Quantitative Hydrogeology: Groundwater Hydrology for Engineers.* San Diego, California: Academic Press. TIC: 208450.

162338 Deer, W.A.; Howie, R.A.; and Zussman, J. 1967. *An Introduction to the Rock-Forming Minerals.* New York, New York: John Wiley and Sons. TIC: 234769.

105778 Deng, Y.; Stjernstrom, M.; and Banwart S. 1996. "Accumulation and Remobilization of Aqueous Chromium (VI) at Iron Oxide Surfaces: Application of a Thin-film Continuous Flow-through Reactor." *Journal of Contaminant Hydrology, 21,* 141-151. Amsterdam, The Netherlands: Elsevier. TIC: 243062.

182051 DOE (U.S. Department of Energy) 2007. *Quality Assurance Requirements and Description.* DOE/RW-0333P, Rev. 19. Washington, D. C.: U.S. Department of Energy, Office of Civilian Radioactive Waste Management. ACC: DOC.20070717.0006.

118564 Drever, J.I. 1988. *The Geochemistry of Natural Waters.* 2nd Edition. Englewood Cliffs, New Jersey: Prentice-Hall. TIC: 242836.

147480 Drever, J.I. 1997. "Evaporation and Saline Waters." Chapter 15 of *The Geochemistry of Natural Waters: Surface and Groundwater Environments.* 3rd Edition. Upper Saddle River, New Jersey: Prentice Hall. TIC: 246732.

105780 Eary, L.E. and Rai, D. 1987. "Kinetics of Chromium(III) Oxidation to Chromium(VI) by Reaction with Manganese Dioxide." *Environmental Science & Technology, 21,* (12), 1187-1193. Washington, D.C.: American Chemical Society. TIC: 243224.

105784 Eary, L.E. and Rai, D. 1988. "Chromate Removal from Aqueous Wastes by Reduction with Ferrous Ion." *Environmental Science & Technology, 22,* (8), 972-977. Washington, D.C.: American Chemical Society. TIC: 243600.

105788 Eary, L.E. and Rai, D. 1989. "Kinetics of Chromate Reduction by Ferrous Ions Derived from Hematite and Biotite at 25C." *American Journal of Science, 289,* 180-213. New Haven, Connecticut: Yale University. TIC: 243614.

100743 Eugster, H.P. and Hardie, L.A. 1978. "Saline Lakes." *Lakes, Chemistry, Geology, Physics.* Lerman, A., ed. Pages 237-293. New York, New York: Springer-Verlag. TIC: 240782.

178836 Evans, N.J.; Wilson, N.S.F.; Cline, J.S.; McInnes, B.I.A.; and Byrne. J. 2005. "Fluorite (U-Th)/He Thermochronology: Constraints on the Low Temperature History of Yucca Mountain, Nevada." *Applied Geochemistry, 20,* 1099-1105. New York, New York: Elsevier. TIC: 259246.

162282 Faust, G.T. 1953. "Huntite, $Mg_3Ca(CO_3)_4$, a New Mineral." *American Mineralogist, 38,* (1-2), 4-24. Washington, D.C.: Mineralogical Society of America. TIC: 252888.

105795 Fitzpatrick, R.W.; Le Roux, J.; and Schwertmann, U. 1978. "Amorphous and Crystalline Titanium and Iron-Titanium Oxides in Synthetic Preparations, at Near Ambient Conditions, and in Soil Clays." *Clays and Clay Minerals, 26,* (3), 189-201. Boulder, Colorado: Clay Minerals Society. TIC: 242847.

162312 Fleischer, M. and Efremov, N. 1954. "New Mineral Names." *American Mineralogist, 39,* (3-4), 402-408. Washington, D.C.: Mineralogical Society of America. TIC: 252897.

162284 Fleischer, M. and Pabst, A. 1983. "New Mineral Names." *Journal of the Mineralogical Society of America, 68,* (1-2), 281-283. Washington, D.C.: Mineralogical Society of America. TIC: 252898.

100033 Flint, L.E. 1998. *Characterization of Hydrogeologic Units Using Matrix Properties, Yucca Mountain, Nevada.* Water-Resources Investigations Report 97-4243. Denver, Colorado: U.S. Geological Survey. ACC: MOL.19980429.0512.

159343 Forgeson, B.W.; Southwell, C.R.; Alexander, A.L.; Mundt, H.W.; and Thompson, L.J. 1958. "Corrosion of Metals in Tropical Environments, (Part 1—Five Non-Ferrous Metals and a Structural Steel)." *Corrosion, 14,* (2), 73t-81t. Houston, Texas: National Association of Corrosion Engineers. TIC: 223373.

144877 Garrels, R.M. and Christ, C.L. 1990. *Solutions, Minerals, and Equilibria.* Boston, Massachusetts: Jones and Bartlett Publishers. TIC: 223483.

154800 Gascoyne, M.; Miller, N.H.; and Neymark, L.A. 2002. "Uranium-Series Disequilibrium in Tuffs from Yucca Mountain, Nevada, as Evidence of Pore-Fluid Flow Over the Last Million Years." *Applied Geochemistry, 17,* (6), 781-792. New York, New York: Elsevier. TIC: 251901.

176844 Gunnarsson, I.; Arnórsson, S.; and Jakobsson, S. 2005. "Precipitation of Poorly Crystalline Antigorite Under Hydrothermal Conditions." *Geochimica et Cosmochimica Acta, 69,* (11), 2813-2828. New York, New York: Elsevier. TIC: 258287.

105175 Haar, L.; Gallagher, J.S.; and Kell, G.S. 1984. *NBS/NRC Steam Tables: Thermodynamic and Transport Properties and Computer Programs for Vapor and Liquid States of Water in SI Units.* New York, New York: Hemisphere Publishing Corporation. TIC: 241793.

170586 Hall, D. and Walton, J. 2003. "Physical Separation Processes and EBS Water Chemistry – A Modeling Study." *Proceedings of the 10th International High-Level Radioactive Waste Management Conference (IHLRWM), March 30-April 2, 2003, Las Vegas, Nevada.* Pages 624-628. La Grange Park, Illinois: American Nuclear Society. TIC: 254559.

100580 Harr, M.E. 1987. *Reliability-Based Design in Civil Engineering.* New York, New York: McGraw-Hill. TIC: 240687.

100814 Harrar, J.E.; Carley, J.F.; Isherwood, W.F.; and Raber, E. 1990. *Report of the Committee to Review the Use of J-13 Well Water in Nevada Nuclear Waste Storage Investigations.* UCID-21867. Livermore, California: Lawrence Livermore National Laboratory. ACC: NNA.19910131.0274.

105965 Hay, R.L. 1966. *Zeolites and Zeolitic Reactions in Sedimentary Rocks.* Special Paper 85. Boulder, Colorado: Geological Society of America. TIC: 238294.

162281 Hay, R.L. and Wiggins, B. 1980. "Pellets, Ooids, Sepiolite and Silica in Three Calcretes of the Southwestern United States." *Sedimentology, 27,* 559-576. Malden, Massachusetts: Blackwell Publishing. TIC: 222806.

162090 He, S. and Morse, J.W. 1993. "The Carbonic Acid System and Calcite Solubility in Aqueous Na-K-Ca-Mg-Cl-SO_4 Solutions from 0 to 90°C." *Geochimica et Cosmochimica Acta, 57,* (15), 3533-3554. New York, New York: Pergamon Press. TIC: 253894.

137246 Helgeson, H.C. 1969. "Thermodynamics of Hydrothermal Systems at Elevated Temperatures and Pressures." *American Journal of Science, 267,* (6), 729-804. New Haven, Connecticut: Scholarly Publications. TIC: 241817.

140382 Helgeson, H.C.; Murphy, W.M.; and Aagaard, P. 1984. "Thermodynamic and Kinetic Constraints on Reaction Rates Among Minerals and Aqueous Solutions, II. Rate Constants, Effective Surface Area, and the Hydrolysis of Feldspar." *Geochimica et Cosmochimica Acta, 48,* 2405-2432. New York, New York: Pergamon Press. TIC: 220177.

115670 Hem, J.D. 1985. *Study and Interpretation of the Chemical Characteristics of Natural Water.* 3rd Edition. Geological Survey Water-Supply Paper 2254. Washington, D.C.: U.S. Government Printing Office. ACC: NNA.19940427.0181.

105854 Hem, J.D.; Lind, C.J.; and Roberson, C.E. 1989. "Coprecipitation and Redox Reactions of Manganese Oxides with Copper and Nickel." *Geochimica et Cosmochimica Acta, 53,* 2811-2822. New York, New York: Pergamon Press. TIC: 243113.

163031 Hrma, P.; Piepel, G.F.; Vienna, J.D.; Cooley, S.K.; Kim, D.S.; and Russell, R.L. 2001. *Database and Interim Glass Property Models for Hanford HLW Glasses.* PNNL-13573. Richland, Washington: Pacific Northwest National Laboratory. TIC: 254061.

181199 Hummel, W. and Curti, E. 2003. "Nickel Aqueous Speciation and Solubility at Ambient Conditions: A Thermodynamic Elegy." *Monatshefte für Chemie, 134,* 941-973. New York, New York: Springer-Verlag. TIC: 259453.

158974 HydroGeoLogic and Allison Geoscience Consultants. 1999. *MINTEQA2/PRODEFA2, A Geochemical Assessment Model for Environmental Systems: User Manual Supplement for Version 4.0.* Athens, Georgia: U.S. Environmental Protection Agency, National Exposure Research Laboratory. TIC: 252456.

163337 Incropera, F.P. and DeWitt, D.P. 2002. *Fundamentals of Heat and Mass Transfer.* 5th Edition. New York, New York: John Wiley & Sons. TIC: 254280.

108184 Incropera, F.P. and DeWitt, D.P. 1996. *Fundamentals of Heat and Mass Transfer.* 4th Edition. New York, New York: John Wiley & Sons. TIC: 243950.

181136 Ishikawa, T.; Yoshida, T.; Kandori, K.; Nakayma, T.; and Hara, S. 2007. "Assessment of Protective Function of Steel Rust Layers by N_2 Adsorption." *Corrosion Science, 49,* 1468-1477. New York, New York: Elsevier. TIC: 259431.

105878 Johnson, C.A. and Xyla, A.G. 1991. "The Oxidation of Chromium (III) to Chromium (VI) on the Surface of Manganite (MnOOH)." *Geochimica et Cosmochimica Acta, 55,* 2861-2866. New York, New York: Pergamon Press. TIC: 243616.

162560 Johnson, T.M. and DePaolo, D.J. 1994. "Interpretation of Isotopic Data in Groundwater-Rock Systems: Model Development and Application to Sr Isotope Data from Yucca Mountain." *Water Resources Research, 30,* (5), 1571-1587. Washington, D.C.: American Geophysical Union. TIC: 252320.

168509 Jovancicevic, V. and Bockris, J.O'M. 1986. "The Mechanism of Oxygen Reduction on Iron in Neutral Solutions." *Journal of the Electrochemical Society, 133,* (9), 1797-1807. Manchester, New Hampshire: Electrochemical Society. TIC: 255668.

181151 Kamimura, T.; Hara, S.; Miyuki, H.; Yamashita M.; and Uchida H. 2006. "Composition and Protective Ability of Rust Layer Formed on Weathering Steel Exposed to Various Environments." *Corrosion Science, 48,* 2799-2812. New York, New York: Elsevier. TIC: 259445.

161606 Kerr, P.F. 1977. *Optical Mineralogy.* 4th Edition. New York, New York: McGraw-Hill. TIC: 252886.

124293 Klein, C. and Hurlbut, C.S., Jr. 1999. *Manual of Mineralogy.* 21st Edition, Revised. New York, New York: John Wiley & Sons. TIC: 246258.

125329 Koorevaar, P.; Menelik, G.; and Dirksen, C. 1983. *Elements of Soil Physics.* Developments in Soil Science 13. New York, New York: Elsevier. TIC: 246286.

105909 Krauskopf, K.B. 1979. *Introduction to Geochemistry.* 2nd Edition. New York, New York: McGraw-Hill. TIC: 242816.

100051 Langmuir, D. 1997. *Aqueous Environmental Geochemistry.* Upper Saddle River, New Jersey: Prentice Hall. TIC: 237107.

106466 Lasaga, A.C.; Soler, J.M.; Ganor, J.; Burch, T.E.; and Nagy, K.L. 1994. "Chemical Weathering Rate Laws and Global Geochemical Cycles." *Geochimica et Cosmochimica Acta, 58,* (10), 2361-2386. New York, New York: Pergamon. TIC: 237441.

133364 Levy, S. and O'Neil, J. 1986. "Moderate Temperature Zeolitic Alteration in a Cooling Pyroclastic Deposit." *Fifth International Symposium on Water-Rock Interaction, Reykjavik, 8-17 August 1986, Extended Abstracts.* LA-UR-86-1248. Pages 361-364. Los Alamos, New Mexico: Los Alamos National Laboratory. TIC: 223793.

159034 Li, G.; Peacor, D.R.; Coombs, D.S.; and Kawachi, Y. 1997. "Solid Solution in the Celadonite Family: The New Minerals Ferroceladonite, $K_2Fe^2{}_2+Fe^3{}_2+Si_8O_{20}(OH)_4$, and Ferroaluminoceladonite, $K_2Fe^2{}_2+Al_2Si_8O_{20}(OH)_4$." *American Mineralogist, 82,* (5-6), 503-511. Washington, D.C.: Mineralogical Society of America. TIC: 252472.

162229 Lide, D.R., ed. 2000. *CRC Handbook of Chemistry and Physics.* 81st Edition. Boca Raton, Florida: CRC Press. TIC: 253056.

166192 Linke, W.F. 1958. *Solubilities, Inorganic and Metal-Organic Compounds.* 4th Edition. Volume I, A–Ir. Washington, D.C.: American Chemical Society. TIC: 255159.

166191 Linke, W.F. 1965. *Solubilities, Inorganic and Metal-Organic Compounds.* 4th Edition. Volume II, K–Z. Washington, D.C.: American Chemical Society. TIC: 222176.

156503 Marshall, B.D. and Futa, K. 2001. "Strontium Isotope Evolution of Pore Water and Calcite in the Topopah Spring Tuff, Yucca Mountain, Nevada." *"Back to the Future - Managing the Back End of the Nuclear Fuel Cycle to Create a More Secure Energy Future," Proceedings of the 9th International High-Level Radioactive Waste Management Conference (IHLRWM), Las Vegas, Nevada, April 29-May 3, 2001.* La Grange Park, Illinois: American Nuclear Society. TIC: 247873.

114637 McCright, R.D. 1998. *Corrosion Data and Modeling, Update for Viability Assessment.* Volume 3 of *Engineered Materials Characterization Report.* UCRL-ID-119564, Rev. 1.1. Livermore, California: Lawrence Livermore National Laboratory. ACC: MOL.19980806.0177.

108954 McLean, J.E. and Bledsoe, B.E. 1992. *Behavior of Metals in Soils.* EPA/540/S-92/018. Washington, D.C.: U.S. Environmental Protection Agency. TIC: 243412.

181601 Miller, J.N. and Miller, J.C. 2000. *Statistics and Chemometrics for Analytical Chemistry.* 4th Edition. New York, New York: Prentice Hall. TIC: 254022.

163274 NRC (U.S. Nuclear Regulatory Commission) 2003. *Yucca Mountain Review Plan, Final Report.* NUREG-1804, Rev. 2. Washington, D.C.: U.S. Nuclear Regulatory Commission, Office of Nuclear Material Safety and Safeguards. TIC: 254568.

181153 Ostwald, C. and Grabke, H.J. 2004. "Initial Oxidation and Chromium Diffusion. I. Effects of Surface Working on 9–20% Cr Steels." *Corrosion Science, 46,* 1113-1127. New York, New York: Elsevier. TIC: 259446.

174513 Paces, J.B. and Neymark, L.A. 2004. "U-Series Evidence of Water-Rock Interaction at Yucca Mountain, Nevada, USA." *Proceedings of the Eleventh International Symposium on Water-Rock Interaction, WRI-11, 27 June-2 July 2004.* Wanty, R.B. and Seal, R.R., II, eds. *1,* 475-479. New York, New York: A.A. Balkema Publishers. TIC: 257516.

156507 Paces, J.B.; Neymark, L.A.; Marshall, B.D.; Whelan, J.F.; and Peterman, Z.E. 2001. *Ages and Origins of Calcite and Opal in the Exploratory Studies Facility Tunnel, Yucca Mountain, Nevada.* Water-Resources Investigations Report 01-4049. Denver, Colorado: U.S. Geological Survey. TIC: 251284.

162280 Palache, C.; Berman, H.; and Frondel, C. 1951. *Halides, Nitrates, Borates, Carbonates, Sulfates, Phosphates, Arsenates, Tungstates, Molybdates, Etc.* Volume II of *The System of Mineralogy of James Dwight Dana and Edward Salisbury Dana, Yale University 1837–1892.* 7th Edition. New York, New York: John Wiley & Sons. TIC: 209332.

181103 Palandri, J.L. and Reed, M.H. 2001. "Reconstruction of In Situ Composition of Sedimentary Formation Waters." *Geochimica et Cosmochimica Acta, 65,* (11), 1741-1767. New York, New York: Pergamon. TIC: 259444.

108991 Palmer, C.D. and Puls, R.W. 1994. *Natural Attenuation of Hexavalent Chromium in Ground Water and Soils.* EPA/540/S-94/505. Washington, D.C.: U.S. Environmental Protection Agency. TIC: 243413.

105952 Pankow, J.F. 1991. *Aquatic Chemistry Concepts.* Chelsea, Michigan: Lewis Publishers. TIC: 242999.

162274 Papke, K.G. 1976. *Evaporites and Brines in Nevada Playas.* Nevada Bureau of Mines and Geology Bulletin 87. Reno, Nevada: University of Nevada, Reno, Mackay School of Mines. TIC: 211869.

142177 Parkhurst, D.L. 1995. *User's Guide to PHREEQC—A Computer Program for Speciation, Reaction-Path, Advective-Transport, and Inverse Geochemical Calculations.* Water-Resources Investigations Report 95-4227. Lakewood, Colorado: U.S. Geological Survey. TIC: 248314.

163030 Perez, J.M., Jr.; Bickford, D.F.; Day, D.E.; Kim, D.S.; Lambert, S.L.; Marra, S.L.; Peeler, D.K.; Strachan, D.M.; Triplett, M.B.; Vienna, J.D.; and Wittman, R.S. 2001. *High-Level Waste Melter Study Report.* PNNL-13582. Richland, Washington: Pacific Northwest National Laboratory. TIC: 254062.

162576 Peterman, Z.E. and Cloke, P.L. 2002. "Geochemistry of Rock Units at the Potential Repository Level, Yucca Mountain, Nevada (includes Erratum)." *Applied Geochemistry, 17,* (6, 7), 683-698, 955-958. New York, New York: Pergamon. TIC: 252516; 252517; 254046.

105955 Pettine, M.; D'Ottone, L.; Campanella, L.; Millero, F.J.; and Passino, R. 1998. "The Reduction of Chromium(VI) by Iron(II) in Aqueous Solutions." *Geochimica et Cosmochimica Acta, 62,* (9), 1509-1519. New York, New York: Pergamon Press. TIC: 243059.

100923 Phipps, P.B.P. and Rice, D.W. 1979. "The Role of Water in Atmospheric Corrosion." Chapter 8 of *Corrosion Chemistry.* Brubaker, G.R. and Phipps, P.B.P., eds. ACS Symposium Series 89. Washington, D.C.: American Chemical Society. TIC: 240725.

181149 Pieragi, B.; MacDougall, B.; and Rapp, R.A. 2005. "The Role of the Metal/Oxide Interface in the Growth of Passive Films in Aqueous Environments." *Corrosion Science, 47,* 247-256. New York, New York: Elsevier. TIC: 259447.

162481 Pitzer, K.S. 1987. "A Thermodynamic Model for Aqueous Solutions of Liquid-Like Density." *Thermodynamic Modeling of Geological Materials: Minerals, Fluids and Melts.* Carmichael, I.S.E. and Eugster, H.P., eds. Reviews in Mineralogy Volume 17. Pages 97-142. Washington, D.C.: Mineralogical Society of America. TIC: 253653.

152738 Pitzer, K.S. 1973. "Thermodynamics of Electrolytes. I. Theoretical Basis and General Equations." *Journal of Physical Chemistry, 77,* (2), 268–277. Washington, D.C.: American Chemical Society. TIC: 239503.

152740 Pitzer, K.S. 1975. "Thermodynamics of Electrolytes. V. Effects of Higher-Order Electrostatic Terms." *Journal of Solution Chemistry, 4,* (3), 249–265. New York, New York: Plenum Publishing. TIC: 248997.

119530 Pitzer, K.S. 1979. "Theory: Ion Interaction Approach." Volume 1, Chapter 7 of *Activity Coefficients in Electrolyte Solutions.* Pytkowicz, R.M., ed. Boca Raton, Florida: CRC Press. TIC: 239527.

168289 Plyasunova, N.V.; Zhang, Y.; and Muhammed, M. 1998. "Critical Evaluation of Thermodynamics of Complex Formation of Metal Ions in Aqueous Solutions. IV. Hydrolysis and Hydroxo-Complexes of Ni^{2+} at 298.15 K." *Hydrometallurgy, 48,* (1), 43-63. New York, New York: Elsevier. TIC: 255758.

179582 Rai, D.; Moore, D.A.; Hess, N.J.; Rao, L.; and Clark, S.B. 2004. "Chromium(III) Hydroxide Solubility in the Aqueous Na^{+}-OH^{-}-$H_2PO^{-}_4$-HPO^{2-}_4-PO^{3-}_4-H_2O System: A Thermodynamic Model." *Journal of Solution Chemistry, 33,* (10), 1213-1242. New York, New York: Springer Science + Business Media. TIC: 259197.

163132 Reheis, M.C.; Budahn, J.R.; and Lamothe, P.J. 2002. "Geochemical Evidence for Diversity of Dust Sources in the Southwestern United States." *Geochimica et Cosmochimica Acta, 66,* (9), 1569-1587. New York, New York: Pergamon. TIC: 254213.

101708 Rimstidt, J.D. and Barnes, H.L. 1980. "The Kinetics of Silica–Water Reactions." *Geochimica et Cosmochimica Acta, 44,* 1683-1699. New York, New York: Pergamon Press. TIC: 219975.

107105 Roberts, W.L.; Campbell, T.J.; and Rapp, G.R., Jr. 1990. *Encyclopedia of Minerals.* 2nd Edition. New York, New York: Van Nostrand Reinhold. TIC: 242976.

154862 Rosenberg, N.D.; Gdowski, G.E.; and Knauss, K.G. 2001. "Evaporative Chemical Evolution of Natural Waters at Yucca Mountain, Nevada." *Applied Geochemistry, 16,* (9-10), 1231-1240. New York, New York: Pergamon. TIC: 249879.

105957 Sass, B.R. and Rai, D. 1987. "Solubility of Amorphous Chromium(III)-Iron(III) Hydroxide Solid Solutions." *Inorganic Chemistry, 26,* (13), 2228-2232. Washington, D.C.: American Chemical Society. TIC: 243717.

100075 Sawyer, D.A.; Fleck, R.J.; Lanphere, M.A.; Warren, R.G.; Broxton, D.E.; and Hudson, M.R. 1994. "Episodic Caldera Volcanism in the Miocene Southwestern Nevada Volcanic Field: Revised Stratigraphic Framework, $^{40}Ar/^{39}Ar$ Geochronology, and Implications for Magmatism and Extension." *Geological Society of America Bulletin, 106,* (10), 1304-1318. Boulder, Colorado: Geological Society of America. TIC: 222523.

105959 Schwertmann, U. and Taylor, R.M. 1995. "Iron Oxides." Chapter 8 of *Minerals in Soil Environments.* 2nd Edition. Dixon, J.B. and Weed, S.B., eds. SSSA Book Series, No. 1. Madison, Wisconsin: Soil Science Society of America. TIC: 237222.

105964 Sedlak, D.L. and Chan, P.G. 1997. "Reduction of Hexavalent Chromium by Ferrous Iron." *Geochimica et Cosmochimica Acta, 61,* (11), 2185-2192. New York, New York: Elsevier. TIC: 243064.

162970 Sequeira, C.A.C. 2000. "Corrosion of Copper and Copper Alloys." Chapter 42 of *Uhlig's Corrosion Handbook.* 2nd Edition. Revie, R.W., ed. New York, New York: John Wiley & Sons. TIC: 248360.

181150 Smith, A.F. 1982. "The Influence of Oxygen Partial Pressure on the Kinetics of Duplex Scale Formation on 316 Stainless Steel." *Corrosion Science, 22,* (9), 857-865. New York, New York: Pergamon Press. TIC: 259459.

162976 Smith, W.H. and Purdy, G.M. 1995. "Chromium in Aqueous Nitrate Plutonium Process Streams: Corrosion of 316 Stainless Steel and Chromium Speciation." *Waste Management, 15,* (7), 477-484. New York, New York: Pergamon. TIC: 254034.

161602 Smith, W.R. and Missen, R.W. 1991. *Chemical Reaction Equilibrium Analysis: Theory and Algorithms.* Malabar, Florida: Krieger Publishing Company. TIC: 252885.

162494 SNL (Sandia National Laboratories) 2003. *Software User's Manual, EQ3/6, Version 8.0.* SDN: 10813-UM-8.0-00. Albuquerque, New Mexico: Sandia National Laboratories. ACC: MOL.20030312.0084.

181267 SNL 2007. *Analysis of Dust Deliquescence for FEP Screening.* ANL-EBS-MD-000074 REV 01 AD 01. Las Vegas, Nevada: Sandia National Laboratories. ACC: DOC.20050829.0002.

177418 SNL 2007. *Dissolved Concentration Limits of Elements with Radioactive Isotopes.* ANL-WIS-MD-000010 REV 06. Las Vegas, Nevada: Sandia National Laboratory.

177404 SNL 2007. *Drift-Scale THC Seepage Model.* MDL-NBS-HS-000001 REV 05. Las Vegas, Nevada: Sandia National Laboratories.

177407 SNL 2007. *EBS Radionuclide Transport Abstraction.* ANL-WIS-PA-000001 REV 03. Las Vegas, Nevada: Sandia National Laboratories.

179476 SNL 2007. *Features, Events, and Processes for the Total System Performance Assessment.* ANL-WIS-MD-000026 REV 00. Las Vegas, Nevada: Sandia National Laboratories.

180778 SNL 2007. *General Corrosion and Localized Corrosion of the Drip Shield.* ANL-EBS-MD-000004 REV 02 ADD 01. Las Vegas, Nevada: Sandia National Laboratories. ACC: DOC.20040921.0002; DOC.20060427.0002; DOC.20070807.0004.

178519 SNL 2007. *General Corrosion and Localized Corrosion of Waste Package Outer Barrier.* ANL-EBS-MD-000003 REV 03. Las Vegas, Nevada: Sandia National Laboratories. ACC: DOC.20070730.0003; DOC.20070807.0007.

181648 SNL 2007. *In-Drift Natural Convection and Condensation.* MDL-EBS-MD-000001 REV 00, AD 01. Las Vegas, Nevada: Sandia National Laboratories. ACC: DOC.20041025.0006; DOC.20050330.0001; DOC.20051122.0005.

177411 SNL 2007. *In-Drift Precipitates/Salts Model.* ANL-EBS-MD-000045 REV 03. Las Vegas, Nevada: Sandia National Laboratories. ACC: DOC.20070306.0037.

180506 SNL 2007. *In-Package Chemistry Abstraction.* ANL-EBS-MD-000037 REV 04 ADD 01. Las Vegas, Nevada: Sandia National Laboratories. ACC: DOC.20050714.0003; DOC.20051130.0007; DOC.20070816.0004.

181383 SNL 2007. *Multiscale Thermohydrologic Model.* ANL-EBS-MD-000049 REV 03 AD01. Las Vegas, Nevada: Sandia National Laboratories. ACC: DOC.20050711.0001.

179287 SNL 2007. *Technical Work Plan for: Revision of Model Reports for Near-Field and In-Drift Water Chemistry.* TWP-MGR-PA-000038 REV 02. Las Vegas, Nevada: Sandia National Laboratories. ACC: DOC.20070110.0004.

179196 SNL 2007. *Thermal Management Flexibility Analysis.* ANL-EBS-MD-000075 REV 01. Las Vegas, Nevada: Sandia National Laboratories. ACC: DOC.20070207.0001.

177414 SNL 2007. *Thermal Testing Measurements Report.* TDR-MGR-HS-000002 REV 01. Las Vegas, Nevada: Sandia National Laboratories. ACC: DOC.20070307.0010.

179354 SNL 2007. *Total System Performance Assessment Data Input Package for Requirements Analysis for EBS In-Drift Configuration.* TDR-TDIP-ES-000010 REV 00. Las Vegas, Nevada: Sandia National Laboratories.

156721 Sonnenfeld, P. 1984. "The Continental Environment." Chapter 5 of *Brines and Evaporites.* Orlando, Florida: Academic Press. TIC: 251436.

118845 Sonnenthal, E.; Spycher, N.; Apps, J.; and Simmons, A. 1998. *Thermo-Hydro-Chemical Predictive Analysis for the Drift-Scale Heater Test.* Milestone SPY289M4. Version 1.0. Berkeley, California: Lawrence Berkeley National Laboratory. ACC: MOL.19980812.0268.

100928 Southwell, C.R. and Bultman, J.D. 1982. "Atmospheric Corrosion Testing in the Tropics." Chapter 64 of *Atmospheric Corrosion.* The Corrosion Monograph Series. Ailor, W.H., ed. New York, New York: John Wiley and Sons. TIC: 240907.

100927 Southwell, C.R.; Bultman, J.D.; and Alexander, A.L. 1976. "Corrosion of Metals in Tropical Environments - Final Report of 16-Year Exposures." *Materials Performance, 15,* (7), 9-25. Houston, Texas: National Association of Corrosion Engineers. TIC: 224022.

153578 Stefansson, A. and Arnorsson, S. 2000. "Feldspar Saturation State in Natural Waters." *Geochimica et Cosmochimica Acta, 64,* (15), 2567-2584. New York, New York: Elsevier. TIC: 249336.

100829 Stumm, W. and Morgan, J.J. 1981. *Aquatic Chemistry, An Introduction Emphasizing Chemical Equilibria in Natural Waters.* 2nd Edition. New York, New York: John Wiley & Sons. TIC: 208448.

125332 Stumm, W. and Morgan, J.J. 1996. *Aquatic Chemistry, Chemical Equilibria and Rates in Natural Waters.* 3rd Edition. New York, New York: John Wiley & Sons. TIC: 246296.

180016 Tao, Z.; Li, W.; Zhang, F.; Ding, Y.; and Yu, Z. 2003. "Am(III) Adsorption on Oxides of Aluminium and Silicon: Effects of Humic Substances, pH, and Ionic Strength." *Journal of Colloid and Interface Sciences, 265,* 221-226. New York, New York: Academic Press. TIC: 258926.

105960 Tebo, B.M.; Ghiorse, W.C.; van Wassbergen, L.G.; Siering, P.L.; and Caspi, R. 1997. "Bacterially Mediated Mineral Formation: Insights into Manganese(II) Oxidation from Molecular Genetic and Biochemical Studies." Chapter 7 of *Geomicrobiology: Interactions Between Microbes and Minerals.* Banfield, J.F. and Nealson, K.H., eds. Reviews in Mineralogy, Volume 35. Washington, D.C.: Mineralogical Society of America. TIC: 236757.

100831 Thorstenson, D.C.; Weeks, E.P.; Haas, H.; and Woodward, J.C. 1990. "Physical and Chemical Characteristics of Topographically Affected Airflow in an Open Borehole at Yucca Mountain, Nevada." *Proceedings of the Topical Meeting on Nuclear Waste Isolation in the Unsaturated Zone, Focus '89, September 17-21, 1989, Las Vegas, Nevada.* Pages 256-270. La Grange Park, Illinois: American Nuclear Society. TIC: 212738.

161603 Van Zeggeren, F. and Storey, S.H. 1970. *The Computation of Chemical Equilibria.* New York, New York: Cambridge University Press. TIC: 252891.

105946 Vaniman, D.T.; Bish, D.L.; Chipera, S.J.; Carlos, B.A.; and Guthrie, G.D., Jr. 1996. *Chemistry and Mineralogy of the Transport Environment at Yucca Mountain.* Volume I of *Summary and Synthesis Report on Mineralogy and Petrology Studies for the Yucca Mountain Site Characterization Project.* Milestone 3665. Los Alamos, New Mexico: Los Alamos National Laboratory. ACC: MOL.19961230.0037.

107066 Vaniman, D.T.; Ebinger, M.H.; Bish, D.L.; and Chipera, S. 1992. "Precipitation of Calcite, Dolomite, Sepiolite, and Silica from Evaporated Carbonate and Tuffaceous Waters of Southern Nevada, USA." *Proceedings of the 7th International Symposium on Water-Rock Interaction, Park City, Utah, July 13-18, 1992.* Kharaka, Y.K. and Maest, A., eds. *1,* 687-691. Brookfield, Vermont: A.A. Balkema. TIC: 208527.

178837 Wallace, P.J.; Dufek, J.; Anderson, A.T.; and Zhang, Y. 2003. "Cooling Rates of Plinian-Fall and Pyroclastic-Flow Deposits in the Bishop Tuff: Inferences from Water Speciation in Quartz-Hosted Glass Inclusions." *Bulletin of Volcanology, 65,* 105-123. New York, New York: Springer-Verlag. TIC: 259101.

162283 Walling, E.M.; Rock, P.A.; and Casey, W.H. 1995. "The Gibbs Energy of Formation of Huntite, $CaMg_3(CO_3)_4$, at 298 K and 1 Bar from Electrochemical Cell Measurements." *American Mineralogist, 80,* (3-4), 355-360. Washington, D.C.: Mineralogical Society of America. TIC: 252890.

127454 Walton, J.C. 1994. "Influence of Evaporation on Waste Package Environment and Radionuclide Release from a Tuff Repository." *Water Resources Research, 30,* (12), 3479-3487. Washington, D.C.: American Geophysical Union. TIC: 246921.

100833 Weast, R.C. and Astle, M.J., eds. 1981. *CRC Handbook of Chemistry and Physics.* 62nd Edition. Boca Raton, Florida: CRC Press. TIC: 240722.

179305 Whelan, J.F.; Neymark, L.A.; Moscati, R.J.; Marshall, B.D.; and Roedder, E. 2006. *Thermal History of the Unsaturated Zone at Yucca Mountain, Nevada, USA.* Denver, Colorado: U.S. Geological Survey.

179312 White, A.F. 1995. "Chemical Weathering Rates of Silicate Minerals in Soils." Chapter 9 of *Chemical Weathering Rates of Silicate Minerals.* White, A.F. and Brantley, S.L., eds. Reviews in Mineralogy Volume 31. Washington, D.C.: Mineralogical Society of America. TIC: 222496.

182474 White, A.F.; Blum, A.E.; Bullen, T.D.; Vivit, D.V.; Schulz, M.; and Fitzpatrick, J. 1999. "The Effect of Temperature on Experimental and Natural Chemical Weathering Rates of Granitoid Rocks." *Geochimica et Cosmochimica Acta, 63,* (19/20), 3277-3291. New York, New York: Elsevier. TIC: 259672.

163589 Wilson, N.S.F.; Cline, J.S.; and Amelin, Y.V. 2003. "Origin, Timing, and Temperature of Secondary Calcite–Silica Mineral Formation at Yucca Mountain, Nevada." *Geochimica et Cosmochimica Acta, 67,* (6), 1145-1176. New York, New York: Pergamon. TIC: 254369.

100836 Wolery, T.J. 1992. *EQ3NR, A Computer Program for Geochemical Aqueous Speciation-Solubility Calculations: Theoretical Manual, User's Guide, and Related Documentation (Version 7.0).* UCRL-MA-110662 PT III. Livermore, California: Lawrence Livermore National Laboratory. ACC: MOL.19980717.0626.

100097 Wolery, T.J. and Daveler, S.A. 1992. *EQ6, A Computer Program for Reaction Path Modeling of Aqueous Geochemical Systems: Theoretical Manual, User's Guide, and Related Documentation (Version 7.0).* UCRL-MA-110662 PT IV. Livermore, California: Lawrence Livermore National Laboratory. ACC: MOL.19980701.0459.

177633 Wolf, M.; Breitkopf, O.; and Puk, R. 1989. "Solubility of Calcite in Different Electrolytes at Temperatures Between 10º and 60ºC and at CO_2 Partial Pressures of About 1 kPa." *Chemical Geology, 76,* 291-301. Amsterdam, The Netherlands: Elsevier. TIC: 258562.

160839 Yang, I.C. 2002. "Percolation Flux and Transport Velocity in the Unsaturated Zone, Yucca Mountain, Nevada." *Applied Geochemistry, 17,* (6), 807-817. New York, New York: Elsevier. TIC: 253605.

100194 Yang, I.C.; Rattray, G.W.; and Yu, P. 1996. *Interpretation of Chemical and Isotopic Data from Boreholes in the Unsaturated Zone at Yucca Mountain, Nevada.* Water-Resources Investigations Report 96-4058. Denver, Colorado: U.S. Geological Survey. ACC: MOL.19980528.0216.

179304 Yund, R.A. 1983. "Diffusion in Feldspars." In *Feldspar Mineralogy,* Volume 2, Chapter 8 of *Reviews in Mineralogy.* 2nd Edition. Washington, D.C.: Mineralogical Society of America. TIC: 259152.

105963 Zachara, J.M.; Girvin, D.C.; Schmidt, R.L.; and Resch, C.T. 1987. "Chromate Adsorption on Amorphous Iron Oxyhydroxide in the Presence of Major Groundwater Ions." *Environmental Science & Technology, 21,* (6), 589-594. Easton, Pennsylvania: American Chemical Society. TIC: 243613.

9.2 CODES, STANDARDS, REGULATIONS, AND PROCEDURES

173273 10 CFR 63. 2005. Energy: Disposal of High-Level Radioactive Wastes in a Geologic Repository at Yucca Mountain, Nevada. ACC: MOL.20050405.0118.

162720 ASTM A 240/A 240M-02a. 2002. *Standard Specification for Chromium and Chromium-Nickel Stainless Steel Plate, Sheet, and Strip for Pressure Vessels and for General Applications.* West Conshohocken, Pennsylvania: American Society for Testing and Materials. TIC: 253994.

165006 ASTM A 276-03. 2003. *Standard Specification for Stainless Steel Bars and Shapes.* West Conshohocken, Pennsylvania: American Society for Testing and Materials. TIC: 254842.

162723 ASTM A 516/A 516M-01. 2001. *Standard Specification for Pressure Vessel Plates, Carbon Steel, for Moderate- and Lower-Temperature Service.* West Conshohocken, Pennsylvania: American Society for Testing and Materials. TIC: 253997.

162724 ASTM A 588/A 588M-01. 2001. *Standard Specification for High-Strength Low-Alloy Structural Steel with 50 ksi [345 MPa] Minimum Yield Point to 4–in. [100–mm] Thick.* West Conshohocken, Pennsylvania: American Society for Testing and Materials. TIC: 253998.

176255 ASTM A 588/A 588M-05. 2005. *Standard Specification for High-Strength Low-Alloy Structural Steel, up to 50 ksi [345 MPa] Minimum Yield Point, with Atmospheric Corrosion Resistance.* West Conshohocken, Pennsylvania: American Society for Testing and Materials. TIC: 258058.

176423 ASTM A 759-00 (Reapproved 2005). 2005. *Standard Specification for Carbon Steel Crane Rails.* West Conshohocken, Pennsylvania: American Society for Testing and Materials. TIC: 258684.

159971 ASTM A 759-00. 2001. *Standard Specification for Carbon Steel Crane Rails.* West Conshohocken, Pennsylvania: American Society for Testing and Materials. TIC: 253176.

103515 ASTM G 1-90 (Reapproved 1999). 1999. *Standard Practice for Preparing, Cleaning, and Evaluating Corrosion Test Specimens.* West Conshohocken, Pennsylvania: American Society for Testing and Materials. TIC: 238771.

151442 ASTM G 101-97. 1997. *Standard Guide for Estimating the Atmospheric Corrosion Resistance of Low-Alloy Steels.* West Conshohocken, Pennsylvania: American Society for Testing and Materials. TIC: 248533.

IM-PRO-003, Rev. 2 ICN 0. *Software Management*. Washington, D.C.: U.S. Department of Energy, Office of Civilian Radioactive Waste Management. ACC: DOC.20070228.0002.

SCI-PRO-001, Rev. 4, ICN 0. *Qualification of Unqualified Data*. Washington, D.C.: U.S. Department of Energy, Office of Civilian Radioactive Waste Management. ACC: DOC.20070725.0002.

SCI-PRO-002, Rev. 2, ICN 0. *Planning for Science Activities*. Washington, D.C.: U.S. Department of Energy, Office of Civilian Radioactive Waste Management. ACC: DOC.20070320.0001.

SCI-PRO-006, Rev. 5, ICN 0. *Models*. Washington, D.C.: U.S. Department of Energy, Office of Civilian Radioactive Waste Management. ACC: DOC.20070810.0004.

9.3 SOURCE DATA, LISTED BY DATA TRACKING NUMBER

162015 GS000308313211.001. Geochemistry of Repository Block. Submittal date: 03/27/2000.

156375 GS010708312272.002. Chemical Data for Pore Water from Tuff Cores of USW NRG-6, USW NRG-7/7A, USW UZ-14, USW UZ-N55 and UE-25 UZ#16. Submittal date: 09/05/2001.

165859 GS011008312272.004. Analysis for Chemical Composition of Pore Water from Boreholes USW WT-24 and USW SD-6 During FY98 and FY99. Submittal date: 12/20/2001.

160899 GS020408312272.003. Collection and Analysis of Pore Water Samples for the Period from April 2001 to February 2002. Submittal date: 04/24/2002.

166569 GS020808312272.004. Analysis of Water-Quality Samples for the Period from July 1999 to July 2002. Submittal date: 09/18/2002.

163118 GS030108312242.001. Temperature, Relative Humidity and Barometric Pressure Behind the Bulkhead in Alcove 8 from June 22, 2000 to August 26, 2002. Submittal date: 02/20/2003.

165226 GS030408312272.002. Analysis of Water-Quality Samples for the Period from July 2002 to November 2002. Submittal date: 05/07/2003.

166570 GS031008312272.008. Analysis of Pore Water and Miscellaneous Water Samples for the Period from December 2002 to July 2003. Submittal date: 11/13/2003.

171287 GS031208312232.003. Deep Unsaturated Zone Surface-Based Borehole Instrumentation Program Data from Boreholes USW NRG-7A, UE-25 UZ #4, USW NRG-6, UE-25 UZ #5, USW UZ-7A and USW SD-12 for the Time Period 10/01/97 - 03/31/98. Submittal date: 07/29/2004.

178750 GS031208312232.008. Deep Unsaturated Zone Surface-Based Borehole Instrumentation Program Data from Boreholes USW NRG-7A, USW NRG-6, UE-25 UZ#4, UE-25 UZ#5, USW UZ-7A, and USW SD-12 for the Time Period 10/01/95 through 3/31/96. Submittal date: 05/24/2004.

178057 GS041108312272.005. Analysis of Pore Water and Miscellaneous Water Samples for the Period from July 2003 to September 2004. Submittal date: 02/25/2005.

179065 GS060908312272.004. Chemical Analysis of Pore Water Samples Extracted from HD-PERM, USW SD-9, and ESF-SAD-GTB#1 Core for the Period from April 29, 2006 to July 21, 2006. Submittal date: 09/14/2006.

182478 GS0703PA312272.001. Analysis of Pore Water Samples Collected from the ESF Cross Drift and Analyzed from November 1, 2005 through January 26, 2006. Submittal date: 03/23/2007.

182307 GS070708312272.002. Analysis of Metabolic Acids in Pore Water Samples Collected from Surface and ESF Boreholes and Analyzed from March 18, 2002 THROUGH JULY 01, 2003. Submittal date: 07/24/2007.

182482 GS911208312271.011. Analysis of CO2 Concentration of Syringe Samples Taken During USW UZ-1 Borehole Gas Sampling, September, 1988. Submittal date: 12/11/1991.

166448 GS930108312271.004. Gas Chromatograph Analysis of Gas Composition (CO2, CH4, SF6) of Syringe Samples Taken During USW UZ-1 Borehole Gas Sampling, 12/9/91 - 12/19/91. Submittal date: 12/22/1992.

145533 GS930408312271.014. Analysis of CO2 Concentration of Syringe Samples Taken During USW UZ-1 Borehole Gas Sampling, May, 1989, thru Jan., 1991. Submittal date: 03/30/1993.

166450 GS940408312271.001. Gas Chromatograph Analysis of Gas Composition (CO2, CH4, SF6) of Syringe Samples Taken During USW UZ-1 Borehole Gas Sampling, December 1993. Submittal date: 03/25/1994.

166451 GS940408312271.006. Gas Chromatograph Analysis of Gas Composition (CO2, CH4) of Syringe Samples Taken During USW UZ-1 Borehole Gas Sampling, January, 1993. Submittal date: 03/25/1994.

145702 GS970908315215.011. Strontium Isotope Ratios and Strontium Concentrations in USW SD-7 Rock and Soils, and ESF Calcite. Submittal date: 09/11/1997.

106752 GS980708312242.010. Physical Properties of Borehole Core Samples, and Water Potential Measurements Using the Filter Paper Technique, for Borehole Samples from USW WT-24. Submittal date: 07/27/1998.

106748 GS980808312242.014. Physical Properties of Borehole Core Samples and Water Potential Measurements Using the Filter Paper Technique for Borehole Samples from USW SD-6. Submittal date: 08/11/1998.

145711 GS990308315215.004. Strontium Isotope Ratios and Strontium Concentrations in Rock Core Samples and Leachates from USW SD-9 and USW SD-12. Submittal date: 03/25/1999.

158426 LA0201SL831225.001. Chemical, Textural, and Mineralogical Characteristics of Sidewall Samples from the Drift Scale Test. Submittal date: 01/10/2002.

174331 LA0506BR831371.001. FEHM Files for Basecase UZ Transport Abstraction Model Particle Tracking Simulations. Submittal date: 06/20/2005.

113495 LA9908JC831321.001. Mineralogic Model "MM3.0" Version 3.0. Submittal date: 08/16/1999.

146451 LB000121123142.003. Isotope Data for CO2 Gas Samples Collected From the Hydrology Holes of the ESF Drift Scale Test for the Period August 9, 1999 through November 30, 1999. Submittal date: 01/21/2000.

158342 LB000718123142.003. Isotope Data for CO2 Gas Samples Collected from the Hydrology Holes of the ESF Drift Scale Test for the Period April 18, 2000 through April 19, 2000. Submittal date: 07/18/2000.

153460 LB0011CO2DST08.001. Isotope Data for CO2 from Gas Samples Collected from Hydrology Holes in Drift-Scale Test. Submittal date: 12/09/2000.

159306 LB0102CO2DST98.001. Concentration Data for CO2 from Gas Samples Collected from Hydrology Holes in Drift-scale Test. Submittal date: 02/28/2001.

156888 LB0108CO2DST05.001. Concentration and Isotope Data for CO2 and H2O from Gas Samples Collected from Hydrology Holes in Drift-Scale Test - May and August 1999, April 2000, January and April 2001. Submittal date: 08/27/2001.

158349 LB0203CO2DSTEH.001. Concentration/Isotope Data for CO2/H2O from Gas Samples Collected from Hydrology Holes in DST up to End of Heating. Submittal date: 03/27/2002.

159303 LB0206C14DSTEH.001. Carbon 14 Isotope Data from CO2 Gas Samples Collected from DST. Submittal date: 06/17/2002.

159672 LB0207REVUZPRP.002. Matrix Properties for UZ Model Layers Developed from Field and Laboratory Data. Submittal date: 07/15/2002.

161638 LB0208ISODSTHP.001. Isotope Data and CO2 Analysis for the Heating Phase of the DST. Submittal date: 08/09/2002.

161243 LB0208UZDSCPMI.002. Drift-Scale Calibrated Property Sets: Mean Infiltration Data Summary. Submittal date: 08/26/2002.

177538 LB0303ISODSTCP.001. Isotope Data and CO2 Analysis for the Cooling Phase of the DST. Submittal date: 03/28/2003.

177539 LB0309ISODSTCP.001. Isotope Data and CO2 Analysis for the Cooling Phase of the DST. Submittal date: 09/24/2003.

177540 LB0403ISODSTCP.001. H2O and CO2 Isotope Analysis for the Cooling Phase of the DST. Submittal date: 03/16/2004.

169254 LB0404ISODSTHP.003. Third Submittal of CO_2/H_20 Isotope Data for the Heating Phase of the DST. Submittal date: 04/15/2004.

177541 LB0410ISODSTCP.001. H2O and CO2 Isotope Analysis for the Cooling Phase of the DST. Submittal date: 11/24/2004.

177542 LB0509ISODSTCP.001. H2O and CO2 Isotope Analysis for the Cooling Phase of the DST. Submittal date: 09/29/2005.

179180 LB0610UZDSCP30.001. Drift-Scale Calibrated Property Set for the 30-Percentile Infiltration Map. Submittal date: 11/02/2006.

179150 LB0612PDPTNTSW.001. Vertical Flux at PTN/TSW Interface for Present-Day Climate of 10th, 30th, 50th, and 90-Percentile Infiltration Maps. Submittal date: 12/19/2006.

179153 LB0701GTPTNTSW.001. Vertical Flux at PTN/TSW Interface for Glacial Transition Climate of 10th, 30th, 50th, and 90th-Percentile Infiltration Maps. Submittal date: 01/03/2007.

179156 LB0701MOPTNTSW.001. Vertical Flux at PTN/TSW Interface for Monsoon Climate of 10th, 30th, 50th and 90th-Percentile Infiltration Maps. Submittal date: 01/03/2007.

179332 LB0702UZPTN10K.002. Vertical Flux at PTN/TSW Interface for Post-10K-Year Climate Infiltration Maps. Submittal date: 02/15/2007.

181164 LB0704DSTHONLY.001. Abstracted TH Information from 2-D Drift-Scale TH Simulations. Submittal date: 05/04/2007.

181217 LB0705DSTHC001.001. Drift-Scale THC Simulation Results with Water HDPERM3 (W0). Submittal date: 05/02/2007.

180854 LB0705DSTHC001.002. Input and Output Files of Drift-Scale THC Simulations with Water HDPERM3 (W0). Submittal date: 05/02/2007.

111471 LB980420123142.005. Isotope Data for CO2 from Gas Samples Collected from Drift Scale Test February 1998 in First Quarter TDIF Submission for the Drift Scale Test. Submittal date: 11/12/1998.

111472 LB980715123142.003. Isotope Data for CO2 from Gas Samples Collected from Drift Scale Test June 4, 1998 in 2nd Quarter TDIF Submission of the Drift Scale Test Heating Phase. Submittal date: 07/13/1998.

111475 LB990501233129.004. 3-D UZ Model Calibration Grids for AMR U0000, "Development of Numerical Grids of UZ Flow and Transport Modeling". Submittal date: 09/24/1999.

111476 LB990630123142.003. Fourth, Fifth, and Sixth Quarters TDIF Submission for the Drift Scale Test, September 1998 to May 1999. Submittal date: 06/30/1999.

144913 LL000202905924.117. Environment on the Surfaces of the Drip Shield and Waste Package Outer Barrier. Submittal date: 02/18/2000.

161677 LL020709923142.023. Aqueous Geochemistry of Borehole Waters Collected in the Heating Phase of the DST. Submittal date: 07/26/2002.

171362 LL040803112251.117. Target Compositions of Aqueous Solutions Used for Corrosion Testing. Submittal date: 08/14/2004.

173659 LL040901831032.008. Results from Boiling Temperature Measurements for Saturated Solutions in the Systems NACL + KNO3 + H2O, NaNO3 + KNO3 + H2O, and NACL + NANO3 + KNO3 + H2O. Submittal date: 02/17/2005.

147298 LL980704605924.035. Engineering Material Characterization Report, Volume 3. Submittal date: 07/17/1998.

120487 LL991008004241.041. Evaporation of Topopah Spring Tuff Pore Water. Submittal date: 10/21/1999.

120489 LL991008104241.042. Evaporation of J13 Water: Laboratory Experiments and Geochemical Modeling. Submittal date: 10/21/1999.

153836 MO0001SEPDSTPC.000. Drift Scale Test (DST) Temperature, Power, Current, and Voltage Data for June 1, 1999 through October 31, 1999. Submittal date: 01/12/2000.

152554 MO0004QGFMPICK.000. Lithostratigraphic Contacts from MO9811MWDGFM03.000 to be Qualified Under the Data Qualification Plan, TDP-NBS-GS-000001. Submittal date: 04/04/2000.

150930 MO0005PORWATER.000. Perm-Sample Pore Water Data. Submittal date: 05/04/2000.

153707 MO0007SEPDSTPC.001. Drift Scale Test (DST) Temperature, Power, Current, and Voltage Data for November 1, 1999 through May 31, 2000. Submittal date: 07/13/2000.

153777 MO0012MWDGFM02.002. Geologic Framework Model (GFM2000). Submittal date: 12/18/2000.

153708 MO0012SEPDSTPC.002. Drift Scale Test (DST) Temperature, Power, Current, and Voltage Data for June 1, 2000 through November 30, 2000. Submittal date: 12/19/2000.

158321 MO0107SEPDSTPC.003. Drift Scale Test (DST) Temperature, Power, Current, and Voltage Data for December 1, 2000 through May 31, 2001. Submittal date: 07/06/2001.

155989 MO0109HYMXPROP.001. Matrix Hydrologic Properties Data. Submittal date: 09/17/2001.

158320 MO0202SEPDSTTV.001. Drift Scale Test (DST) Temperature, Power, Current, and Voltage Data for June 1, 2001 through January 14, 2002. Submittal date: 02/28/2002.

161767 MO0208SEPDSTTD.001. Drift Scale Test (DST) Temperature Data for January 15, 2002 through June 30, 2002. Submittal date: 08/29/2002.

165698 MO0303SEPDSTTM.000. Drift Scale Test (DST) Temperature Data for July 1, 2002 through December 31, 2002. Submittal date: 03/17/2003.

165699 MO0307SEPDST31.000. Drift Scale Test (DST) Temperature Data for 01/01/2003 through 06/30/2003. Submittal date: 07/07/2003.

167409 MO0312SPAPCEML.003. EBS P&CE Model Longevity of Materials Evaluation. Submittal date: 12/18/2003.

177813 MO0403SEPDST32.000. Drift Scale Test (DST) Temperature Data for July 1, 2003 through December 31, 2003. Submittal date: 03/08/2004.

170616 MO0406SEPTVDST.000. Temperature and Volume Water Content for Drift Scale Test (DST) Heating Phase for Boreholes 79 and 80. Submittal date: 06/29/2004.

177814 MO0408SEPDSTTD.000. Drift Scale Test (DST) Temperature Data for January 1, 2004 through June 30, 2004. Submittal date: 08/18/2004.

171714 MO0409MWDUGCMW.000. Updated General Corrosion Model of the Waste Package Outer Barrier. Submittal date: 09/17/2004.

172059 MO0409SPAACRWP.000. Aqueous Corrosion Rates for Non-Waste Form Waste Package Materials. Submittal date: 09/16/2004.

177815 MO0509SEPDSTTD.000. Drift Scale Test (DST) Temperature Data for July 1, 2004 through June 30, 2005. Submittal date: 09/01/2005.

177816 MO0603SEPDSTTD.000. Drift Scale Test (DST) Temperature Data for July 1,2005 through December 31, 2005. Submittal date: 03/09/2006.

180552 MO0612MEANTHER.000. Mean Thermal Conductivity of Yucca Mountain Repository Units. Submittal date: 04/27/2007.

179290 MO0701EQ36IDPS.000. EQ3/6 Input and Output Files Used for IDPS Model Validation Simulations of Evaporation of Dilute Salt Solutions at 25C and 100C, Seawater, Binary and Ternary Salt Solutions, Synthetic Topopah Springs Tuff Pore Water at 95C and in the Carbonate System. Submittal date: 01/16/2007.

179085 MO0701VENTCALC.000. Analytical Ventilation Calculation for the Base Case Analysis with a 1.45 KW/M Initial Line Load. Submittal date: 01/23/2007.

179343 MO0702PAGLOBAL.000. Global 10th and 90th Percentile Mean Thermal Conductivity of Yucca Mountain Repository Units. Submittal date: 02/22/2007.

181613 MO0706SPAFEPLA.001. FY 2007 LA FEP List and Screening. Submittal date: 06/20/2007.

182333 MO0708ISOTOPES.000. Strontium Isotope Ratios and Isotope Dilution Data for Rubidium and Strontium Collected 08/16/96 to 02/19/97. Submittal date: 08/07/2007.

113644 MO9807DSTSET01.000. Drift Scale Test (DST) Temperature, Power, Current, Voltage Data for November 7, 1997 through May 31, 1998. Submittal date: 07/09/1998.

113662 MO9810DSTSET02.000. Drift Scale Test (DST) Temperature, Power, Current, Voltage Data for June 1 through August 31, 1998. Submittal date: 10/09/1998.

113673 MO9906DSTSET03.000. Drift Scale Test (DST) Temperature, Power, Current, Voltage Data for September 1, 1998 through May 31, 1999. Submittal date: 06/08/1999.

164196 SN0307T0510902.003. Updated Heat Capacity of Yucca Mountain Stratigraphic Units. Submittal date: 07/15/2003.

169129 SN0404T0503102.011. Thermal Conductivity of the Potential Repository Horizon Rev 3. Submittal date: 04/27/2004.

179067 SN0609T0502404.012. Pitzer Thermodynamic Database (DATA0.YP2). Submittal date: 09/28/2006.

179335 SN0611T0509206.007. Estimated Model Uncertainties in IDPS Model Outputs. Submittal date: 11/29/2006.

178850 SN0612T0502404.014. Thermodynamic Database Input File for EQ3/6 - DATA0.YMP.R5. Submittal date: 12/15/2006.

180451 SN0702PAIPC1CA.001. In-Package Chemistry Calculations and Abstractions. Submittal date: 04/19/2007.

9.4 OUTPUT DATA, LISTED BY DATA TRACKING NUMBER

SN0701PAEBSPCE.001. PCE TDIP Potential Seepage Water Chemistry Lookup Tables. Submittal date: 04/25/2007.

SN0701PAEBSPCE.002. PCE TDIP PCO2 and Total Carbon Lookup Tables. Submittal date: 01/30/2007.

SN0703PAEBSPCE.006. Physical and Chemical Environment (PCE) TDIP Water-Rock Interaction Parameter Table and Salt Separation Tables with Supporting Files. Submittal date: 06/27-2007.

SN0703PAEBSPCE.007. Physical and Chemical Environment (PCE) TDIP Uncertainty Evaluations and Supporting Files. Submittal date: 04/06/2007.

SN0705PAEBSPCE.008. P&CE Abstraction Models Validations. Submittal date: 05/31/2007.

SN0705PAEBSPCE.009. P&CE Normative Calculation of Mineral Abundances and Other Supporting Miscellaneous Calculations. Submittal date: 05/31/2007.

SN0705PAEBSPCE.010. Justification of the DATA0.PCE Thermodynamic Database for One Time Use in the P&CE. Submittal date: 05/31/2007.

SN0705PAEBSPCE.011. P&CE Sensitivity Study of the Interaction between Introduced Materials and Seepage Waters. Submittal date: 05/31/2007.

SN0705PAEBSPCE.012. P&CE Alternative Conceptual Model. Submittal date: 05/31/2007.

SN0705PAEBSPCE.013. P&CE Validation Exercise: Comparing NFC Model Outputs to THC Model Outputs. Submittal date: 05/31/2007.

SN0705PAEBSPCE.014. P&CE Validation Exercise: Comparing NFC Model Outputs to Ambient Field Data. Submittal date: 05/31/2007.

SN0705PAEBSPCE.015. P&CE Selection of Pore Water Data. Submittal date: 05/31/2007.

MO0705OXYBALAN.000. Oxygen Balance Analysis for Physical and Chemical Environment. Submittal date: 05/23/2007.

9.5 SOFTWARE CODES

162228 EQ3/6 V. 8.0. 2003. WINDOWS 2000, WIN NT 4.0, WIN 98, WIN 95. STN: 10813-8.0-00.

178965 FEHM V. 2.24. 2006. 5.9/2.4.21/WINXP/WIN 2000. STN: 10086-2.24-00.

173680 GetEQData V. 1.0.1. 2002. WINDOWS 2000. STN: 10809-1.0.1-00.

165753 ppptrk V. 1.0. 2003. Red Hat 7.1, Linux 2.4.18, Win2000, SOLARIS 7, 8. STN: 11030-1.0-00.

180937 TOUGHREACT V. 3.1.1. 2007. OSF1 V5.1/Linux/WINDOWS XP. STN: 10396-3.1.1-00.

APPENDIX A

CRITICAL REVIEW

INTENTIONALLY LEFT BLANK

A critical review by Brian Viani (Lawrence Livermore National Laboratory) was performed in accordance with SCI-PRO-006, Attachment 4, as a model validation method for two model abstractions, seepage dilution/evaporation and integrated invert chemistry. The critical reviewer is independent of the development, checking, and review of the these model abstractions.

A facsimile of the critical review letter identifying review criteria is attached below. The letter identifies a few suggestions for clarification of model documentation and concludes that the model abstractions are valid for their intended use. It should be noted that, subsequent to the letter, many of the suggestions were incorporated into the final version of the report.

Interdepartmental letterhead

Mail Station L- 221

Ext: 925-423-2001

July 6, 2007

MEMORANDUM

To: James Blink

From: Brian Viani for James A. Blink 9 July 07

Subject: Critical Review of Seepage Evaporation Abstraction Model and the Invert Pore-Water Abstraction Model - Documented in the EBS: Physical and Chemical Environment AMR (ANL-EBS-MD-000033, Rev 06)

A critical review for two model abstractions (the Seepage Evaporation Abstraction Model and the Invert Pore-Water Abstraction Model) documented in the EBS: Physical and Chemical Environment (P&CE AMR (ANL-EBS-MD-000033 REV 06)) by technical specialist Brian Viani (LLNL) has been performed in accordance with SCI-PRO-006 Rev 3, Attachment 4 as a model validation method per *Technical Work Plan for: Revision of Model Reports for Near-Field and In-Drift Water Chemistry* (TWP-MGR-PA-000038 REV 02). The group manager for the Near-Field Environment (NFE) team (Geoff Freeze) directed the critical review per Section 6.3.2 of SCI-PRO-006, as part of the NFE group manager's determination regarding the adequacy of model validation. The intent of this review is to provide input to the manager's determination regarding the adequacy of model validation and whether the abstraction submodels are valid and appropriate for their intended use.

Qualifications of the technical specialist Brian Viani include that he has a PhD in soil chemistry and 29 years experience working in the field of low temperature aqueous geochemistry. He is currently a chemist at LLNL where he has been employed for the past 21 years. He has worked as an experimentalist in the area of clay mineralogy, radionuclide sorption, and transport relevant to high-level waste storage and decontamination of materials, and mineral transformations under earth surface and hydrothermal conditions. He is also experienced in the use of geochemical modeling codes such as EQ3/6, the Geochemists Workbench, and PHREEQ for modeling radionuclide interactions with materials, and the formation of new phases. He has worked with such models for 29 years.

The review criteria specified by the NFE manager include the following:

- The technical approaches capture all physical and chemical processes that are significant to the intended uses of the models for representing seepage and invert porewater chemistry.
- Modeling assumptions are clearly defined and justified as appropriate for the intended uses of the models.
- Uncertainties in model parameters, process representation, and assumptions are sufficiently described, and impacts of these uncertainties on model confidence and model output, as appropriate for the intended uses of the models, are adequately discussed.
- The overall technical credibility of the approaches, including assumptions, parameters, equations, and numerical implementation, is appropriate for the intended uses of the models.

University of California
Lawrence Livermore National Laboratory

July 6. 2007 Page 2 of 3
To: James Blink
From: Brian Viani
Subject: Critical Review of Seepage Evaporation Abstraction Model and the Invert Pore-Water Abstraction Model - Documented in the EBS: Physical and Chemical Environment AMR (ANL-EBS-MD-000033, Rev 06)

Critical Review

Introduction – I reviewed the sections of the P&CE AMR (ANL-EBS-MD-000033 REV 06) in which the Seepage Evaporation Abstraction Model and the Invert Pore-Water Abstraction Model (herein referred to as the abstraction model) were developed and validated. I did not review the IDPS model which was used to develop the abstraction model, except its use to develop the look-up table which forms the basis of the abstraction model.

I find that that the model abstractions are valid for their intended use. I suggest that additional validation tests would increase the confidence in the abstraction. Alternatively, a specific discussion justifying the use of a limited number of validation tests could be added to the validation section of the P&CE AMR.

I've identified some minor corrections/suggestions to the sections of the P&CE AMR that I reviewed. These are noted on the accompanying DRCS.

My comments follow each of the review criteria specified by the NFE manager.

The technical approaches capture all physical and chemical processes that are significant to the intended uses of the models for representing seepage and invert porewater chemistry.

The two abstraction models are based on the IDPS model, which is a process model used to predict various solution chemical properties for various seepage, temperature, and relative humidity scenarios. My review focuses on the validity of the abstraction model to accurately represent, within the stated uncertainty of the IDPS model, the output from the IDPS models for the same input. Although I am familiar with the approach taken for the IDPS model, this Critical Review is restricted to the abstraction models only. Based on the description of the abstraction model and its intended use, I believe it captures the significant physical and chemical processes embodied in the IDPS model. A separate review, that is beyond the scope of this review, is necessary to assess whether the physical and chemical processes embodied in the IDPS model are appropriate for its intended use; i.e., to represent seepage and porewater chemistry.

Modeling assumptions are clearly defined and justified as appropriate for the intended uses of the models.

The assumptions used to produce the lookup table, which is the basis for the abstraction model are clearly defined and appear appropriate to its intended use. One clarification regarding the 77 evaporative pathway calculations made with huntite removed from the mineral suppression list might useful. I assume that the evaporative pathway calculations did not include mineral precipitation kinetics; i.e., minerals were assumed to precipitate and reach equilibrium with the fluid whenever their saturation index (SI) was exceeded. Under these conditions, the method used to choose the IDPS evaporative calculations to repeat by including huntite in the model is appropriate. However, if the evaporative calculations included precipitation kinetics for any minerals containing elements common to huntite, then all intermediate output from EQ6 (not just

the output at each reaction progress point) would need to scrutinized for huntite SI above unity. This could capture additional calculations that would have to be redone.

Uncertainties in model parameters, process representation, and assumptions are sufficiently described, and impacts of these uncertainties on model confidence and model output, as appropriate for the intended uses of the models, are adequately discussed.

Interpolation – The validation of the abstraction model was based on comparing the output interpolated from the abstraction model (i.e., the look-up table) with the output from the IDPS model for two validation cases (two water groups, two temperatures, two pCO_2 levels, and one WRIP). The methodology and approach used appears to be an appropriate means of validating the abstraction. The results clearly show that for the cases chosen, the interpolation in the look-up table returns pore water chemistry values that are well within the stated uncertainty of the IDPS model. Hence, the abstraction is a valid means to reproduce the IDPS model within the uncertainty of the IDPS model for the validation cases considered.

My only suggestion is that the author includes some discussion justifying why two validation scenarios are sufficient to validate the entire look-up table. There are four regions within temperature – pCO_2 space that would require interpolation. The validation process addressed two of them. Additionally, only two water types and one WRIP were considered, out of four and eleven, respectively. It may be useful to include additional validation test scenarios.

Extrapolation – The abstraction model was also shown to match, within the uncertainty of the IDPS model, key water chemistry parameters for pCO_2 levels outside the range for which the abstraction was developed. This validation test was based on comparison of the full IDPS model output with the look-up table output for validation cases based on one temperature, one WRIP, two RH's and two pCO_2 values outside the look-up table bounds. Extrapolation of the key parameters was based on a log-linear function of pCO_2. The results again clearly show that for the cases chosen the, extrapolation based on the look-up table returns pore water chemistry values that are within the stated uncertainty of the IDPS model. Again, similar to the interpolation validation, it may be useful to include additional validation scenarios, or a discussion supporting the use of a single temperature and WRIP for the validation test.

The overall technical credibility of the approaches, including assumptions, parameters, equations, and numerical implementation, is appropriate for the intended uses of the models.

The development of the abstracted models and their validation used an approach that is technically defensible and appropriate for the intended use of the model. In particular, the ability of the abstraction model to represent pore water chemistry within the uncertainty defined for the full IDPS model, when used in an interpolative mode, and for limited extrapolation, has been shown. There may be benefit in more fully documenting the interpolative aspect of the model as a means of developing additional confidence in the abstraction model's ability to match the IDPS output.

APPENDIX B

DATA QUALIFICATION PLANS

INTENIONALLY LEFT BLANK

Data Qualification Plan

Complete only applicable items.

QA: QA

Page 1 of 1

Section I. Organizational Information

Qualification Title

Qualification of corrosion rate data

Requesting Organization

Near Field Environment

Section II. Process Planning Requirements

1. List of Unqualified Data to be Evaluated

1. **Bomberger, H.B.; Cambourelis, P.J.; and Hutchinson, G.E. 1954 [DIRS 163699]**. "Corrosion Properties of Titanium in Marine Environments."
2. **Southwell, C.R.; Bultman, J.D.; and Alexander, A.L. 1976 [DIRS 100927]**. "Corrosion of Metals in Tropical Environments – Final Report of 16-Year Exposures."

2. Type of Data Qualification Method(s) [Including rationale for selection of method(s) (Attachment 3) and qualification attributes (Attachment 4)]

These data will be qualified using Method 2 Corroborating Data in accordance with SCI-PRO-001 Attachment 3. The rationale for selecting this methodology is that corroborating data are available for comparison with the unqualified data set and any inferences drawn to corroborate the unqualified data can be clearly identified, justified and documented. The accuracy, precision and representativeness of the corroborating data will be documented. The data qualification tasks (i.e. work) specified in this plan will be conducted under suitably controlled conditions and any prerequisites for the specified activities, such as personnel training, have been satisfied. There are no special controls, processes, test equipment, tools, skills or tests needed to attain the required quality/verification of quality. Verification of quality will be by inspection and evaluation alone.

3. Data Qualification Team and Additional Support Staff Required

Katheryn B. Helean Ph.D. Qualification Chairperson
Wendy Mitcheltree

4. Data Evaluation Criteria

Evaluation Criteria Used:
1. Conditions for use from Attachment 3, Method 2 of SCI-PRO-001 REV04
   a. Corroborating data are available for comparison with the unqualified data set(s).
   b. Inferences drawn to corroborate the unqualified data can be clearly identified, justified, and documented.
2. Qualification Attributes from Attachment 4 of SCI-PRO-001 REV04:
   (3) The extent to which the data demonstrate the properties of interest (e.g., physical, chemical, geologic, mechanical);
   (8) Prior peer and other professional reviews of the data
   (10) Extent and quality of corroborating data

5. Identification of Procedures Used

This plan was constructed according to SCI-PRO-001, SCI-PRO-006

6. Plan coordinated with the following known organizations providing input to or using the results of the data qualification

This plan is internal to the Performance Assessment, Near Field Environment organization.

Section III. Approval

Qualification Chairperson Printed Name	Qualification Chairperson Signature	Date
Katheryn Helean	Kathryn Helean	8/24/2007
Responsible Manager Printed Name	**Responsible Manager Signature**	**Date**
Geoff Freeze	Geoff Freeze	8/24/07

SCI-PRO-001.1-R1

Data Qualification Plan

Complete only applicable items.

QA: QA

Page 1 of 1

Section I. Organizational Information

Qualification Title

Qualification of the activation energy for feldspar dissolution

Requesting Organization

Near Field Environment

Section II. Process Planning Requirements

1. List of Unqualified Data to be Evaluated

Blum and Stillings 1995 [DIRS 126590], Table 2; activation energies of albite and K-feldspar at near neutral pH.

2. Type of Data Qualification Method(s) [Including rationale for selection of method(s) (Attachment 3) and qualification attributes (Attachment 4)]

These data will be qualified using Method 2 Corroborating Data in accordance with SCI-PRO-001 Attachment 3. The rationale for selecting this methodology is that corroborating data are available for comparison with the unqualified data set and any inferences drawn to corroborate the unqualified data can be clearly identified, justified and documented. The accuracy, precision and representativeness of the corroborating data will be documented. The data qualification tasks (i.e. work) specified in this plan will be conducted under suitably controlled conditions and any prerequisites for the specified activities, such as personnel training, have been satisfied. There are no special controls, processes, test equipment, tools, skills or tests needed to attain the required quality/verification of quality. Verification of quality will be by inspection and evaluation alone.

3. Data Qualification Team and Additional Support Staff Required

Katheryn B. Helean Ph.D. Qualification Chairperson
Wendy Mitcheltree

4. Data Evaluation Criteria

Evaluation Criteria Used:
1. Conditions for use from Attachment 3, Method 2 of SCI-PRO-001 REV04
   a. Corroborating data are available for comparison with the unqualified data set(s).
   b. Inferences drawn to corroborate the unqualified data can be clearly identified, justified, and documented.
2. Qualification Attributes from Attachment 4 of SCI-PRO-001 REV04:
   (3) The extent to which the data demonstrate the properties of interest (e.g., physical, chemical, geologic, mechanical);
   (8) Prior peer and other professional reviews of the data
   (10) Extent and quality of corroborating data

5. Identification of Procedures Used

This plan was constructed according to SCI-PRO-001, SCI-PRO-006

6. Plan coordinated with the following known organizations providing input to or using the results of the data qualification

This plan is internal to the Performance Assessment, Near Field Environment organization.

Section III. Approval

Qualification Chairperson Printed Name	Qualification Chairperson Signature	Date
Katheryn Helean	Katheryn Helean	8/21/2007
Responsible Manager Printed Name	**Responsible Manager Signature**	**Date**
Geoff Freeze	Geoff Freeze	8/21/07

SCI-PRO-001.1-R1

Data Qualification Plan

Complete only applicable items.

QA: QA
Page 1 of 1

Section I. Organizational Information

Qualification Title

Qualification of inputs to the pH uncertainty analysis

Requesting Organization

Near Field Environment

Section II. Process Planning Requirements

1. List of Unqualified Data to be Evaluated

LL991008104241.042 [DIRS 120489] "Evaporation of J-13 water"

LL000202905924.117 [DIRS 144913] "Evaporation of 100x Conc. J13 Water"

LL991008004241.041 [DIRS 120487] "Evaporation of Topopah Spring Tuff Water at 75°C"

2. Type of Data Qualification Method(s) [Including rationale for selection of method(s) (Attachment 3) and qualification attributes (Attachment 4)]

These data will be qualified using Method 2 Corroborating Data in accordance with SCI-PRO-001 Attachment 3. The rationale for selecting this methodology is that corroborating data are available for comparison with the unqualified data set and any inferences drawn to corroborate the unqualified data can be clearly identified, justified and documented. The accuracy, precision and representativeness of the corroborating data will be documented. The data qualification tasks (i.e. work) specified in this plan will be conducted under suitably controlled conditions and any prerequisites for the specified activities, such as personnel training, have been satisfied. There are no special controls, processes, test equipment, tools, skills or tests needed to attain the required quality/verification of quality. Verification of quality will be by inspection and evaluation alone.

3. Data Qualification Team and Additional Support Staff Required

Katheryn B. Helean Ph.D. Qualification Chairperson
Wendy Mitcheltree

4. Data Evaluation Criteria

Evaluation Criteria Used:
1. Conditions for use from Attachment 3, Method 2 of SCI-PRO-001 REV04
   a. Corroborating data are available for comparison with the unqualified data set(s).
   b. Inferences drawn to corroborate the unqualified data can be clearly identified, justified, and documented.
2. Qualification Attributes from Attachment 4 of SCI-PRO-001 REV04:
   (3) The extent to which the data demonstrate the properties of interest (e.g., physical, chemical, geologic, mechanical);
   (10) Extent and quality of corroborating data

5. Identification of Procedures Used

This plan was constructed according to SCI-PRO-001, SCI-PRO-006

6. Plan coordinated with the following known organizations providing input to or using the results of the data qualification

This plan is internal to the Performance Assessment, Near Field Environment organization.

Section III. Approval

Qualification Chairperson Printed Name	Qualification Chairperson Signature	Date
Katheryn Helean	Katheryn Helean	8/21/2007
Responsible Manager Printed Name	**Responsible Manager Signature**	**Date**
Geoff Freeze	Geoff Freeze	8/21/07

SCI-PRO-001.1-R1

Data Qualification Plan

Complete only applicable items.

QA: QA
Page 1 of 1

Section I. Organizational Information

Qualification Title

Qualification of the age of the Topopah Springs Tuff

Requesting Organization

Near Field Environment

Section II. Process Planning Requirements

1. List of Unqualified Data to be Evaluated

Sawyer et al. 1994 [DIRS 100075], Table 1; Age of the Topopah Spring Tuff, 12.8 Ma

2. Type of Data Qualification Method(s) [Including rationale for selection of method(s) (Attachment 3) and qualification attributes (Attachment 4)]

These data will be qualified using Method 2 Corroborating Data in accordance with SCI-PRO-001 Attachment 3. The rationale for selecting this methodology is that corroborating data are available for comparison with the unqualified data set and any inferences drawn to corroborate the unqualified data can be clearly identified, justified and documented. The accuracy, precision and representativeness of the corroborating data will be documented. The data qualification tasks (i.e. work) specified in this plan will be conducted under suitably controlled conditions and any prerequisites for the specified activities, such as personnel training, have been satisfied. There are no special controls, processes, test equipment, tools, skills or tests needed to attain the required quality/verification of quality. Verification of quality will be by inspection and evaluation alone.

3. Data Qualification Team and Additional Support Staff Required

Katheryn B. Helean Ph.D. Qualification Chairperson
Wendy Mitcheltree

4. Data Evaluation Criteria

Evaluation Criteria Used:
1. Conditions for use from Attachment 3, Method 2 of SCI-PRO-001 REV04
   a. Corroborating data are available for comparison with the unqualified data set(s).
   b. Inferences drawn to corroborate the unqualified data can be clearly identified, justified, and documented.
2. Qualification Attributes from Attachment 4 of SCI-PRO-001 REV04:
   (3) The extent to which the data demonstrate the properties of interest (e.g., physical, chemical, geologic, mechanical);
   (8) Prior peer and other professional reviews of the data
   (10) Extent and quality of corroborating data

5. Identification of Procedures Used

This plan was constructed according to SCI-PRO-001, SCI-PRO-006

6. Plan coordinated with the following known organizations providing input to or using the results of the data qualification

This plan is internal to the Performance Assessment, Near Field Environment organization.

Section III. Approval

Qualification Chairperson Printed Name	Qualification Chairperson Signature	Date
Katheryn Helean	Katheryn Helean	8/21/2007
Responsible Manager Printed Name	**Responsible Manager Signature**	**Date**
Geoff Freeze	Geoff Freeze	8/21/07

SCI-PRO-001.1-R1